UNIVERSITY OF KWAZULU-NATAL

HIGH GAIN WIDEBAND MICROSTRIP PATCH ANTENNAS WITH DEFECTED GROUND STRUCTURE FOR SUB-6 GHZ 5G COMMUNICATIONS

Taiwo Oluwafemi Olawoye

2021

HIGH GAIN WIDEBAND MICROSTRIP PATCH ANTENNAS WITH DEFECTED GROUND STRUCTURE FOR SUB-6 GHZ 5G COMMUNICATIONS

Taiwo Oluwafemi Olawoye

218088305

Submitted in fulfillment of the academic requirements of
Master of Science (MSc) in Electronic Engineering

Discipline of Electrical, Electronic and Computer Engineering
School of Engineering, College of Agriculture, Engineering and Science
University of KwaZulu-Natal, Durban, South Africa

Supervisor: Dr Pradeep Kumar

January 2021

Preface

The research discussion in this dissertation was conducted at the University of Kwazulu-Natal under the supervision of Dr Pradeep Kumar, Discipline of Electrical, Electronic and Computer Engineering, College of Agriculture, Engineering and Science, University of Kwazulu-Natal, Howard College, South Africa.

I hereby declare that all materials incorporated in this dissertation are my own original work except where acknowledgement is made by name or in the form of reference. The work contained herein has not been submitted in part or whole for a degree at any other university.

_____

January 18, 2021

Declaration - Supervisor

As the candidate's Supervisor, I agree to the submission of this dissertation.

_____

Dr Pradeep Kumar

Date: January 18, 2020

Declaration 1

Plagiarism

I, Taiwo Oluwafemi Olawoye, declare that:

  i. the research reported in this dissertation, except where otherwise indicated, is my original research;

 ii. this dissertation has not been submitted for any degree or examination at any other university;

iii. this dissertation does not contain other person's data, pictures, graphs or other information unless specifically acknowledged as being sourced from other persons;

iv. this dissertation does not contain other person's writing unless specifically acknowledged as being sourced from other researchers. Where other written sources have been quoted, then

   a. their words have been re-written but the general information attributed to them has been referenced,

   b. where their exact words have been used, then their writing has been placed in italics and inside quotation marks, and referenced;

 v. this dissertation does not contain texts, graphics or tables copied from the internet, unless specifically acknowledged, and the source being detailed in the dissertation and in the reference section.

Signed:

_____

Taiwo Oluwafemi Olawoye

Date: January 18, 2020

Declaration 2

Publications

DETAILS OF CONTRIBUTION TO PUBLICATIONS that form part and/or include research presented in this dissertation (include publications in preparation, submitted, *in press* and published and give details of the contributions of each author to the experimental work and writing of each publication).

Publication 1:

T. O. Olawoye and P. Kumar, "A High Gain Microstrip Patch Antenna with Slotted Ground Plane for Sub-6 GHz 5G Communications," 2020 International Conference on Artificial Intelligence, Big Data, Computing and Data Communication Systems (icABCD), Durban, South Africa, 2020, pp. 1-6, (IEEE Xplore) doi:10.1109/icABCD49160.2020.9183820.

Publication 2:

T. O. Olawoye and P. Kumar, "A High Gain Antenna with DGS for Sub-6 GHz 5G Communications", Progress in Electromagnetic Research Journals (Submitted).
Signed:

Taiwo Oluwafemi Olawoye

_____

Candidate name

Date: January 18, 2021

Dedication

This dissertation is dedicated to the glory of God who has bestowed grace, good health, wisdom to complete this work and the benefit of all mankind.

Acknowledgment

My appreciation goes to Almighty God for grace, strength and courage to begin the pursuit of this programme and how He made available financial provision to make it possible. I will also appreciate my Supervisor Dr Pradeep Kumar, a gentle but firm individual for his professional and excellent supervision, counselling and encouragement throughout the research study. I am grateful and indebted to him for his assistance, invaluable advice that has continually propelled me further to carry out this research and get it to a reasonable conclusion. I take the opportunity to work with such a wonderful person a good fortune.

I will like to appreciate Dr. Patrick Adeyeye, who introduced me to the University of Kwazulu Natal and through whom I met wonderful people that has been instrumental to the success of this work. I will also like to appreciate my friends and colleagues at the University of Kwazulu Natal. They are all beautiful people. I want to appreciate Oluwafemi Oni, a wonderful gentleman, Ayodeji Bamisaye a dependable friend, Oyedeji Okikioluwa, Emanuel Ogunwole, Babatunde Adewolu, Oluwole Osaloni and many more that space will not allow me to mention.

My colleagues at Rufus Giwa polytechnic, Owo deserve some praise as well. People like Engr. Arobieke O., Mr. Adedeji O., Dr. Oluwajobi I., Dr. Osafehinti S., Engr. Ijarotimi O., Engr. Idowu A. etc. you are all wonderful people to work with, I appreciate you all. I should not forget to appreciate the people of God at UKZN. My spiritual father and Pastor, Dr. Moses Okpeku and the rest of the family of the Lord that space will not allow me to mention. You are all wonderful people. The family of God in Nigeria, you are appreciated for your prayers support, encouragement, good wishes etc. I appreciate you all. God will reward your labour of love in Jesus name, amen.

Finally, I recognize my wife and children for your love and prayers. You have endured lonesomeness while I am away in pursuit of this noble course. I appreciate you all for supporting me and creating an enabling environment for me to carry out this research

work. I am most grateful.

Abstract

5G communication utilizes the two frequency ranges i.e. frequency range 1 (FR1) and frequency range 2 (FR2). The FR1 is the low frequency band with the frequency range from 450 MHz to 6 GHz. As FR1 contains the frequency range upto 6 GHz, it is also known as sub-6 GHz frequency band. The FR2, known as mm-wave frequency range, uses the frequencies above 24 GHz. The lower frequency including electromagnetic (EM) waves can travel farther as these are less affected by the weather such as rain, snow etc. The low frequency EM waves can penetrate the solid objects like buildings etc. The sub-6 GHz 5G radio band will handle the wider bandwidth needed for high speed 5G communication devices. This research work presents the design of 5 GHz microstrip patch antennas for use in sub-6 GHz 5G communication. Antennas designed for 5G network must have high gain and necessary wideband capabilities to handle the large data requirements at high speed.

This research proposes the design of a high gain rectangular microstrip patch antenna (HGRMPA) for use in sub-6 GHz 5G communication. A HGRMPA, that utilizes the patch with T-shaped slot, is designed. The defected ground structure (DGS) technology is used to improve the performance of the HGRMPA. The DGS of the proposed HGRMPA consists a C-shaped slot. The C-shaped slot along with cuts at its upper and lower parts is incorporated in the ground plane to further improve the performance of the HGRMPA. A reflective plate is placed at the back of the proposed HGRMPA to reduce the side lobes and back lobes produced by the antenna. This will improve the main lobe of the radiated signal and the gain of the HGRMPA. The proposed HGRMPA is fed using inset feeding technique and the antenna is mounted on the FR-4 epoxy substrate. The size of the proposed HGRMPA is $28.03 \times 23.45 \times 5.35 \ mm^3$ and it provides the maximum gain and maximum directivity of 5.49 dB and 7.12 dB, respectively. The bandwidth of the proposed HGRMPA is from $4.775 \ GHz$ to $5.049 \ GHz$, which covers the $4.8 \ GHz - 5 \ GHz$

sub-6 GHz 5G communication band.

Further, a high gain wideband microstrip patch antenna (HGWBMPA), using partial ground plane with triangular strip, is also presented. The proposed HGWBMPA operates in the sub-6 GHz 5G wireless networking band. The HGWBMPA utilizes the reflective plate to reduce the development of the back lobes and increasing the gain. The inset feed technique is used to feed the antenna and the antenna is mounted on the FR-4 epoxy substrate. The proposed design is simulated and optimized with commercially available EM software i.e. CST studio suite. The size of the proposed HGWBMPA is compact with the patch dimension of $18.43 \times 13.85\ mm^2$. The maximum gain, maximum directivity and efficiency of the HGWBMPA are 6.21 dB, 7.56 dB and 78%, respectively. The proposed HGWBMPA works from 4.921 GHz to 5.784 GHz, which covers the 4.9 GHz - 5.8 GHz sub-6 GHz 5G communications range.

Contents

List of Figures

List of Tables

List of Acronyms

5G	5th Generation
dB	Decibel
DGS	Defected Ground Structure
EBG	Electromagnetic Band Gap
EM	Electromagnetic
FSS	Frequency Selective Surface
GHz	Giga Hertz
GP	Ground Plane
HPBW	Half-Power Beamwidth
HGRMPA	High Gain Rectangular Microstrip Patch Antenna
HGWBMPA	High Gain Wideband Microstrip Patch Antenna
MHz	Megahertz
MPA	Microstrip Patch Antenna
PBG	Photonic Band Gap
RF	Radio Frequency
VSWR	Voltage Standing Wave Ratio

Chapter 1

Introduction

1.1   Background

Communication technologies have developed from the days of the wired machine or net-work to the age of cellular communication. Wireless communication is the preferred means of communication because of its various advantages such as it can be deployed where the wired infrastructure is inoperative etc. The antennas is a key device of a wireless commu-nication system. For long distance communications, high gain antennas are required. The high capacity wireless systems require wideband antennas. Additionally, practical anten-nas are necessary to maximize the reception of the transmitted radiation or power in a particular direction. The antennas with directional patterns are known as directional an-tennas. The design of antennas play an important role in the performance of the wireless communications systems. The successful design and implementation of the transmitting and receiving antennas increase the overall efficiency of the wireless system [1–4].

The invention of the microstrip patch antenna (MPA), that became popular in the 1970s, has given rise to a new generation of lightweight antennas. These antennas consist of a metallic radiating element and a metallic ground plane with a dielectric material sandwiched between them. The top metallic layer, the dielectric material and the metallic material at the bottom are known as patch, substrate and the ground plane, respectively. The radiating metallic patch may have several different configurations depending on their function. These antennas have the advantage of the low profile, flat and curve geometry, and low fabrication cost using the advanced print-circuit technology. Fig. 1.1 shows the general form of the microstrip patch antenna.
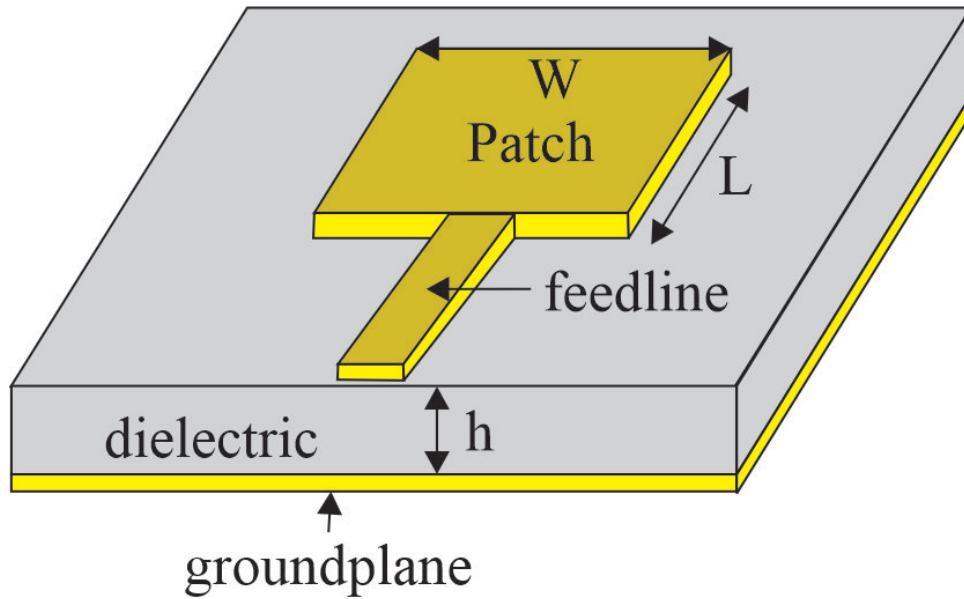
Figure 1.1: Rectangular MPA [3]

Fig. 1.1 displays a rectangular microstrip patch antenna (MPA). Other examples of microstrip patch include oval, triangular, square, eclipse, and several different geometries. Rectangular and circular MPA are commonly used geometries because of their good radiation characteristics and ease analysis [4, 5].

1.1.1 Merits of MPA

MPA has many advantages. These advantages have made these antennas popular for many lightweight applications. Following are the advantages of MPAs: [5–8]:

(a) Lightweight, low profile, small volume.

(b) These antennas can take the shape of their host such as conformal antennas.

(c) Multi-frequency operations can be achieved.

(d) Ease of fabrication.

(e) Printed-circuit board technology reduces their fabrication cost.

(f) Compact design is possible.

(g) Both linear and circular polarisation are possible.

(h) These antennas can be mass-produced.

(i) Matching networks for these antennas can be easily designed.

(j) These antennas can be mounted on airplanes, missiles, rockets and satellites etc.

1.1.2 Demerits of MPA

The major disadvantages of MPA are stated bellow [7, 9]:

(a) Narrow bandwidth.

(b) Low gain.

(c) Feeding for arrays may be complicated.

(d) Polarisation purity may be difficult.

(e) Low power handling capability.

The significant disadvantages of MPA are low gain and narrow bandwidth. To overcome these disadvantages, several methods of improving gain and bandwidth have been proposed. Several MPA properties can effectively be strengthened by Defected Ground Structure (DGS). DGS is created by etching the desired shape on the ground plane of conventional MPA. The DGS at the ground plane introduces impedance into the antenna circuit, which, when properly placed, improves the antenna properties [10,11]. DGS is easy to incorporate in the design as compared to electromagnetic bandgap (EBG). Both, DGS and EBG, significantly benefit the antenna properties. These technologies have gained the great recognition for improving the performance of MPAs. In a modern communication device, the use of DGS in MPAs maintains the compact size of the antennas [12–15]. DGS is accomplished by etching the required form in the ground plane of the antenna, which causes disruption in the distribution of current in the circuit. Hence, incorporation of defects in ground plane increases the inductance and capacitance of the MPA line. DGS is easy to analyze and integrate with the MPAs, hence it achieved the significant attention in the MPA technology.

DGS implementation has made MPAs deployment possible for wide bandwidth applications. It has helped in size reduction, in improving polarisation, in achieving multi-band operation, and in improving the return loss level.

1.2   Research Problem

Conventional MPA has the major disadvantages such as low gain, large profile size at low frequencies and narrow bandwidth etc [4, 5, 7, 9]. To improve the properties of traditional MPA, researchers have proposed several techniques which include stacking, photonic bandgap (PBG), EBG, DGS, frequency selective surface (FSS), metamaterial, etc. These techniques address the problem of low gain, narrow bandwidth, and the large size of the MPA at low frequencies [16–19]. DGS has drawn the interest of researchers over the last few years and continues to grow in achieving popularity due to its ability to improve the antenna performance with easy implementation.

DGS improves the antenna's efficiency by modifying the ground plane metal of the MPA. DGS deforms the ground plane by deliberately etching the slot(s) or defect(s) into the antenna's ground plane. It creates the imperfection or flaw in the circuit. This resulting the disruption in current flow in the ground plane of the MPA, hence resulting in the spread of EM waves across the substrate layers [11, 20–22]. This interference alters the capacitance of the line and the inductance of the transmission line. Tuning the output of the circuit may entail changing the shape from a basic to a complex one. The DGS technology is utilized in the proposed antennas to improve the performance of the antennas.

1.3   Research Questions

This research addresses the problem associated with the low gain and narrow bandwidth of the conventional MPAs. These limitations are improved by designing the antennas with slotted patch and DGS. The research seeks to answer the following questions:

(a) How can we significantly improve the gain and bandwidth of the MPA?

(b) How can the performance of the antenna be improved with simple and compact antenna structure?

(c) What motivates the choice of DGS in effecting a simple solution of gain and bandwidth of MPA in this design?

1.4 Research Aim and Objectives

Good antennas are desired in wireless communications due to the ever-increasing connectivity of the devices. The aim of the research is to design and develop MPAs with improved parameters for sub-6 GHz applications.

The following are the objectives in meeting the aim of this research:

(a) To design the compact rectangular MPA operating at the resonant frequency of 5 GHz in the sub-6 GHz frequency band.

(b) To design, simulate and optimize the antennas with high gain, wide bandwidth.

(c) To fabricate and test the designed compact antennas.

1.5 Research Contributions

The research proposes the design and development of MPAs for $\text{sub}-6\ GHz$ 5G communications. The research contributions are summarized below:

(a) To understand MPA problem of large size and design the compact MPAs for sub-6 GHz 5G applications.

(b) The wideband MPAs with DGS for $5G$ communication in the $\text{sub}-6\ GHz$ frequency band are proposed. A high gain of 6.21 dB is achieved.

(c) The design is fabricated and tested. The measured results are in agreement with the simulated results.

1.6 Structure of the Dissertation

This structure of the dissertation is given below:

Chapter 1 presents the introduction of MPAs, background, thesis motivation, thesis objectives, research contribution etc.

Chapter 2 discusses the fundamentals of MPAs, review of relevant literature that includes technical expertise in the application of DGS in antenna design. The concept

focuses on the rectangular microstrip patch antenna with DGS. Also, the strategies followed to enhance MPA properties are discussed in this chapter. The different techniques of enhancing the antenna properties are briefly discussed.

Chapter 3 discusses the methodology for HGRMPA and HGWBMPA. The mathematical calculations and design analysis used in the proposed antennas are discussed. The methods for improving the antenna performance are presented. The necessary criteria for evaluating the height and material for the substrate are discussed. Finally, the procedure for fabrication and necessary software tools are briefly discussed.

Chapter 4 presents the design and development of HGRMPA. The proposed HGRMPA uses the DGS to improve the radiation properties of the antenna. The antenna is mounted on the FR-4 substrate. The proposed HGRMPA was fabricated and measured. The measured results are compared with the simulated results. The simulation is carried out using the CST microwave studio, a commercial EM antenna tool.

Chapter 5 presents the design and development of the HGWBMPA. The proposed HGWBMPA utilizes the partial ground plane with triangular strp for improving the performance of the antenna. The antenna is fabricated and tested. The measured results agree with the simulated results.The proposed wideband high gain antenna is suitable for sub-6 GHz 5G communications.

In chapter 6, the conclusions of the work and future scope of the work are presented.

1.7 Summary

The introduction of MPAs, background, thesis motivation, thesis objectives, research contribution, structure of the thesis etc have been discussed in this chapter. The general introduction of the research work is given. MPAs have many advantages as compared to other antennas which make these antennas suitable for many light weight applications. These antennas suffer with low gain and narrow bandwidth. MPAs have many advantages which has encouraged a lot of research for improving their disadvantages. This dissertation presents the design of the compact high gain wideband MPAs for sub-6 GHz 5G wireless communication systems.

Chapter 2

Basic Antenna Parameters and Literature Review

2.1 Brief Introduction to the Antenna

An antenna is a metallic device that is typically used to radiate or receive the EM waves. The behavior of the antenna is same in transmitting mode and receiving mode. This is referred to as the reciprocal properties of an antenna i.e. the characteristics of the antenna as a transmitter or as a receiver are the same given that there is no use of non-linear or unilateral equipment. However, the reciprocity theorem does not ensure that the distribution of current on the antenna in receiving mode and transmitting mode remains the same [4,5]. In a smart wireless device, it is expected to maximize or boost the radiation energy in a specific direction and reduce or eliminate the radiation in other directions. This requirement for an antenna requires the directional patterns of the antenna. The antenna must take different forms such as wire antenna, aperture antenna, MPA, an assembly of elements (array), a reflector etc to satisfy the specific need for the transfer of the energy. An antenna is a vital part of the wireless communication system.

In 1953, Deschamps first introduced the microstrip antenna [23]. By the 1970s, several substrates with good thermal and mechanical properties were available for the rapid production of microstrip patch antennas. Advances in photolithography and progress in analytic antenna architecture models have lent a hand to the success of MPAs. [5, 24]. The first practical microstrip antenna was designed by Munson in 1972 and was first patented in 1973 [25]. Since then, the practical antenna production has proceeded at an

enormous pace. The researchers are actively making efforts to discover many more of the benefits of microstrip patch antennas and to minimize the disadvantages.

2.2 Antenna Parameters

For discussing the antenna parameters, we need to look the energy radiated by the antenna. To determine the radiation energy, we need to understand the radiation mechanism of the conductor first. A conductive wire can radiate when it carries the time-varying current or the charge associated with it accelerates (or decelerates). This means that when there is no charge movement taking place in the wire, there is no radiation occurring, and there is no flow of current in the wire. Also, the radiation would not occur even though charges travel over a straight wire at a uniform velocity. However, charges traveling at a constant velocity over a curved wire can emit the radiation. The changing oscillating charge over time creates radiation even when moving through a straight wire. [5]. Fig. 2.1 shows a two-wire transmission line with an attached voltage source. When an alternating voltage is applied to the transmission line, it generates a sinusoidal electric field.

As a consequence, an electrical line of force is developed which works in tangent to an electric field. The amplitude of the electric field is demonstrated by the bundling of the electric lines of the force, which passes the free electrons onto the conductors. The acceleration of these charges produces a magnetic field as a function of the current flowing in the conductor. The time-varying electrical and magnetic fields produce the EM waves. These waves are radiated into the free space. Electromagnetic waves are sustained by the charges inside the transmission line and the antenna. When the waves reach the free space as shown in Fig. 2.1, these form the closed loop.

2.3 Far Field and Near Field Regions

The antenna is surrounded by two regions i.e. near field region and far field region. In the near field region, the field patterns change with the distance. The field patterns in near field region can be represented by the two energy types i.e. radiative energy and reactive energy. Therefore, we can divide near field region in to two sub regions i.e. reactive near field region and radiative near-field region. Hence, the space surrounded by the antenna can be divided into three regional parts:
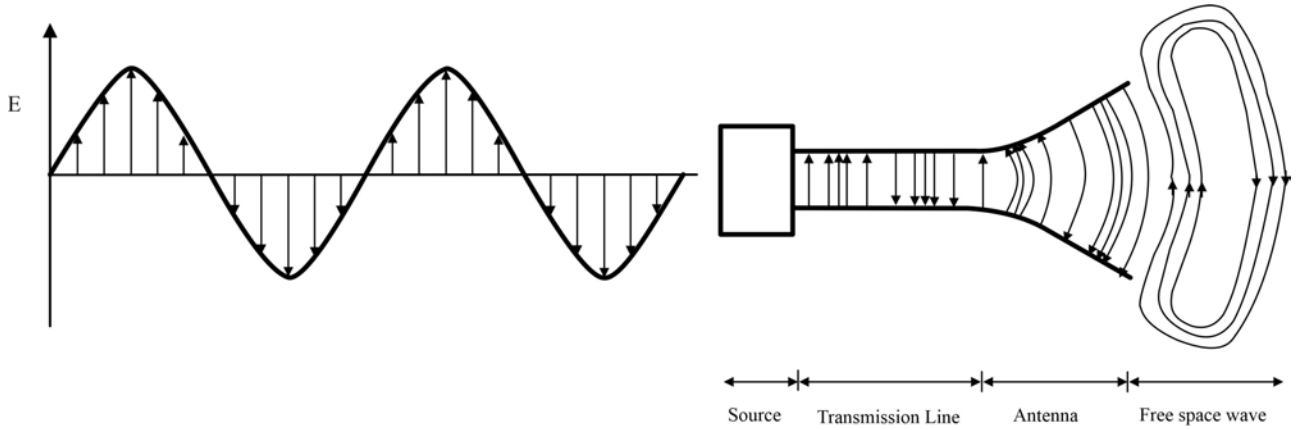
Figure 2.1: Antenna radiation mechanism [26]

   (a) The reactive near field region,

   (b) The radiative near-field region, and

   (c) The far-field region.

Fig. 2.2 shows the antenna field regions in the space.

2.3.1 The Reactive Near-Field Region

The energy here occurs as a reaction because the reactive field is dominant in this region. There is no dissipation of the energy in this region. $R_1 = 0.62\sqrt{\frac{D^3}{\lambda}}$ is the distance between the antenna and the outermost boundary of this region as shown in Fig. 2.2. Where R_1, D and λ are the distance between the antenna surface and the outer boundary, the maximum antenna diameter and the operating wavelength, respectively.

2.3.2 The Radiating Near-Field Region

This region is also known as the Fresnel region. From the Fig. 2.2, it can be observed that this region separates the near-field reactive region and the far-field region. The angular field distribution is dominant in this region. The outermost limit of this region is at a distance R_2 which is given by $R_2 = \frac{2D^2}{\lambda}$, where R_2 is the distance from the antenna surface to the outer boundary of this region.

2.3.3   The Far-Field Region

The far-field region is also called the Fraunhofer region. From Fig. 2.2, it can be observed that this region goes beyond near-field radiating region, i.e. $R_2 = \frac{2D^2}{\lambda}$. There are no reactive fields in this region. The angular field distribution of the far-field region does not depend on the distance from the antenna surface and its power density changes is inversely proportional to the square of the radial distance.
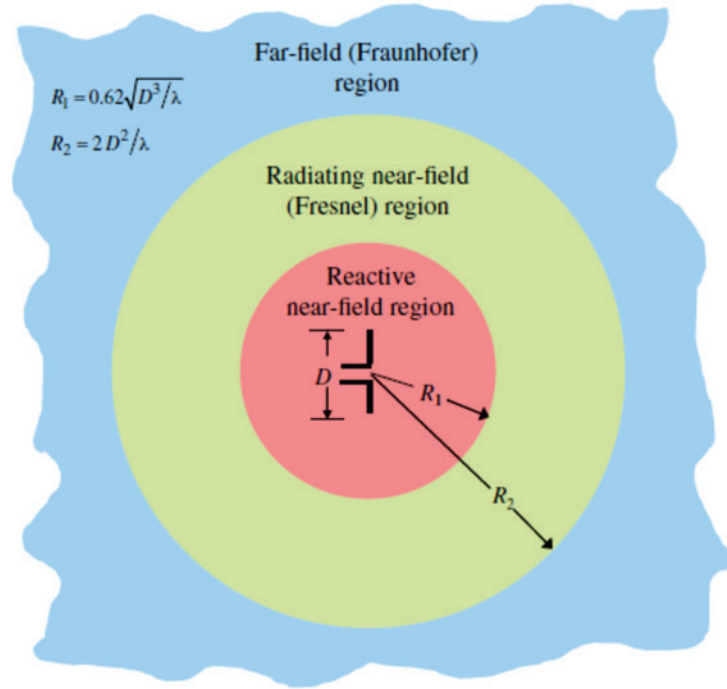
Figure 2.2: Antenna field regions [5]

2.4   Radiation Parameters of Antenna

The radiating parameters of an antenna determine the directional capabilities of the antenna. Some of the important parameters are discussed in this section.

2.4.1   Radiation Pattern

The radiation pattern of the antenna gives the information about the directional behavior of the antenna. The antenna can radiate or receive a signal when it acts as a transmitter or as a receiver. The radiation pattern of the antenna is a mathematical relationship or function that indicates the radiation properties of the antenna. The radiation pattern

of the antenna is typically calculated in the far-field region and is interpreted using the spatial coordinate system. The isotropic antennas radiate equally in all directions. The total radiated power is P is distributed over the radius of sphere r. The power density S at the distance r in any direction is given by [5]:

$$S = \frac{P}{area} = \frac{P}{4\pi r^2} \tag{2.1}$$

The radiation intensity U_i for the isotropic source is given by:

$$U_i = r^2 S = \frac{P}{4\pi} \tag{2.2}$$

In reality, however, it is difficult to realize an isotropic antenna. A directional antenna is more practical than an isotropic antenna. A directional antenna produces more radiation power in one direction while it radiate less power in other directions. The omni-directional antenna is a special case of the directional antenna. It may have a continuous radiation pattern in one plane (e.g. in the E-plane) and may differ in the orthogonal plane (e.g. in the H-plane).
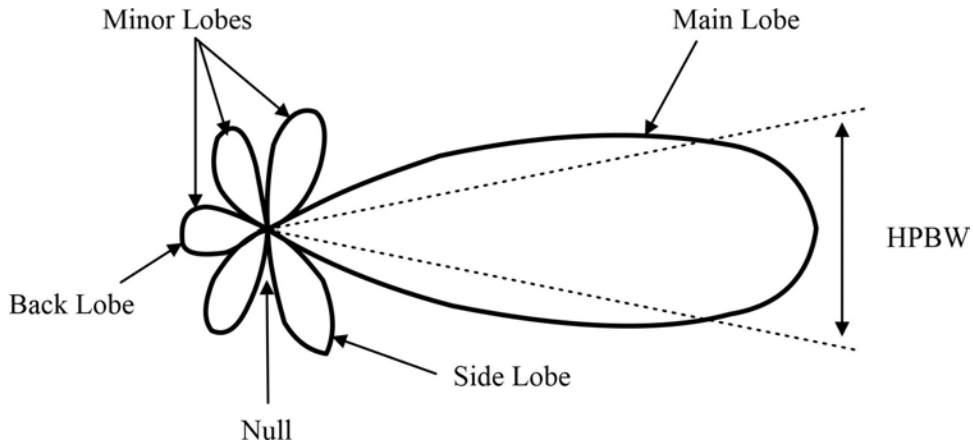
Figure 2.3: Antenna radiation pattern [27]

From Fig. 2.3, we define the following:

(a) Beamwidth: This is the aperture angle from where the antenna radiates most of its power.

(b) Half Power Beamwidth (HPBW): This refers to the angular separation from where the full power of the antenna radiation has reduced by half. It is also called the $3dB$ beamwidth.

(c) Main Lobe: The main lobe radiates power in the desired direction of maximum radiation.

(d) Minor Lobes: All lobes that do not radiate power in the direction of maximum radiation are called minor lobes.

(e) Back Lobe: This refers to a minor lobe that usually radiates in the opposite direction to the main lobe.

(f) Side Lobe: This is a minor lobe that is usually sideways to the main lobe. They are generally the largest among the minor lobes.

(g) Null: The null area is the area with no radiation of power.

We want to avoid minor lobes in the radiation pattern because they are generally undesired and reduce the antenna performance.

2.4.2 Antenna Directivity

The directivity of an antenna is a very important or critical property of the antenna. It is defined as the ratio of the radiated power by the antenna in a specified direction to the radiated power of an isotropic antenna. This means that the directivity of an antenna is the ability to aggregate or focus the radiation power in a specified direction. From [5],

$$D = \frac{U}{U_0} = \frac{4\pi U}{P_{rad}} \tag{2.3}$$

Maximum directivity is given by:

$$D_m = D_0 = \frac{U_m}{U_0} = \frac{4\pi U_m}{P_{rad}} \tag{2.4}$$

where,

D = directivity (dimensionless)

D_0 = maximum directivity (dimensionless)

U = radiation intensity (W/unit solid angle)

U_m = maximum radiation intensity (W/unit solid angle)

U_0 = radiation intensity of isotropic source (W/unit solid angle)

P_{rad} = total radiated power (W)

$$D_0 = D_\theta + D_\phi \tag{2.5}$$

$$D_\theta = \frac{4\pi U_\theta}{(P_{rad})_\theta + (P_{rad})_\phi} \tag{2.6}$$

$$D_\phi = \frac{4\pi U_\phi}{(P_{rad})_\theta + (P_{rad})_\phi} \tag{2.7}$$

where,

U_θ = radiation intensity in a specified direction contained in θ field component

U_ϕ = radiation intensity in a specified direction contained in ϕ field component

$(P_{rad})_\theta$ = radiated power in all directions contained in θ field component

$(P_{rad})_\theta$ = radiated power in all directions contained in θ field component

2.4.3 Gain

The antenna gain is the ratio of the power radiated by an isotropic antenna to the input power of the antenna. The gain of the antenna includes the directional characteristics of the antennas as well as the efficiency of the antenna. The gain of an antenna can be determined by using [28]:

$$Gain = 4\pi \frac{Radiated\ intensity}{Total\ power} = 4\pi \frac{U(\theta, \phi)}{P_{in}} \tag{2.8}$$

2.4.4 Input Impedance

The input impedance for an antenna is the resistance or impedance as seen at the input terminals of the antenna. It is the voltage to the current ratio at the antenna terminals. For an antenna to have maximum power, the characteristic impedance of the transmission line that feeds the antenna and the impedance of the antenna should be matched. A mismatch of the impedance will cause the overall efficiency of the system to be reduced because full power cannot be delivered over the terminals. This is because it generates a reflected wave at the terminals of the antenna, which causes power to be reflected back to the source of power. Therefore, the characteristic impedance of the transmission line and the input impedance must be balanced for maximum power transfer to take place between the transmission line and the antenna. Mathematically, we write the impedance

as [5]:

$$Z_i = R_i + jX_i \tag{2.9}$$

Here Z_i is the impedance at the input terminal of the antenna,

R_i is the resistance of the antenna at the input terminal, and

X_i is the reactance of the antenna at the input terminal.

The imaginary part of the input impedance X_i indicates the power stored in the near field region of the antenna. The resistive part of the input impedance, R_i, contains two components i.e. the radiation resistance R_r and the loss resistance R_L. The power radiated by the antenna is associated with the radiation resistance while the loss is dissipated as heat.

2.4.5 Bandwidth

Bandwidth of an antenna is defined as the range of frequencies for which antenna is operating properly. Optimal antenna bandwidth is one of the major parameters used to evaluate the performance of the antenna. When an antenna has narrow bandwidth, it can not be used as a wideband antenna. If the highest frequency and the lowest frequency of the antenna bandwidth are f_H and f_L, respectively, the bandwidth of the antenna is given by [4, 5]:

$$BW = f_H - f_L \tag{2.10}$$

Bandwidth can also be defined as fractional or percentage bandwidth. To do this, the central frequency must be calculated, which is either the arithmetic or geometric mean of the maximum and minimum frequency [28].

$$f_C = \frac{f_H + f_L}{2} \tag{2.11}$$

The arithmetic means to produce the centre frequency f_C when the frequency is considered on an arithmetic scale. The geometric average is an alternative to the arithmetic average.

$$f_C = \sqrt{f_H f_L} \tag{2.12}$$

The centre frequency generated by the geometric mean is essential when the centre

15

frequency is viewed on a logarithmic scale and is not widely used. Unless otherwise stated, the arithmetic average or mean should be inferred. The phrase fractional bandwidth, which is the ratio of the bandwidth to the middle frequency, can also be used.

$$BW = \frac{BW}{f_C} \tag{2.13}$$

Percentage bandwidth is given by

$$BW\% = \frac{BW}{f_C}100\% \tag{2.14}$$

2.4.6 Voltage Standing Wave Ratio (VSWR)

The Voltage Standing Wave Ratio (VSWR) of an antenna is defined as the ratio of the highest amplitude to the lowest amplitude of the standing wave. The VSWR is a measure of the efficiency of the antenna. It depicts how efficiently the impedance of the antenna is matched with the characteristic impedance of the transmission line. The VSWR closer to 1 is better as more power flows from the transmission line to be radiated by the antenna. Usually, the normal range of values for VSWR to achieve a successful impedance is between 2.0 and 1.0 i.e. ≤ 2. The condition for the matching is defined by:

$$Z_i = Z_S^* \tag{2.15}$$

where Z_i is the impedance at the input terminals of the antenna and Z_S^* is the complex conjugate of the impedance of the transmission line.

$$Z_S = R_S + jX_S \tag{2.16}$$

where R_S is the resistance and X_S is the reactance.
Similarly,

$$Z_i = R_i + jX_i \tag{2.17}$$

R_i is the resistance and X_i is the reactance at the input terminals of the antenna.

$$R_i = R_L + R_r \tag{2.18}$$

where R_r and R_L are the loss resistance and the radiation resistance, respectively.

The Voltage standing wave ratio is given by [5]

$$VSWR = \frac{1 + |\Gamma|}{1 - |\Gamma|} \tag{2.19}$$

$$\Gamma = \frac{V_r}{V_i} = \frac{Z_i - Z_S}{Z_i + Z_S} \tag{2.20}$$

where Γ denotes the reflection coefficient,

V_r represents the amplitude of the reflected wave, and

V_i is the amplitude of the incident wave.

A practical antenna design is usually designed for 50Ω or 75Ω input impedance.

2.4.7   Return Loss (RL)

The Return Loss (RL) of an antenna is a measure of the impedance matching of the antenna. Due to mismatching, the power delivered to the load is not maximum. The wasted power which returned to the source and not transferred to the load, is called the Return Loss (RL). When RL is less than or equal to $10dB$, the matching is adequate and the sufficient power is transferred to the load. When $\Gamma = 1$ and $RL = 0dB$, all the power fed to the antenna is reflected back to the source. The return loss is given by [29]:

$$RL = -20log_{10}|\Gamma| \tag{2.21}$$

where Γ is the reflection coefficient.

2.4.8   Antenna Efficiency

In determining the efficiency of an antenna, we must consider the power at the input and output terminals of the antenna. Following are the various types of losses in antenna:

(a) The reflection losses due to mismatching.

(b) The conductor and dielectric losses.

Putting these together, the total antenna efficiency of the antenna is given by: [5]

$$e_t = e_r e_c e_d \qquad (2.22)$$

where e_t is the total efficiency of the antenna,

$e_r = (1 - |\Gamma^2|)$ is the reflection efficiency,

$e_c =$ conduction efficiency,

$e_d =$ dielectric efficiency.

The e_c and e_d together are represented by e_{cd}. The e_{cd} is known as the radiation efficiency and is given by:

$$e_{cd} = e_c e_d = \frac{R_r}{R_r + R_L} \qquad (2.23)$$

2.4.9   Polarization

The antenna field consists of the magnetic and electric components. These fields are always perpendicular to each other and are also perpendicular to the direction of propagation. The direction in which the electric field component oscillates is known as polarization. The direction of the electrical field with respect to the earth's surface determines the polarization of the wave, as shown in Fig. 2.4. Common types of polarization includes the linear polarization, which is horizontal or vertical in nature, and circular polarization, which is right-hand or left-hand polarization.

2.5   Antenna Types

There are mainly five types of antennas $[1, 5, 30]$. Those are:

  (a) Wire Antennas,

  (b) Aperture Antennas,

  (c) Microstrip Antennas,

  (d) Array Antennas and

  (e) Reflector Antennas.

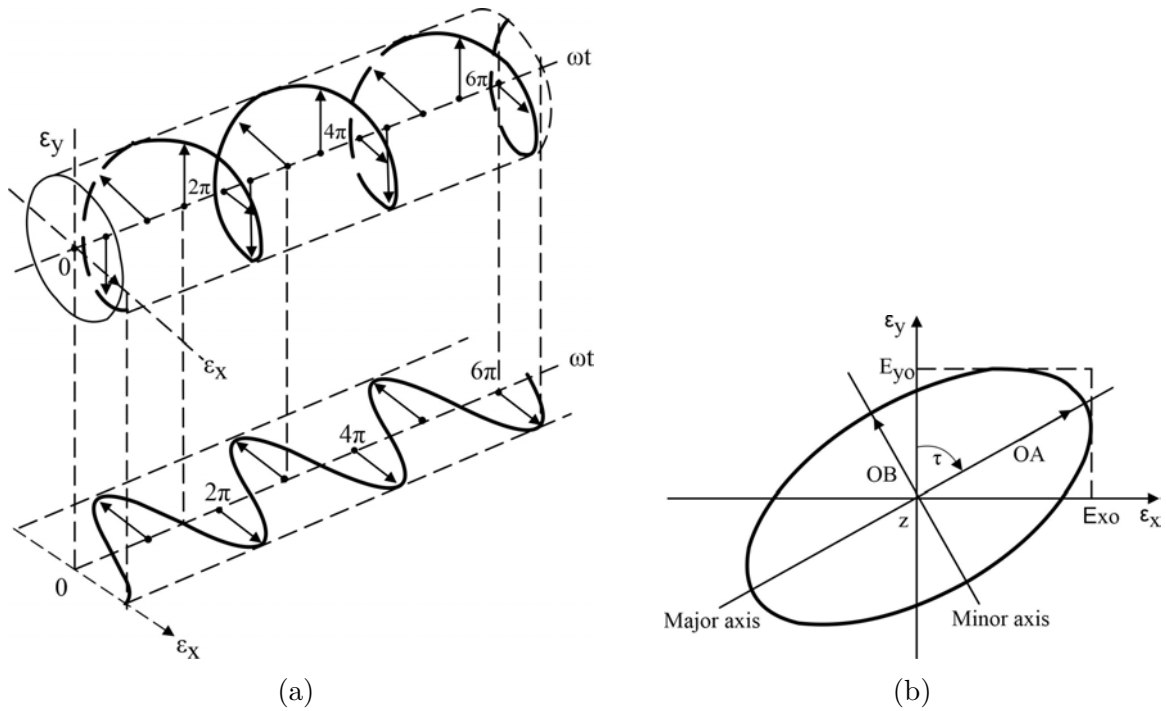Figure 2.4: (a) Rotation of a plane electromagnetic wave (b) Polarization ellipse [5]

2.5.1 Wire Antennas

Wire antennas are the most commonly used antennas and are quite familiar. These antennas are usually mounted on vehicles, houses, spacecraft, etc., and can take any shape from a straight wire (dipole) to a helix. Fig. 2.5 shows the examples and types of wire antennas.
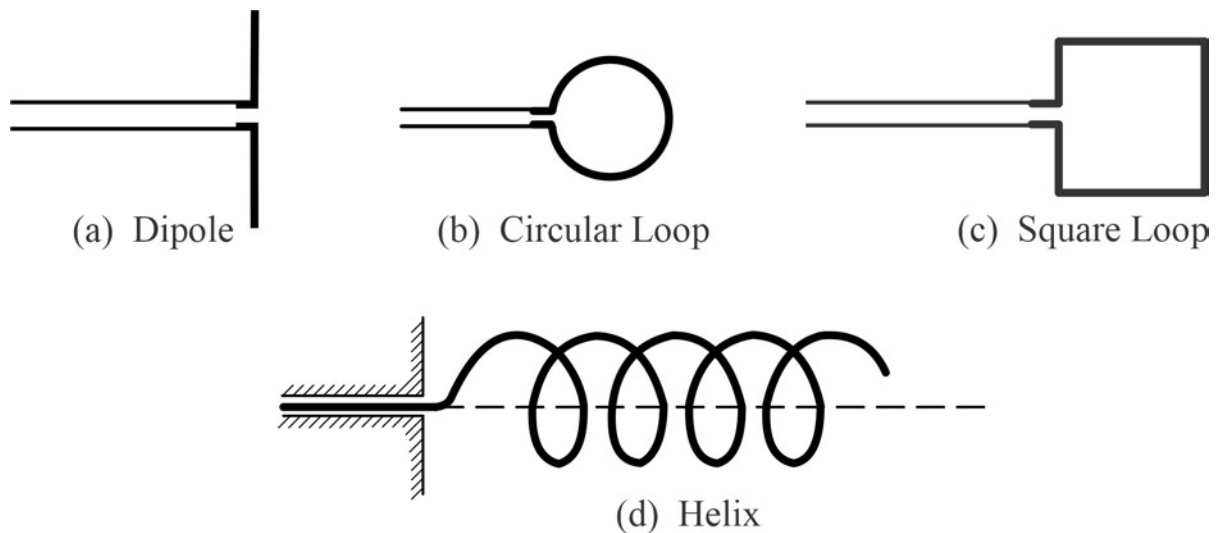
Figure 2.5: Wire antenna configurations [5]

2.5.2 Aperture Antennas

Aperture antennas are required for higher frequency and high power utilization. Some forms of the aperture antennas are shown in Fig. 2.6. These antennas are suitable for applications in spacecraft because they can conveniently take the shape of the body or skin of the craft. Also, protection from hazardous environmental elements can be achieved by covering them with the dielectric materials.

(a) Pyramidal Horn   (b) Conical Horn   (c) Rectangular Waveguide

Figure 2.6: Aperture antennas [5]

2.5.3 Microstrip Antennas

Microstrip patch antennas (MPAs) consist of a dielectric material or substrate sandwiched between the two metallic layers. The upper metallic layer is called the patch and the lower metallic layer is called the ground plane. These antennas have the advantages of low profile, conformable to planar and non-planar surfaces, inexpensive and straightforward to design, mass production using advanced printed-circuit technology etc. These antennas can be designed for multi-band operations, polarization diversity etc. MPAs can be installed on vehicle bodies or surfaces, high-speed aircraft, satellites, high-speed missiles, mobile phones, etc.

2.5.4 Array Antennas

Antenna arrays consist of more than one antenna element to achieve the specific propagation characteristics. These antennas are known as the array antennas. The elements of the antenna arrays are arranged in such a way so that these antennas have maximum cumulative radiation in the desired direction and minimum radiation in the other directions.

2.5.5 Reflector Antennas

The reflector antennas are parabolic dishes or reflectors to reflect signals over a far distance. These antennas are employed for communication to outer space or planets. These antennas are suitable for long distance applications. However, they are always very bulky because of their large size.

2.6 Feeding Techniques of MPA

Various feeding techniques are used to excite or power the MPA. The feeding techniques are classified as direct feeding techniques and indirect feeding techniques. In the direct feeding techniques, the antennas are in direct contact with the feeding line/probe, while in the indirect feeding techniques, the antennas are not directly in contact with the feeding line/probe. The four most popular methods for feeding MPA are the coaxial probe feeding method, microstrip line feeding method, aperture coupling feeding method, and the proximity coupling feeding method. Aperture and proximity coupling are non-contacting feeding techniques. These techniques use electromagnetic field coupling to transfer power from the feeding line to the radiating patch. On the other hand, contacting feeding techniques include the coaxial probe feed and microstrip line feed, where the RF feed power is transferred to the radiating patch using the direct contact between the patch and feeding probe/line [5, 31–33].

2.6.1 Aperture Coupling

Aperture coupled feed consists of a ground plane sandwiched between the two different substrates. The bottom substrate has a microstrip feed line. The EM energy is coupled to the patch through a slot that passes to the ground plane. Normally, a low dielectric constant substrate is used for the upper substrate, while a higher dielectric substrate is used for the lower substrate in aperture coupling. The ground plane, which separates the substrates, isolates the feed from the radiation components and reduces the interference from the spurious radiation. Aperture coupling is the most difficult feeding technique to fabricate because it requires multi-layer fabrication. The use of aperture coupling usually results in a narrow bandwidth of the antenna. Fig. 2.7 (a) and Fig. 2.8 (c) show the aperture coupled MPA and the equivalent circuit, respectively.

(a) Aperture-coupled feed   (b) Proximity-coupled feed

(c) Microstrip line feed   (d) Probe probe feed
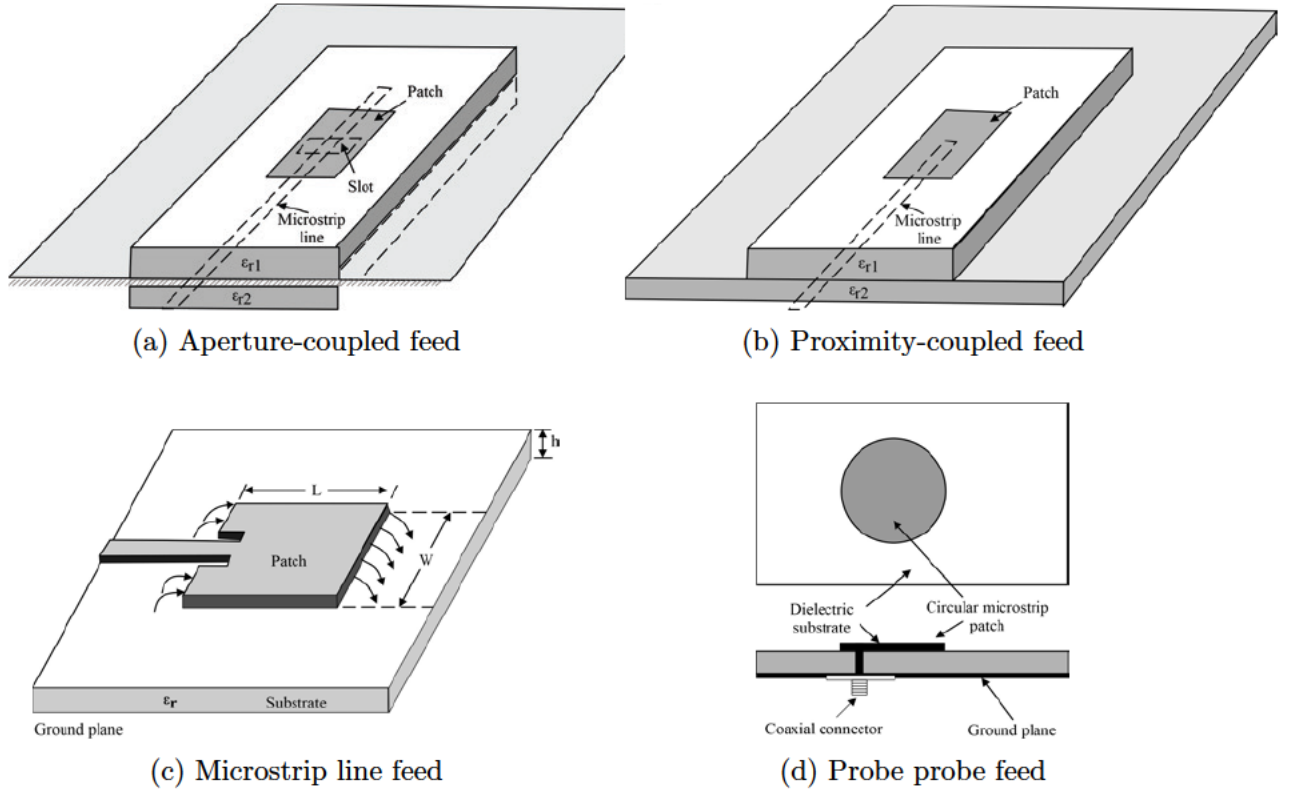
Figure 2.7: Feeding methods for MPA. [5]

2.6.2 Proximity Coupling

Two methods can be used to accomplish proximity coupling or electromagnetic coupling. The first is to separate the patch and the feed line by a small gap, while the other method is to mount the patch and the feed line on different substrate layers. This coupling has the advantage of the wide bandwidth and low spurious radiation. Fig. 2.7 (b) and Fig. 2.8 (d) depict the proximity coupled MPA and its equivalent circuit, respectively.

2.6.3 Microstrip Line Feed

The microstrip line feed is very simple to model and easy to fabricate. Impedance matching is also easy as it can be done by controlling the position of the inset cut into the patch. There is the possibility of increased surface wave and spurious feed radiation as the thickness of the substrate increases. Due to high spurious radiation, this method provides the narrow bandwidth. We have adopted this feeding technique for the work reported in this dissertation. Fig. 2.7 (c) and Fig. 2.8 (a) show the microstrip feed line fed MPA and the equivalent circuit, respectively. The dimension, which is opposite to the feed line of the patch, is the width of the patch.
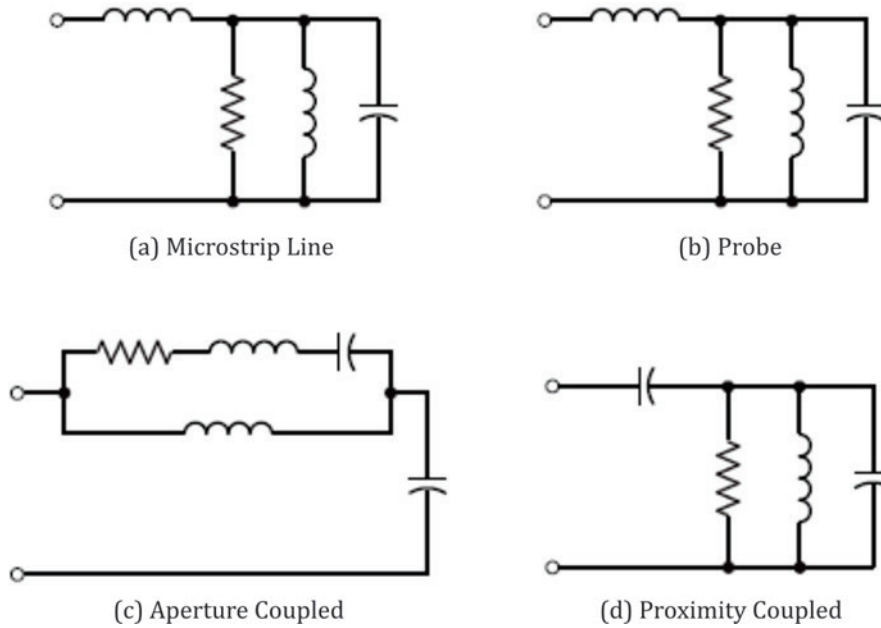
Figure 2.8: Equivalent circuits of the feeding methods, (a) equivalent circuit of microstrip feed, (b) equivalent circuit of Probe feed, (c) equivalent circuit of aperture coupled feed, (d) equivalent circuit of proximity coupled feed [5]

2.6.4 Coaxial Probe Feed

Coaxial probe feed is another commonly used method for feeding MPAs due to its simplicity in manufacturing and matching. Coaxial feed uses a coaxial cord to energise the radiating patch. The inner conductor of the coaxial cable is connected to the radiating patch, and the outer conductor is connected to the ground plane. It has a major drawback of narrow bandwidth and is difficult to model. Fig. 2.7 (d) and Fig. 2.8 (b) show the coaxial probe fed MPA and the equivalent circuit, respectively. Table 2.1 shows the comparison of feeding techniques of MPA [34].

2.7 Microstrip Patch Antenna (MPA)

As stated early in this dissertation, a Microstrip Patch Antennas (MPA), or Patch Antenna, or Microstrip Antenna is made up of a metallic patch that is mounted on the grounded substrate [5, 35]. Due to their inherent advantages, these antennas are used in low profile applications. These antennas are suitable in aircraft, missiles, satellite, mobile devices etc [1, 5]. Fig. 1.1 shows the typical example of a MPA. Let us briefly see some of the methods of enhancing the properties of an MPA in the following section.

Table 2.1: Comparison of different feeding methods [9]

Characteristics	Microstrip line feed	Coaxial feed	Aperture coupled feed	Proximity coupled feed
Configuration	Coplanar	Non-planar	Planar	Planar
Spurious feed radiation	More	More	More	More
Polarization purity	Good	Good	Excellent	Poor
Ease of fabrication	Easy	Soldering and drilling	Poor	Poor
Reliability	Better	Poor due to soldering	Good	Good
Impedance matching	Easy	Easy	Easy	Easy
Bandwidth	2–5%	2–5%	2–5%	13%

2.7.1 Methods of Improving MPA Properties

Several researchers have proposed different methods in the literature for improving the properties of MPA. These properties include the size reduction, gain enhancement, bandwidth enhancement, improving the radiation efficiency etc. In [36–38], Frequency Selective Surface (FSS) was implemented to improve the antenna parameters. In [36], a wideband circular polarised FSS based dual-slot antenna was implemented. The designed antenna achieves an improved axial ratio bandwidth. It achieves the 56% circular polarization bandwidth (3.5 GHz, 4.5 − 8.0 GHz). The 10 dB impedance bandwidth of the antenna is 84.8% (5.48 GHz, 3.72–9.20 GHz). By introducing the FSS into the design, the antenna achieved a 10 dB peak gain at 5.6 GHz. In [37], a compact ultra-wideband monopole antenna was designed. The antenna achieved a compact size of 52 $mm \times 62.5\ mm \times 23.2\ mm$ and a high gain of 9.4 dB across the entire UWB range of 3.1–18.6 GHz. In [38], FSS implementation resulted in a wideband and high gain antenna. The antenna has the wide bandwidth and a maximum gain of 16.8 dB.

In [39–43], metamaterial superstrate was used to improve the gain and bandwidth of the antenna. Metamaterial superstrate has proved to be very useful in enhancing antenna properties that recent research has shown. Though metamaterial is non-natural occurring materials as these materials are artificial to have the properties which are not found in natural materials. They have the properties that can be utilized in antenna design for improving the parameters of the antenna. In [39], the performance of a circular

patch antenna was enhanced with a new dual-layer metasurface material. The design achieved a maximum gain of 7.5 dB up from 2.31 dB and a 30% increase in the antenna bandwidth. The dimensions of the antenna are compact at $1.01\lambda g \times 1.01\lambda g \times 0.025\lambda g$ over an operating frequency of $2.37 - 2.49~GHz$. In [40, 41], a $5G$ antenna was designed. The antenna achieved a high gain while maintaining a low profile or compact design. An operating frequency of 3.5 GHz was used in both antennae, while [40] achieves a gain of 7.43 dB, and [41] achieves the gain of 10.43 dB. [42] presents the novel metamaterial element. The material shows negative permittivity and permeability characteristics at distinct frequency ranges. The material exhibited superior electromagnetic characteristics in the frequency range of 8.5 GHz–10.3 GHz. In [44–46], slots were used to improve the antenna bandwidth by changing the behaviour of the conventional MPA from a single band antenna to multi-band antenna while keeping the size of the antenna compact. [44, 45] uses slots to obtain multiple radiating frequencies, thereby creating a multi-band antenna. In [44], a tri-band antenna was obtained, in [45], a four-band antenna was achieved. Both antennae performed with good gain in the required frequency band of operation. In [47–50], antenna arrays were implemented to improve the properties of the MPA.

2.8 Ground Plane Geometry

Various ground plane geometries have been proposed by researchers to improve the properties of MPA over the years. Using Photonic Band Gap (PBG) [51,52], the Electromagnetic Band Gap (EBG) [53], and Defected Ground Structure (DGS) [54–56], the performance of the MPAs can be improved. Table 2.2 shows the comparison of these three technologies [17].

In the DGS structure, slots are incorporated in the GP for modifying the MPA circuit. The ground plane of MPA is made defected by etching the slots in the GP. Several shapes of defects are used to disturb the wave propagation in the MPA. This disruption also affects the inductance and the capacitance of the transmission line. The defects in the MPA GP can modify the capacitance and inductance of the antenna. The slots in the GP of the MPA interrupt the current movement. This interference also influences the characteristics impedance of the transmission line of the antenna.

Table 2.2: Comparison of PBG, EBG, and DGS [17]

	PBG	EBG	DGS
Definition	Photonic Band Gap (PBG) is regular shape and ground-based structure and have the ability to monitor the radiation properties of the antenna.	Electromagnetic Band Gap (EBG) is similar to PBG technique and is also periodic compact structure.	Ground Plane (GP) with slots are known as Defected Ground Structure (DGS).
Geometry	Periodic structures engraved on the GP	Periodic but compact structures etched on the GP	One or a few structures etched on the GP.
Parameter extraction	Quite complicated, very difficult	Very difficult	It is pretty easy
Size	Large	It is not as big as PBG and bigger than DGS	DGS is smaller in size.
Fabrication	Difficult	Difficult	Easy

2.8.1 Unit Cell DGS

A unit cell DGS consists the single element/slot in the GP. The dumbbell-shaped DGS etched on the GP is the first type of DGS model that has been reported in the literature [57]. Fig. 2.9 shows the unit cell DGS with the dumbbell-shaped structure. It has some merits over PBG. Table 2.2 shows that the DGS has some significant advantages over the PBG and EBG. These are given below:

(a) Periodic structures cover a wide area in the PBG structure, while DGS can have smaller area using few slots in the GP.

(b) The DGS structure is easy to fabricate as slots can be etched easily on the GP.

(c) Better accuracy is obtained in DGS structures.

[58–60] shows the different commonly used geometry forms on the GP under the microstrip line. The commonly used shapes are rectangular dumbbell [61], circular [62], spiral [63], U shape [58], C shape [64], H shape [65] etc. Much more complex shapes continue to appear in literature as technology and analysis allow.
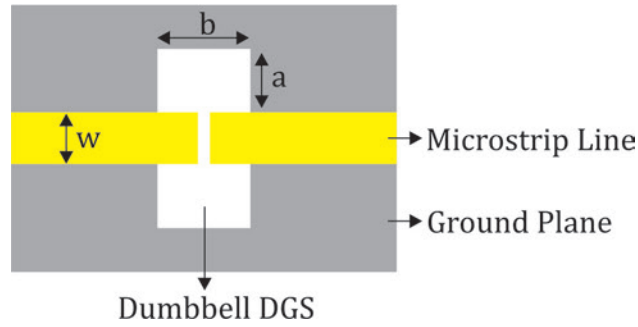
Figure 2.9: Dumbbell unit DGS [17]

2.8.2 Periodic DGS

In the periodic DGS structure, the same element/slot is repeated multiple times in a linear pattern or in a planar pattern. Periodic DGS for microwave components has attracted the attention of many researchers today. Microstrip antenna with a periodic DGS is presented in [66, 67]. By using the periodic structure, we can achieve a suitable antenna property as well as a greater degree of miniaturization. Cascading defects or resonating cells in the GP improve the antenna performance such as minimizes the return loss, improves the gain and bandwidth. The shape, height, spacing between the units, and the spread are important factors for improving the antenna parameters. Periodic DGS can be arranged either vertically, horizontally, or in a planar geometry. The pattern must be repetitive in order to make a periodic structure. Fig. 2.10 shows the structure of a periodic DGS. Fig. 2.10 (a) and Fig. 2.10 (b) depict the horizontal DGS and vertical DGS, respectively.
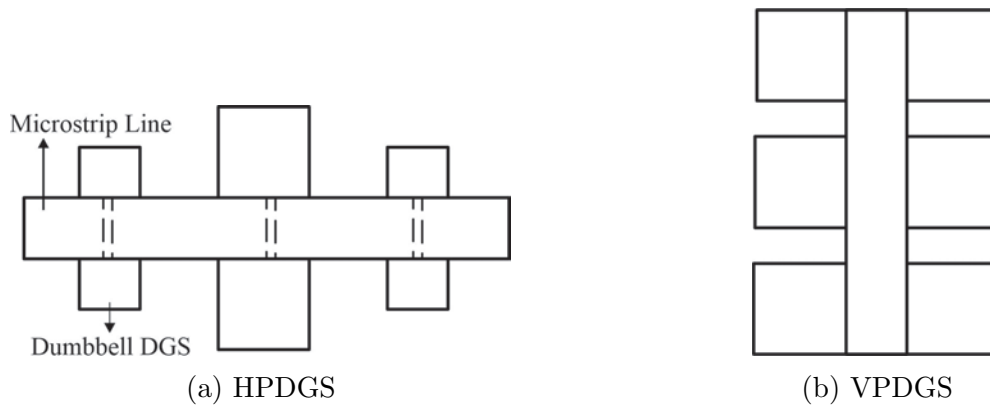

(a) HPDGS

(b) VPDGS

Figure 2.10: Periodic DGS [17]

27

2.9 DGS Equivalent Circuit

The metallic part of the microstrip antenna can be represented as a combination of resistance, inductance, and capacitance. Its equivalent circuit model can then represent the antenna model. Using the theory of Babinate, any slot or flaw on the antenna is a reciprocal of its metallic structure. Also, we can represent it by its equivalent reactance, i.e., RLC. A full-wave method is used to evaluate the reaction of the DGS to find an equivalent circuit model. However, this does not explain the physical measurements and location of the DGS on the antenna. Usually, conventional trial and error iterative methods were used to analyse the DGS. These are the time-consuming methods with the probability of not getting optimum results [68–70]. Fig. 2.11 shows the flowchart of conventional DGS design.
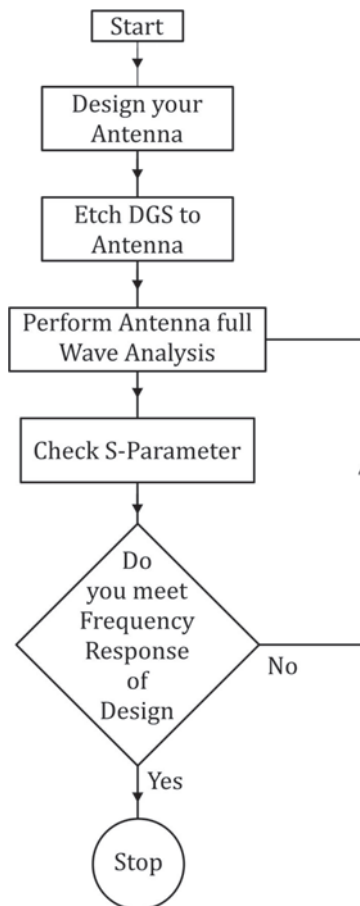
Figure 2.11: Design process of MPA with DGS [17]

There are four methods used to derive an equivalent circuit of DGS. These methods are given below:

(a) Inductance capacitance (LC) and Resistance, inductance and capacitance (RLC)

28

equivalent circuits,

(b) π equivalent circuit,

(c) Quasi-static equivalent circuit,

(d) Ideal transformer equivalent circuit.

2.9.1 LC and RLC Equivalent Circuits

Fig. 2.12 (a) and 2.12 (b) show the LC, and RLC equivalent circuit models of the DGS, respectively. The Butterworth low pass filter equivalent circuit model is given in [71]. The inductance and capacitance of the microstrip line are adjusted effectively by the rectangular sections of the DGS dumbbell, which elongate the current direction in the circuit. The two rectangular slots of the DGS dumbbell create the capacitive effect in the circuit. The thin rectangular defective slot, which joins the two rectangular faults, creates an inductance through the circuit. The combined effect of the capacitance and inductance creates a total impedance in the antenna circuit, which causes the shifting in the resonant frequency. The slotted DGS area size affects the inductance and capacitance of the circuit. If the DGS area increases, a resultant increase occurs in the effective inductance of the antenna circuit, which will cause the cut-off frequency to be reduced. On the other hand, the decrease in the DGS slotted decreases the effective capacitance of the antenna circuit, thereby an increase in the resonant frequency. The reactance of a Butterworth low pass filter is given by [56]:

$$X_{LC} = \frac{1}{\omega_0 C}\left(\frac{\omega_0}{\omega} - \frac{\omega}{\omega_0}\right) \tag{2.24}$$

where ω_0 is the resonance angular frequency. To calculate L and C we use:

$$C = \frac{\omega_C}{Z_0 g_1} \cdot \frac{1}{\omega_0^2 - \omega_C^2} \tag{2.25}$$

$$L = \frac{1}{4\pi^2 f_0^2 C} \tag{2.26}$$

where f_0 is the resonant frequency and f_c is cut-off frequency respectively.

DGSs with the same form as the dumbbell DGS have about the same characteristics as the dumbbell DGS. This implies that they can be studied as the Butterworth low-pass filter as shown in the Fig. 2.12. A parallel R, L, and C resonant circuit can also be
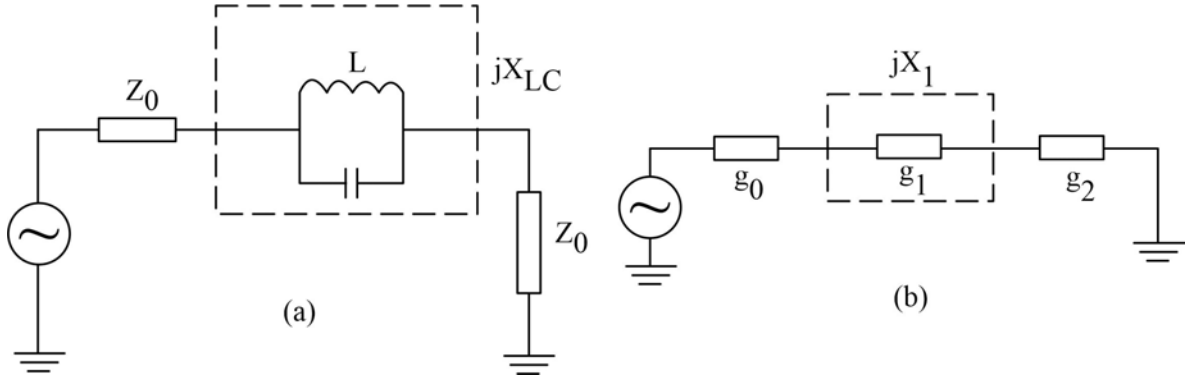
Figure 2.12: LC equivalent circuit, (a) equivalent circuit of the dumbbell DGS, (b) Butterworth-type one-pole prototype low-pass filter circuit [57,71]

used to analyse a DGS unit more effectively. The circuit is shown in the Fig. 2.13 with a resistance of R applied to the LC circuit, which is modeled for radiation losses, conductor losses, and dielectric losses. The circuit elements, i.e., capacitance C, inductance L, and resistance R, can be computed as following:

$$C = \frac{\omega_c}{2Z_0(\omega_0^2 - \omega_c^2)} \tag{2.27}$$

$$L = \frac{1}{4\pi^2 f_0^2 C} \tag{2.28}$$

$$R = \frac{2Z_0}{\sqrt{\frac{1}{|S_{11}(\omega_0)|^2} - \left[2Z_0\left(\omega_0 C - \frac{1}{\omega_0 L}\right)\right]^2 - 1}} \tag{2.29}$$
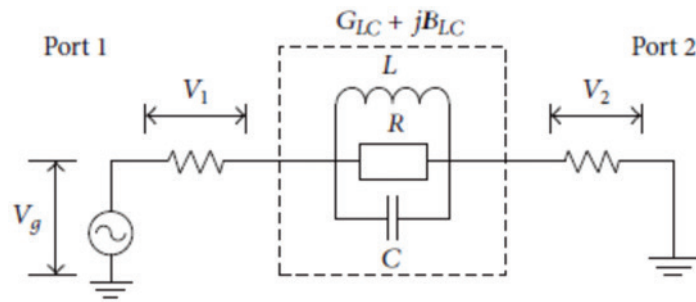

Figure 2.13: Equivalent circuit of unit DGS RLC [57,72]

2.9.2　π Equivalent Circuit Model

Fig. 2.14 shows the π model equivalent circuit which was suggested for use after LC and RLC equivalent circuit [71,73] [47], [48]. The π model equivalent circuit produces more accurate results as compared to the LC and RLC circuit models. A circuit similar to the

π model was suggested by Park. The model describes the amplitude in comparison to the frequency as well as the phase-to-frequency properties of the circuit [74]. The extraction of all the parameters of the circuit is little more complex and difficult using the π equivalent circuit. However, an equivalent circuit formed by π provides more precise results. The equivalent circuit of π is shown in Fig. 2.14. To determine the ABCD parameters for this equivalent circuit model of the DGS unit cell, we use the following:

$$\begin{bmatrix} A & B \\ C & D \end{bmatrix} = \begin{bmatrix} 1 + \frac{Y_b}{Y_a} & \frac{1}{Y_a} \\ 2Y_b + \frac{Y_b}{Y_a} & 1 + \frac{Y_b}{Y_a} \end{bmatrix} \tag{2.30}$$

$$Y_a = \frac{1}{R_g} + jB_r \tag{2.31}$$

$$Y_b = \frac{1}{R_p} + jB_p \tag{2.32}$$

$$C_g = \frac{B_r}{\omega_2 \left(\frac{\omega_2}{\omega_1} - \frac{\omega_1}{\omega_2} \right)} \tag{2.33}$$

$$L_g = \frac{1}{\omega_2^2 C_g} \tag{2.34}$$

$$C_p = \frac{B_p}{\omega_1} \tag{2.35}$$
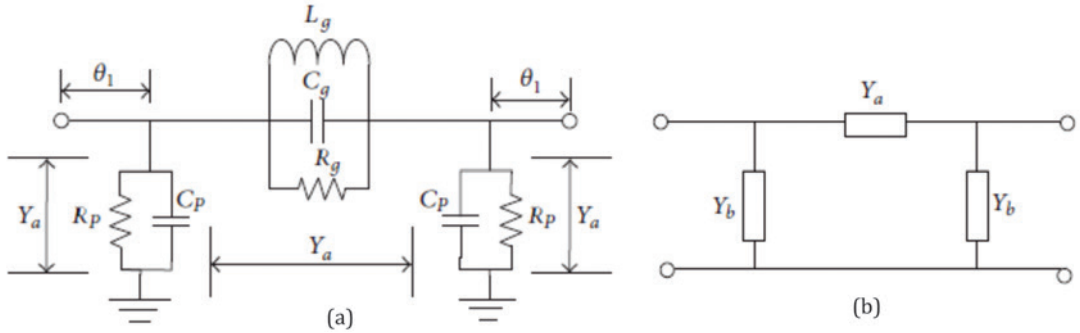
Figure 2.14: π-shaped equivalent circuit for unit DGS [74]

2.9.3   Quasi-Static Equivalent Circuit

Karmakar et al. proposed a quasi-static equivalent circuit model for a dumbbell-shaped DGS in [75]. The physical size of a dumbbell-shaped DGS plays an important role in determining the equivalent circuit model. A quasi-static circuit is shown in Fig. 2.15. In the quasi-static approach, there is no need for full-wave simulations of the structure

(except for the qualitative observation of the current path). However, a better outcome can also be obtained in this case by following an adjustment of the values of the parameters based on the curve fitting of the full-wave simulations [28]. We use the optimization approach to compare the various shapes of the DGS since the shapes produce different characteristics as a result of the different shapes and sizes of the DGS [10].
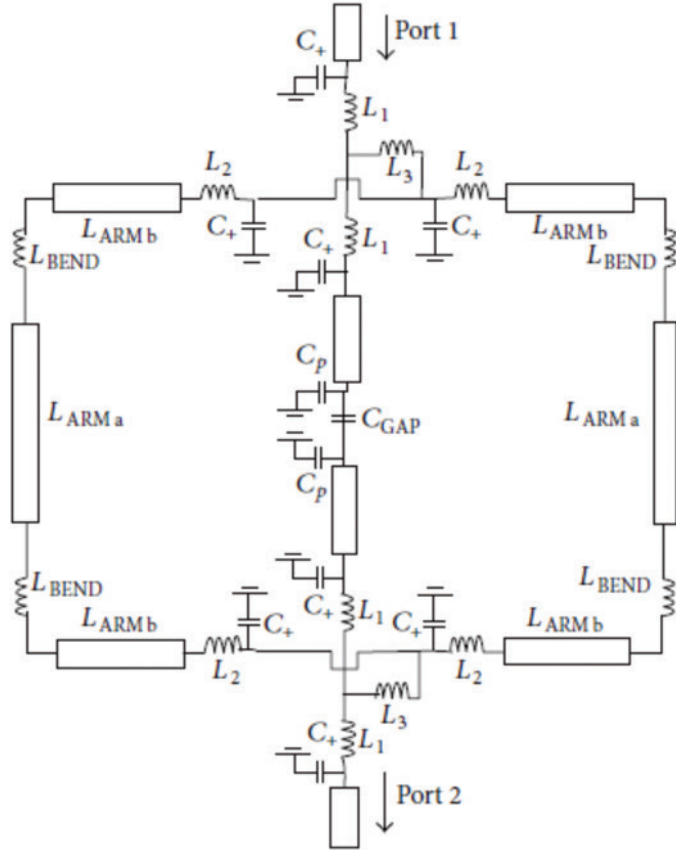
Figure 2.15: Quasi-Static equivalent circuit model of unit cell DGS [75]

2.9.4 Ideal Transformer Model

Caloz et al. suggest a precise and straightforward circuit model for a slot-loaded GP with a microstrip line [76]. The structure proposed in [76] together with its equivalent circuit model is shown in Fig. 2.16. The inductance L and the capacitance C represent the inductance in series and the capacitance in parallel of the microstrip line, and n is the ratio of the number of turns of the ideal transformer. The ideal transformer was used to model the coupling between the microstrip line and the slots inserted on the GP of the microstrip line. The ideal transformer model the microstrip line of length θ. The positioning of the etched slots inserted into the GP separates the microstrip line into two

sections of length θ_1 and θ_2, where $\theta_1 + \theta_2 = \theta$.

$$C_\mu = \frac{\sqrt{\varepsilon_{eff}^{\mu \ strip}}}{C_0 Z_0^{\mu \ strip}} \frac{l}{N_s}$$

$$L_\mu = (Z_0^{\mu \ strip})^2 C_\mu$$

Where Ns and l are the number of cells of the unit corresponding to the number of slots and the length of the line, respectively. The slots modeling was done by an ideal transmission line with the characteristic impedance of Z_0^{slot}.
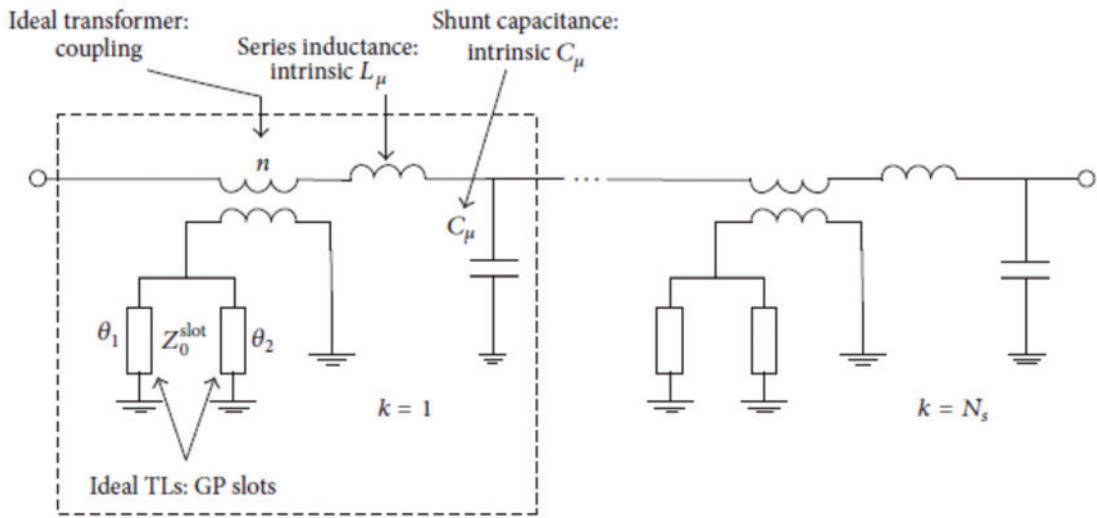
Figure 2.16: Ideal transformer circuit model for the slotted GP MPA [76]

2.10 DGS Applications in Microwave Circuits

DGS is common in microwave circuits and has been used in both active and passive systems. The various shapes and geometries of DGS have an influence on the efficiency of the microwave circuit. In [77], DGS was used to fabricate band-pass (narrowband/wideband), dual-band band-pass, and low pass filters. The design was compact and conventional. In [78–80], DGS has been widely used to accomplish the desired signal filtering. In [81], a coplanar waveguide (CPW) band-stop filter tuning was designed by short-cutting shaped like spirals to modify the resonant frequency. In [82], microwave amplifier size was reduced by using a new method. The method reduces rejection harmonic by using spiral DGS.

2.10.1 Applications of DGS in Antenna Design

DGS has been beneficial in improving the different MPA parameters such as gain, bandwidth, polarization, etc [11, 12]. In [13], DGS has been used to minimize the antenna size by 32.9% and to enhance the antenna gain. In [14], DGS was implemented to minimize the size of the MPA with a reduction of 67% in the patch size of the antenna.

In [51], (PBG) was used to boost the radiation properties of the antenna. In [83], slots were inserted in a parallel position to the patch of an MPA to induce performance improvement in the bandwidth of the MPA. This resulted in an increase of the bandwidth with the gain of 8 dB. The use of DGS to improve the cross-polarization characteristic has been shown in [54]. The design aims to create a simple and physically implementable geometry loaded DGS, with a noticeable effect in the antenna's cross-polarization (XP) properties. Bandwidth and antenna gain have been increased in [38] by using the Fabry-Perot cavity and the printed ridge-gap waveguide technology. The combined effect resulted in a maximum gain of 16.8 dB, which is a significant improvement over the slotted configuration alone. DGS technology was employed to design a dual-band MPA [84, 85] and also to design a triple-band MPA [86]. In [55], the DGS and the reflected surface were combined to enhance the antenna gain.

In [87], a slotted antenna configuration was proposed for use in wideband applications. This design achieves a total bandwidth of 4.4 GHz to 7.7 GHz, and the antenna has a uniform radiation pattern for a circularly polarized bandwidth with a gain of 6 dB. A compact MPA implementing U-shaped slots for dual-band operations was proposed in [88]. The resultant gain of the antenna is 2.06 dB and 2.46 dB, respectively in both frequency bands. It has excellent efficiency and radiation characteristics. In [89], a high-efficiency compact size antenna was suggested for wideband applications. The antenna has a unique slotted design, with an efficiency of about 78% and a gain of 5.72 dB.

2.11 Summary

In this chapter, the introduction to antennas, MPAs, feeding techniques of MPAa, the literature review of MPA antenna with DGS etc have been presented. The important parameters of antennas like gain, efficiency, bandwidth etc have been briefly discussed. The antennas with DGS technology are easy to fabricate. The DGS shapes along with

the equivalent circuit models have been presented. The DGS technology improves the antenna performance such as size reduction, gain enhancement, improvement in radiation properties, improvement in bandwidth etc.

Chapter 3

Methodology

3.1 Introduction

MPA are popular antennas for various compact wireless applications. They have several advantages such as compact size, easy to fabricate, easy to mount etc. This chapter presents the methodology for the design of the proposed HGRMPA and HGWBMPA.The design analysis is also given to achieve good performance by the antenna. The design procedure and the software tools used in the design are presented in this chapter. Prototype fabrication and measurement procedure is also given.

3.2 Substrate Material Selection

In the design of the MPA, we first consider the appropriate substrate for which the antenna will perform optimally. The substrate properties affect the performance of MPAs significantly. To achieve the optimum performance, the dielectric material should be strong for mechanical support and should provide the electrical insulation between the antenna plates. This influences the efficiency of the antenna and the characteristics of the transmission line. The substrate must meet the electrical as well as the mechanical requirements of the antenna.

3.3 Substrate Selection Criteria

When selecting the substrate material for the MPA, we should consider the following points:

(a) Surface wave excitation effects,

(b) The implications of the dielectric constant and the loss tangent effect of the substrate,

(c) Effect of losses of the material,

(d) Substrate anisotropy,

(e) Ageing, temperature and humidity effects on the substrate,

(f) Mechanical requirements of the substrate,

(g) Cost requirement of the substrate.

3.4 Surface Wave Excitation Effects

In MPAs, there is generation of surface waves. The surface waves travel within the substrate of the MPA. This implies that the surface waves keep propagating along the surface unless a discontinuity appears. These waves give rise to spurious radiation and produce unwanted coupling in array elements. This effect causes the losses and limit the performance of MPAs. Surface waves effect depends on the dielectric constant ε_r and the thickness of the substrate h. The cut-off frequency of the (TM_n and TE_n) modes is given by [5] :

$$f_c^{(n)} = \frac{n.c}{4h\sqrt{\varepsilon_r - 1}}, n = 1, 2, ... \tag{3.1}$$

Where c is the speed of light and the cut-off frequencies for the TE_n modes are the odd values of n, whereas the cut-off frequencies for the TM_n modes are given by the even values of n. The thickness of the substrate is carefully chosen so that the ratio $\frac{h}{\lambda_0}$ is well below $\frac{h}{\lambda_c^{(1)}}$.

where λ_0 is the free-space wavelength at the frequency of operation.

$$h \leq \frac{c}{4f_u\sqrt{\varepsilon_r - 1}} \tag{3.2}$$

Where the upper-frequency is denoted as f_u and the bandwidth of operation is f_h. It should be noted that h should be chosen as close as possible to the maximum value of h obtainable to allow for maximum efficiency without degrading the performance of the antenna. Also, h has to be cost-effective and can be practically computed using:

$$h \leq \frac{0.3c}{2\pi f_u \sqrt{\varepsilon_r}} \tag{3.3}$$

The TM_0 mode is always present because it has no cut-off frequency. In general, if the dielectric constant ε_r and the height h of the substrate is reduced, it will cause the suppression of the TM_0 modes. Unfortunately, when the dielectric constant ε_r is reduced, the size of the antenna will increase. Similarly, when the height h of the substrate is decreased, it causes a reduction in the efficiency and bandwidth of the MPAs.

3.5 Dielectric Constant and Loss Tangent Effect of the Substrate

The dielectric constant ε_r and the loss tangent of the substrate vary with frequency. This is known as frequency dispersion. The dielectric constant ε_r dispersion is practically negligible at low frequencies. However, as the frequency of operation increases, the losses begins to be significant. Generally, there is a direct proportionality between frequency and losses i.e. an increase in frequency results in the corresponding increase in losses [90].

3.6 Design Consideration of Rectangular MPA

This design is focused on a basic MPA with a rectangular-shaped patch operating at $5\ GHz$ resonant frequency. To select a suitably good geometry, considerations must be made of three properties: the dielectric constant of the substrates material, the loss tangent, and the thickness or height h of the substrate. The properties of the substrate help in deciding a good substrate for the design. When the dielectric constant of the substrate material is low, the fringing fields around the patch of the antenna will increase, which will lead to an increase in radiated power. Conversely, a high dielectric constant reduces antenna efficiency as it leads to increased loss tangent value. The effect of the

Table 3.1: Typical substrates and their parameters [5]

Company	Substrate	Thickness (mm)	Frequency (GHz)	ε_r	$\tan\delta$
Rogers	Duroid® 5880	0.127	$0-40$	2.20	0.0009
Corporation	RO 3003	1.575	$0-40$	3.00	0.0010
	RO 3010	3.175	$0-10$	10.2	0.0022
	RO 4350	0.168	$0-10$	3.48	0.0037
		0.508			
		1.524			
−	FR4	$0.05-100$	0.001	4.70	−
DuPont	HK 04J	0.025	0.001	3.50	0.005
Isola	IS 410	$0.05-3.2$	0.1	5.40	0.035
Arlon	DiClad 870	0.091	$0-10$	2.33	0.0013
Polyflon	Polyguide	0.102	$0-10$	2.32	0.0005
Neltec	NH 9320	3.175	$0-10$	3.20	0.0024
Taconic	RF-60A	0.102	$0-10$	6.15	0.0038

width of the patch on resonant frequency and the radiation pattern is very small, however, the bandwidth of the antenna is affected considerably. This means that when the patch width is increased, the bandwidth and radiation efficiency are increased. For a rectangular antenna, the width of the patch should be more than the length of the patch without exciting undesired modes. Table 3.1 shows some popular substrates and their parameters. From [5, 28, 91], the patch length L is given by:

$$L = \frac{c}{2f_r\sqrt{\varepsilon_r}} \tag{3.4}$$

The fields are not completely limited to the patch of the antenna. The fringing field, which is a small part of the fields, lies out of the antenna. To include the fringing field effect, we must compute the effective dielectric constant ε_{reff}.

$$L = \frac{c}{2f_r\sqrt{\varepsilon_{reff}}} \tag{3.5}$$

To design a good rectangular patch antenna, we need the following essential parameters for the design:

(a) The resonant frequency f_r of the antenna.

(b) The dielectric constant ε_r of the substrate.

(c) Substrate height h.

To calculate the width of the patch, we use the following equation:

$$W = \frac{c}{2f_r\sqrt{\frac{\varepsilon_r+1}{2}}} \tag{3.6}$$

$$W = \frac{c}{2f_r}\sqrt{\frac{2}{\varepsilon_r+1}} \tag{3.7}$$

Where the speed of light is denoted by c, the resonating frequency is given by f_r, and the dielectric constant of the substrate is given by ε_r. Fringing causes a small change in the dielectric constant. Considering the fringing effect, the effective dielectric constant of the substrate is given by [5, 92]:

$$\varepsilon_{reff} = \frac{\varepsilon_r+1}{2} + \frac{\varepsilon_r-1}{\sqrt{1+\frac{12h}{W}}} \tag{3.8}$$

$$\varepsilon_{reff} = \frac{\varepsilon_r+1}{2} + \frac{\varepsilon_r+1}{2}\left(1+12\frac{h}{W}\right)^{-0.5} \tag{3.9}$$

The actual length of the patch is given by [5]:

$$L = L_{eff} - 2\Delta L \tag{3.10}$$

$$L = \frac{c}{2f_r\sqrt{\varepsilon_{reff}}} - 2\Delta L \tag{3.11}$$

$$\Delta L = \frac{h(0.412)(\varepsilon_{reff}+0.3)(\frac{W}{h}+0.264)}{(\varepsilon_{reff}-0.258)(\frac{W}{h}+0.8)} \tag{3.12}$$

Where h is the substrate thickness.

To calculate the effective length L_{eff} of the antenna, the equation (3.5) is used.

$$L_{eff} = \frac{c}{2f_r\sqrt{\varepsilon_{reff}}} \tag{3.13}$$

Total length of the antenna patch is given by equation 3.10. The width of the ground plane W_g is given by:

$$W_g = 6h + W \tag{3.14}$$

The length of the ground L_g is given by

$$L_g = 6h + L \qquad\qquad (3.15)$$

3.7 Antenna Simulation Software

There are many softwares available for designing and optimizing the antennas. Three of these software programs are briefly discussed.

IE3D modular EM simulation solution program is developed by the Mentor Graphics, formerly Zeland Software. It is one of the first scalable EM design and verification tool that provides the simulation accuracy of choice for high-frequency circuit design. IE3D was replaced mainly by HFSS and CST studios for high-frequency EM architecture due to the ease of use and more reliable solvers.

Another commonly used software for antenna engineers is the High-Frequency Structure Simulator (HFSS). HFSS is a versatile EM simulation program. It uses excellent and efficient solvers and an excellent user-friendly GUI to produce the satisfactory simulation performance. It uses an automated adaptive meshing strategy that makes the results more reliable; thus, it is preferred over IE3D.

CST Studio Suite is an electromagnetic (EM) software for the design, simulation, study, and optimisation of EM components. CST Studio is an extremely scalable product used for creative innovation in engineering and science for a wide range of functions. Dassault Systèmes purchased the CST studio in 2016. It is simple to use, scalable, and iterative GUI. Hence, CST microwave studio is chosen for the study in this dissertation.

3.8 Simulation with CST

Full-wave analysis techniques were used to analyse the whole geometry of the antenna with no prior assumption as to the field interactions that are most relevant. Full-wave analysis models is a reliable modular model. It can handle the single antenna elements, stacked antennas, antennas arrays, randomly generated elements and couplings etc. The CST microwave studio uses the full-wave methodology which means the electromagnetic wave analysis of the solution will be generated using Maxwell's equations for both electrical
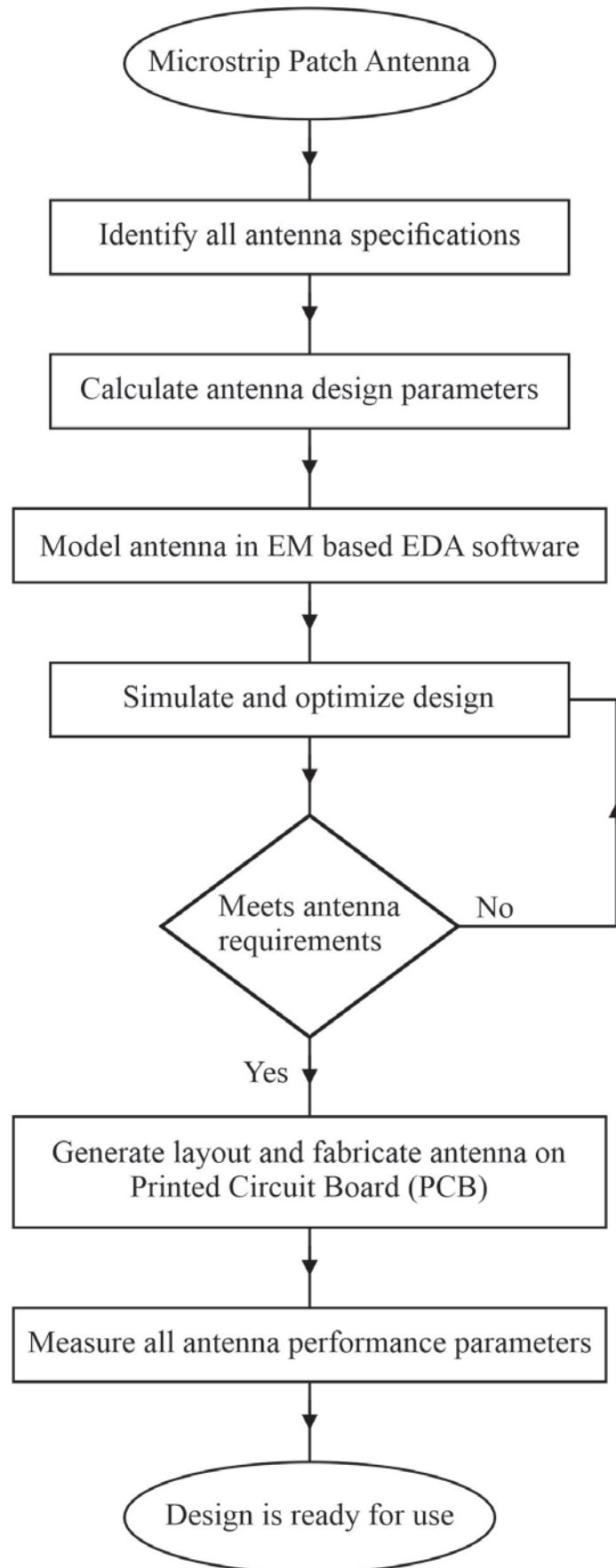
Figure 3.1: Design and fabrication process of MPA [61]

and magnetic fields in either the time domain or the frequency domain.

In the proposed antennas, the inset feeding method is used. The antennas are matched to 50Ω at the input by adjusting the position and depth of the inset on the feed line for a perfect impedance matching. CST microwave studio, a commercially available EM tool software, is used to simulate the design after the dimensions of the antenna have been computed. CST studio suite 2019 is the software of choice because of its ease of use and excellent solvers. Simulation and optimization ensure the optimum design of MPAs. The Fig. 3.1 shows the flowchart of the design, simulation and fabrication of the MPAs.

3.9   Antenna Fabrication and Measurement

The first step in fabricating the antenna prototype is to extract the Gerber files, which is then used to create the artwork from the template. The artwork is used to exposing the photoresist that is spun over the substrate. The mask is mounted on the substrate and held using a vacuum frame or other technique to ensure the fine-line resolution. When exposed to sufficient wavelength radiation, the exposed photoresist is polymerized and make it insoluble in the developer solution. The substrate is produced in a developer, which removes soluble photoresist material. The substrate is now able to be engraved. After etching, the excess photoresist is stripped with a stripping solution. The layer is then rinsed in water and dried. Then the antenna is cut into the small sizes necessary. Measurement of reflection coefficient is done using the network analyser. The measured results are compared with the simulation results. The radiation patterns are measured in an anechoic chamber. RF signal generator is used to feed the fabricated antenna, which is working as a transmitting antenna. A horn antenna is used as a receiver, and the received power is obtained using the signal analyzer. The obtained results are compared with the simulated result, and the antenna agrees largely with simulation with little variations as a result of losses in the materials and equipment error.

3.10   Summary

In this chapter, the methodology for the design and development of a rectangular microstrip patch antenna (MPA) has been presented. The criteria for selection of the substrate and substrate thickness for the proposed HGRMPA and HGWBMPA are also

discussed. The equations for the computation of the antenna dimensions, like width of the patch, length of the patch etc are presented. The software tool for the simulation and optimisation of the proposed antennas is CST microwave studio. CST microwave studio enables the visualisation of the antenna radiation properties before actual fabrication and testing. Finally, the procedure for fabrication and measurement of the antenna are discussed.

Chapter 4

Design and Development of the HGRMPA for Sub-6 GHz 5G Communications

4.1 Introduction

This chapter presents the design and development of the HGRMPA. The antenna is designed on the FR4 substrate which is a widely available and cheap substrate with satisfactory electrical and mechanical properties. The substrate height h is also an important design criterion in antenna design. This height and dielectric constant of the substrate are 1.6 mm and 4.3. respectively. The geometry of the proposed design, antenna prototype, simulated results and measured results of the HGRMPA are presented in this chapter.

4.2 Geometry of HGRMPA

The geometry of the proposed HGRMPA is presented in Fig. 4.1. Transmission model approach is adopted in designing the antenna [5]. Fig. 4.1 (a) and Fig. 4.1 (b) present the top view and GP view of the proposed HGRMPA, respectively. Fig. 4.1 (c) and Fig. 4.1 (d) show the back view and the side view of the HGRMPA, respectively. Fig. 4.1 (e) shows the complete antenna. As shown in Fig. 4.1 (e), the proposed HGRMPA utilizes the rectangular patch with the inset feeding. The inset feed is designed such that the antenna is matched to 50Ω impedance. The T-slot is etched in the patch to improve the

radiation characteristics of the antenna. The slot introduces impedance in the antenna structure, which, when correctly located, contributes to improve the radiation properties of the antenna. The GP of the antenna has a special lacerated C slot defected structure as shown in the Fig. 4.1 (b). Finally, a reflective plate is placed at 2 mm below the antenna. The reflective plate uses the single-sided FR-4 substrate. The top layer copper coating is etched off. The bottom coating serves as the reflector for minimizing the side lobes and back lobes of the antenna. The reflective plate helps to enhance the gain and directivity of the HGRMPA. The spacing between the reflective plate and the antenna is optimised as 2 mm to obtain the maximum gain and directivity. The dimensions of the antenna are shown in Table 4.1. The antenna is designed for the $5GHz$ broadband applications. The antenna is designed using the transmission line model equations $(3.5) - (3.16)$.

Table 4.1: Dimensions of HGRMPA

| S. No.	Parameter	Dimension (mm)
1	Wg	28.0289
2	Lg	23.4493
3	h	1.6
4	Gpf	0.08114
5	Wf	3.0389
6	Fi	5.1954
7	Wp	19.7189
8	Lp	13.8493
9	a, b, c	6, 0.4, 0.8
10	r, g, e, f	4, 1.2, 8, 10

4.3 Antenna Input Characteristics

The proposed antenna is built on the FR-4 substrate as described. The simulation is done using the CST Studio Suite, which is a commercially available EM software. The antenna gain is enhanced by using a reflector plate at the bottom of the antenna. The T slot on the patch helps to improve the performance of the antenna. Fig. 4.3 (a) displays the simulated and measured reflection coefficient of the proposed HGRMPA. The HGRMPA shows the good agreement between the simulated and the measured reflection coefficient. The antenna has the bandwidth of 274 MHz with the frequency range from 4.775 GHz to 5.049 GHz. The resonant frequency of the HGRMPA is 4.95 GHz. The C slot in GP introduces more radiation by the antenna that minimizes the reflection losses and
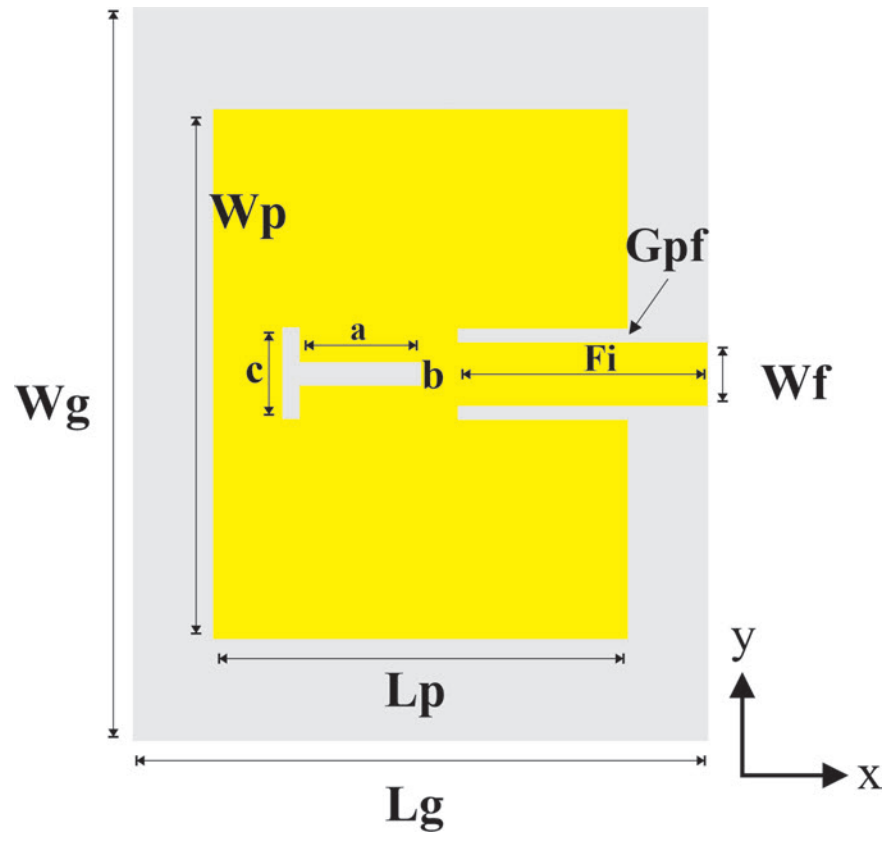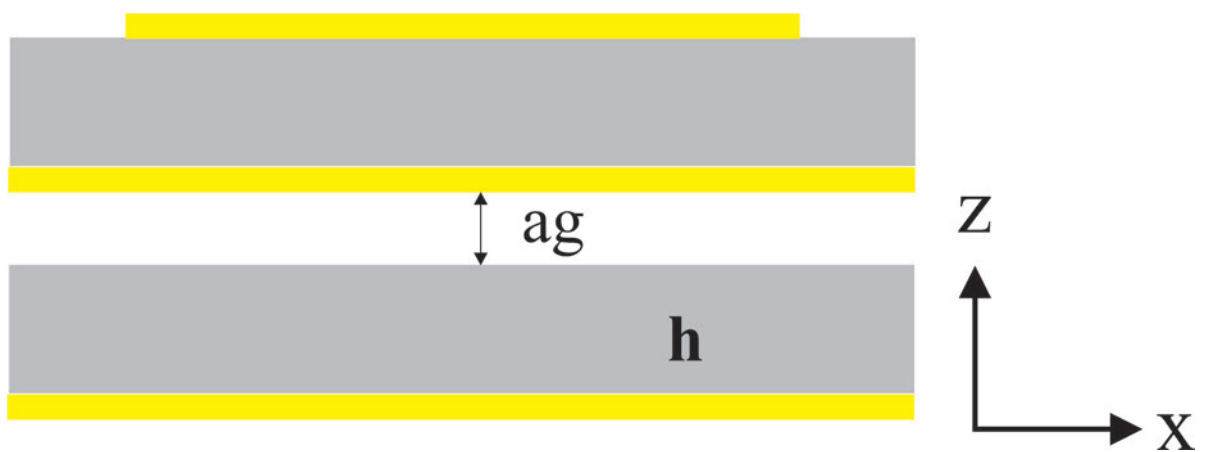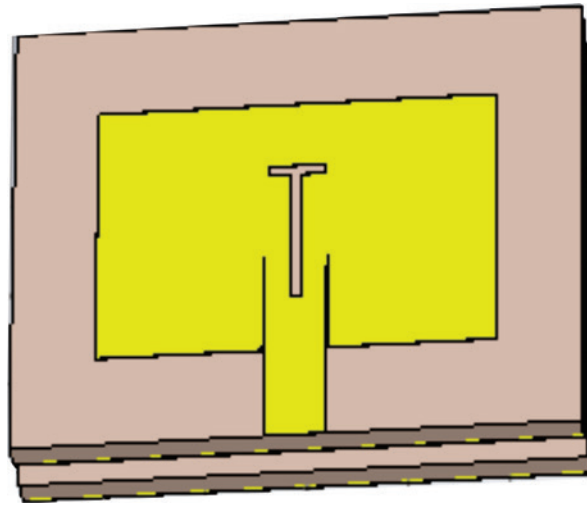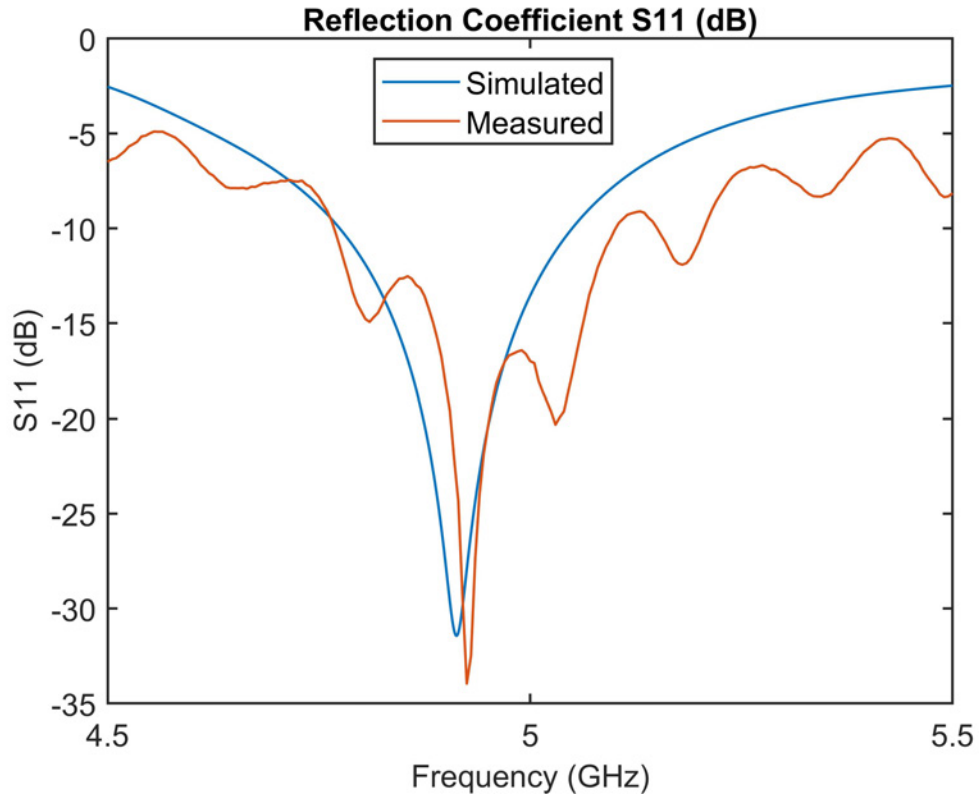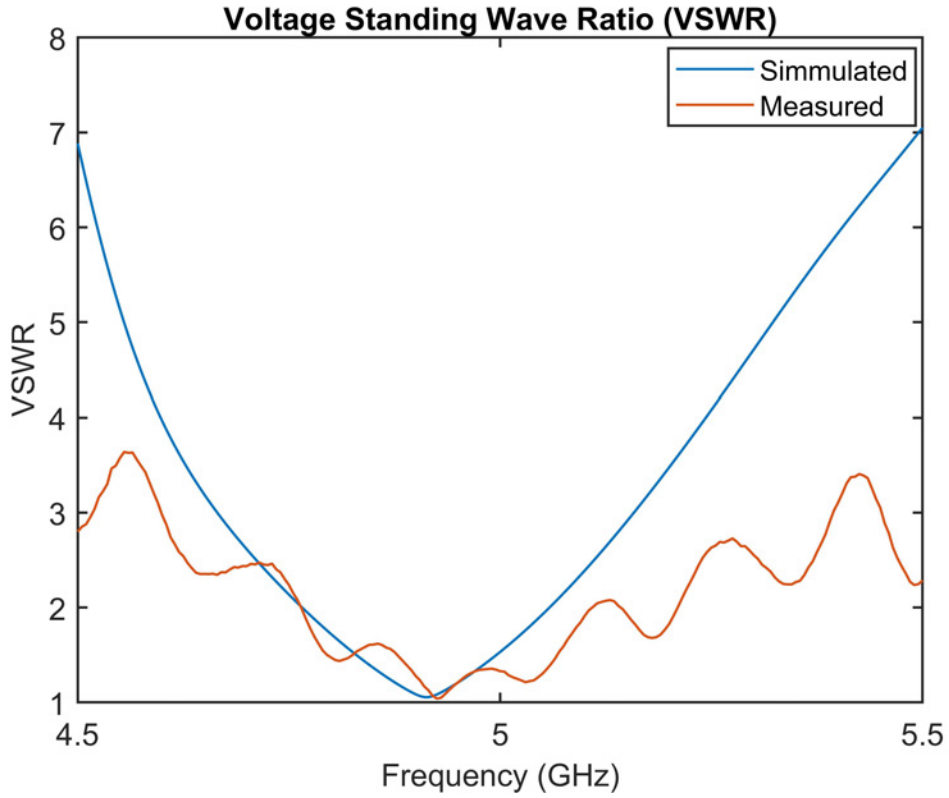
(a)
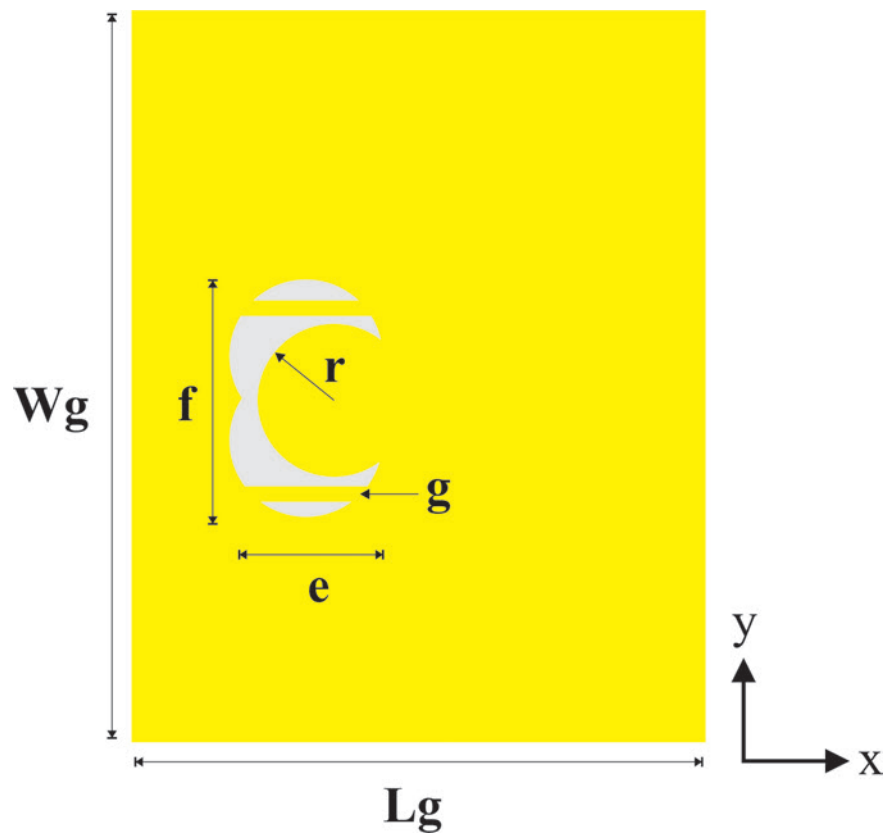
(b)
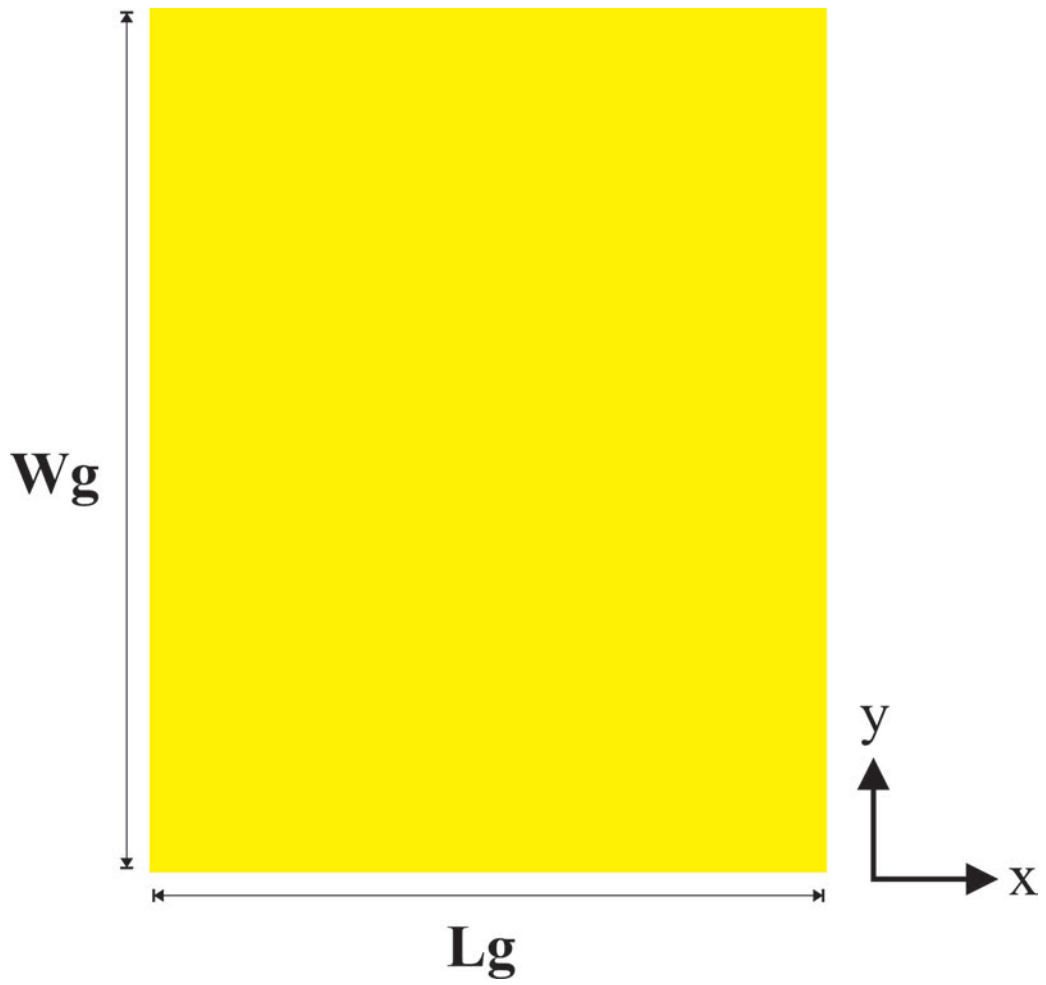
(c)

(d)

(e)

Figure 4.1: Antenna geometry, (a) top view, (b) ground plane, (c) antenna back view, (d) antenna side view, (e) complete antenna

Figure 4.2: Fabricated HGRMPA

(a)

(b)

Figure 4.3: Reflection coefficient and VSWR of the HGRMPA, (a) reflection coefficient (S11), (b) VSWR

improves the antenna performance. Fig. 4.3 (b) shows the voltage standing wave ratio (VSWR) of the proposed HGRMPA. Fig. 4.3 (b) indicates that the VSWR is less than 2 for the entire bandwidth i.e. from 4.775 GHz to 5.049 GHz.

4.4 Radiation Patterns

Fig. 4.4 presents the radiation patterns of the HGRMPA. The 3-d gain pattern and the 3-d directivity pattern are shown in Fig. 4.4 (a) and Fig. 4.4 (b), respectively. It can be seen from the Fig. 4.4 that the overall gain and maximum directivity of the designed antenna are 5.49 dB and 7.12 dB, respectively. The simulated and measured normalized radiation patterns of the HGRMPA at 4.8 GHz, 4.9 GHz, and 5.0 GHz are presented in Fig. 4.5, Fig. 4.6, and Fig. 4.7, respectively. From these patterns, it can be observed that the patterns are constant throughout the bandwidth of the antenna with the high gain and high directivity.

Table 4.2: Main lobe direction and beamwidth at various frequencies

S./No.	Frequency (GHz)	Main lobe direction (phi = 0 deg plane) (in degrees)	Main lobe direction (phi = 90 deg plane) (in degrees)	3 dB Beamwidth (phi = 0 deg) (in degrees)	3 dB Beamwidth (phi = 90 deg) (in degrees)
1	4.80	1.0	0.0	88.6	83.9
2	4.85	1.0	0.0	89.4	84.3
3	4.90	1.0	0.0	90.0	84.4
4	4.95	1.0	0.0	90.4	84.5
5	5.00	1.0	0.0	90.6	84.4
6	5.05	1.0	0.0	90.8	84.4

The 3 dB beamwidth and the main lobe direction of the proposed HGRMPA are shown in Table 4.2. We can observe from Table 4.2 that the HGRMPA presents a good directional property in the entire bandwith. The main lobe directions in $phi = 0$ deg. plane and in $phi = 90$ deg. plane are at 1 degree and 0 degree, respectively. The maximum gain, maximum directivity, radiation efficiency, and total efficiency of the HGRMPA are shown in Table 4.3. From the Table 4.3, it can be observed that the HGRMPA provides the maximum gain and maximum directivity at the frequency of 4.8 GHz. The total efficiency and the radiation efficiency of the HGRMPA are shown in Fig. 4.8. The radiation efficiency and total efficiency of the HGRMPA at 4.8 GHz are -1.625 dB and -1.94 dB,
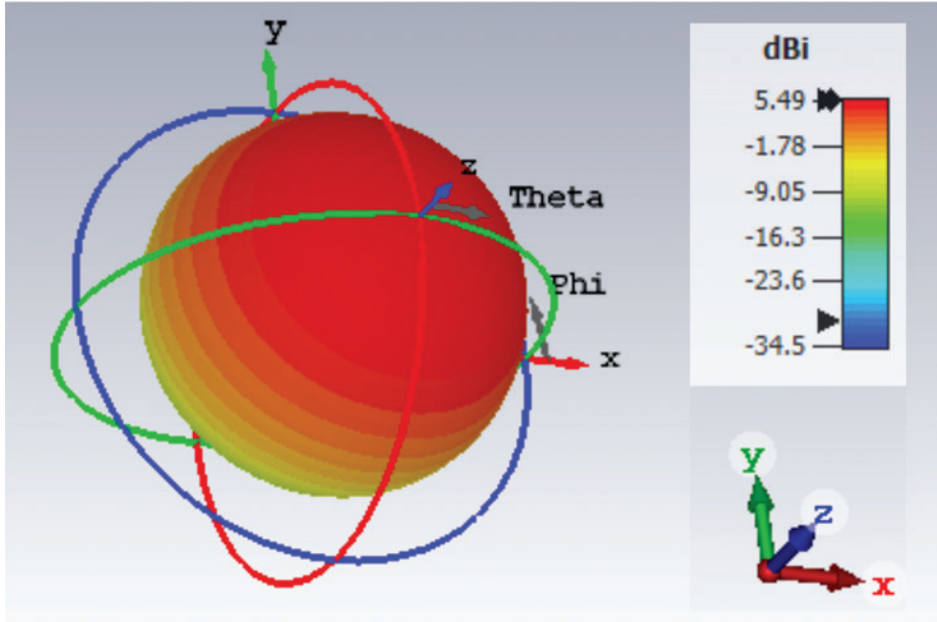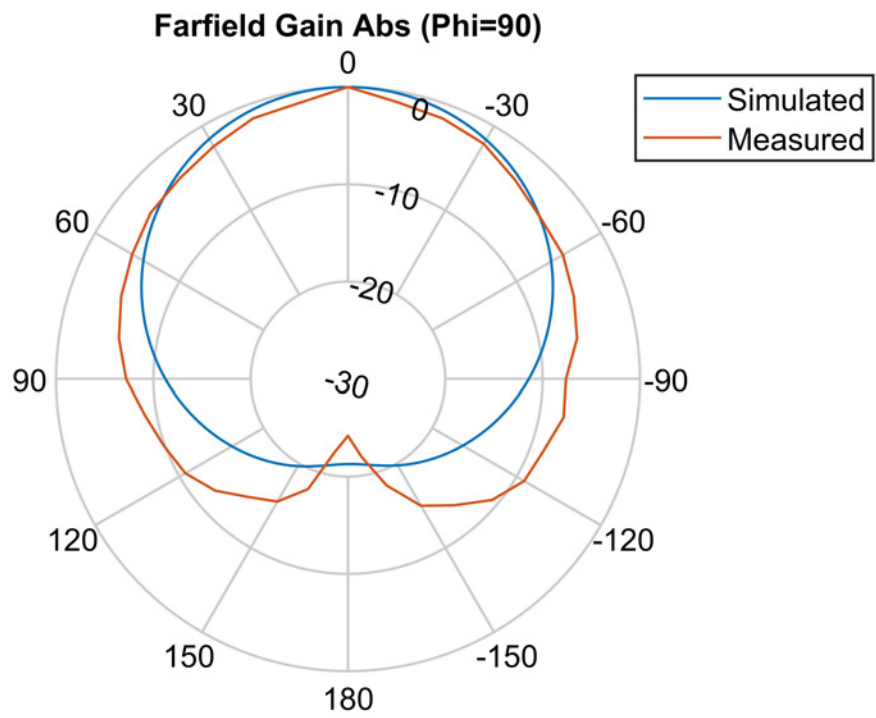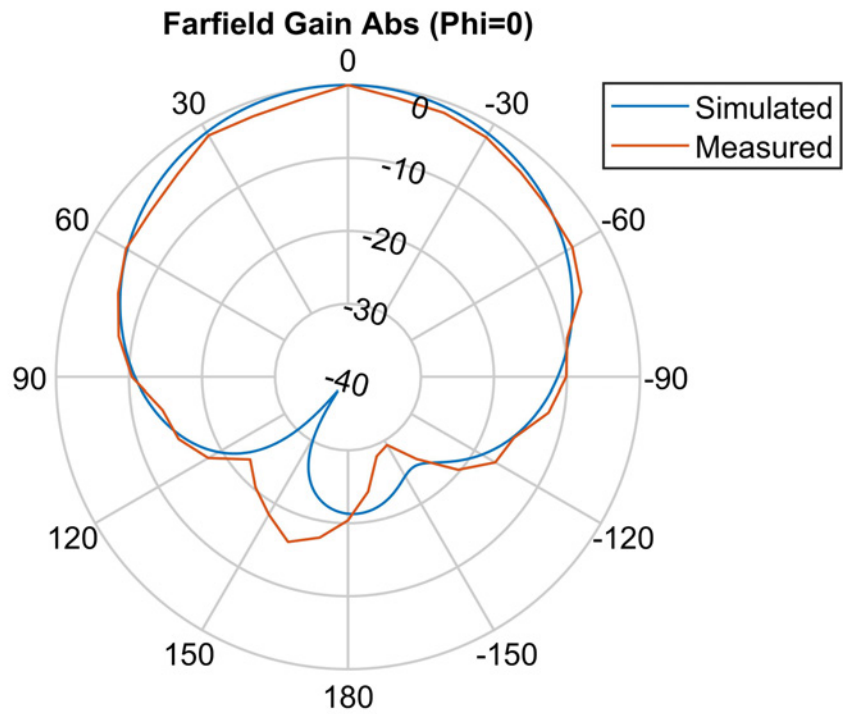
(a)
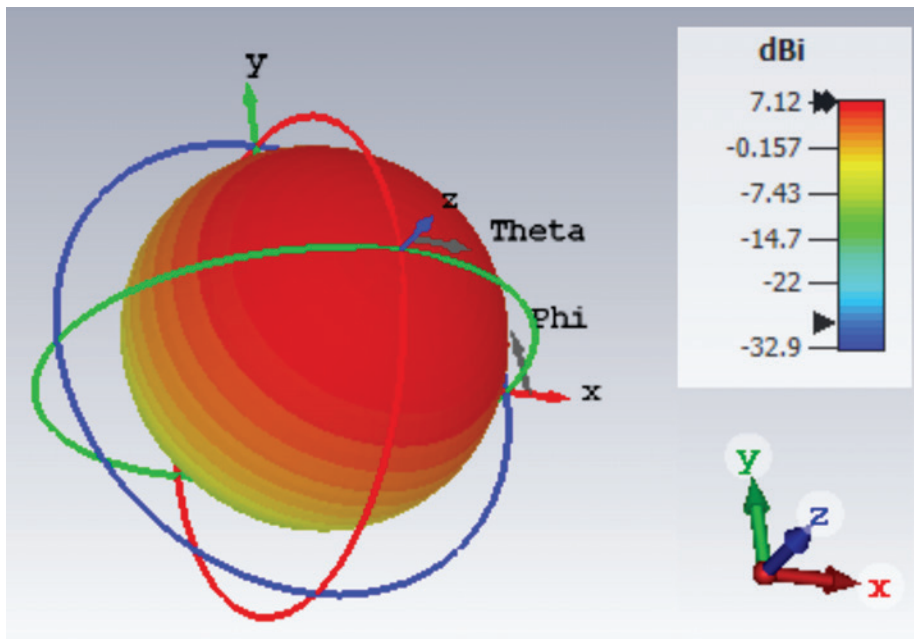
(b)

Figure 4.4: 3D patterns of HGRMPA (a) gain, (b) directivity
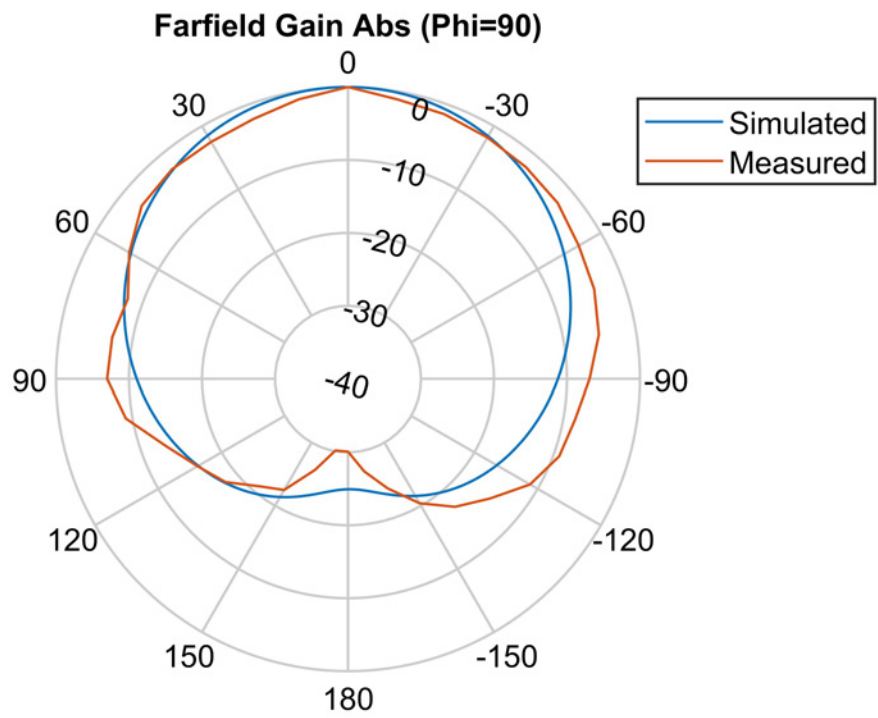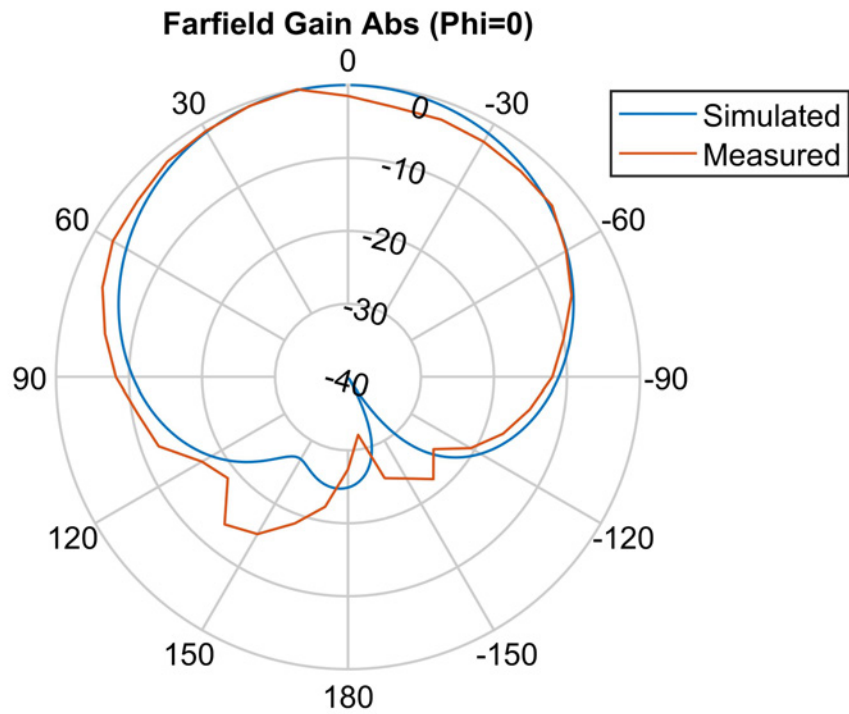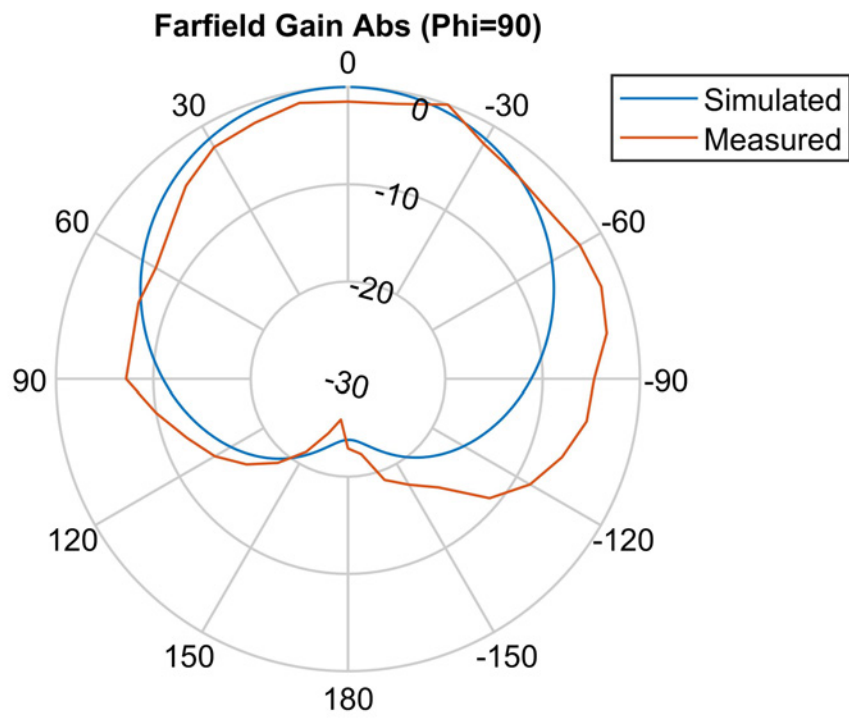
(a)

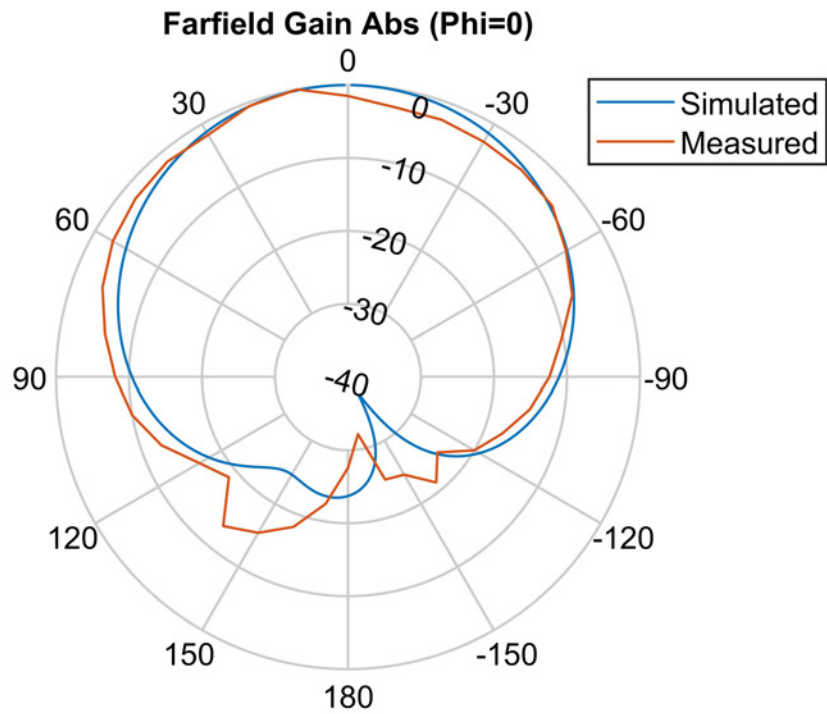(b)

Figure 4.5: Antenna normalized patterns at $4.8GHz$ (a) $Phi = 90$ deg. (b) $Phi = 0$ deg.

(a)

(b)

Figure 4.6: Antenna normalized patterns at $4.9GHz$ (a) $Phi = 90$ deg. (b) $Phi = 0$ deg.

Farfield Gain Abs (Phi=90)

(a)

Farfield Gain Abs (Phi=0)

(b)

Figure 4.7: Antenna normalized patterns at $5.0GHz$ (a) $Phi = 90$ deg. (b) $Phi = 0$ deg.

respectively. From the input and radiation characteristics of the proposed HGRMPA, it can be stated that the HGRMPA is suitable for sub-6 GHz 5G communications.

Table 4.3: Maximum gain, maximum directivity and efficiencies of the HGRMPA

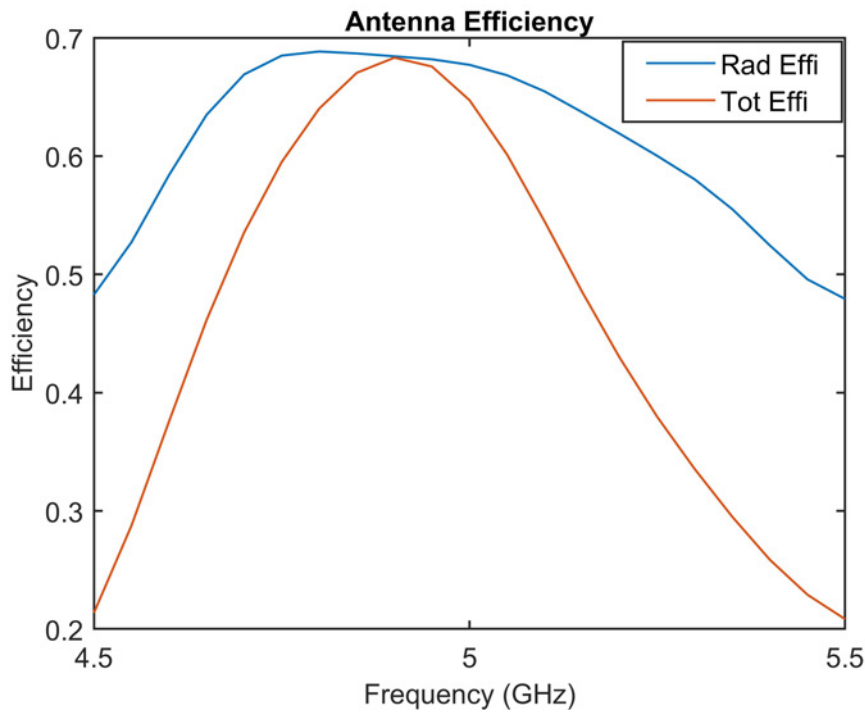| S./No.	Frequency (GHz)	Max. gain (dB)	Max. directivity (dB)	Total efficiency (dB)	Radiation efficiency (dB)
1	4.80	5.49	7.12	-1.94	-1.63
2	4.85	5.44	7.07	-1.74	-1.64
3	4.90	5.39	7.04	-1.66	-1.65
4	4.95	5.35	7.02	-1.70	-1.67
5	5.00	5.31	7.01	-1.89	-1.70
6	5.05	5.24	6.99	-2.21	-1.75

Figure 4.8: Radiation efficiency and total efficiency of the HGRMPA

4.5   Summary

In this chapter, the HGRMPA has been designed and developed. The antenna is simulated and optimized using the CST Studio Suite, which is a commercial EM tool software. The proposed HGRMPA has a maximum gain and maximum directivity of 5.49 dB and 7.12 dB, respectively. The HGRMPA has utilized the reflecting plane to improve the gain and directivity of the proposed HGRMPA significantly. Slots in the patch and GP has

improved the performance of the HGRMPA. The complete antenna is compact with the size of $28.03 \times 23.45 \times 5.35$ mm^3. The proposed HGRMPA is suitable for sub-6 GHz 5G applications.

Chapter 5

Design and Development of the HGWBMPA for Sub-6 GHz 5G Communications

5.1 Introduction

This chapter presents the design and development of the HGWBMPA. The proposed design utilizes the DGS to improve the gain and the bandwidth of the antenna. A slotted triangle plate is attached to the partial GP for achieving the wide bandwidth. A reflective plane is placed at the back of the antenna to improve the directional properties of the antenna. The HGWBMPA achieves a bandwidth of $4.9\ GHz$ to $5.8\ GHz$, which is quite considerable and makes the antenna suitable for $sub-6\ GHz$ $5G$ wireless applications. The gain and directivity of the proposed HGWBMPA are $6.21\ dB$ and $7.56\ dB$, respectively.

5.2 Design and Geometry of HGWBMPA

The geometry of the proposed HGWBMPA is shown in Fig. 5.1 (a) to (e). The top view, the ground plane, the side view, the back view, and the combined antenna are shown in Fig. 5.1 (a), Fig. 5.1 (b), Fig. 5.1 (c), Fig. 5.1 (d) and Fig. 5.1 (e), respectively. The proposed HGWBMPA design utilizes the transmission model approach. By applying equations (3.4) - (3.16) and optimizing using CST microwave studio, the dimensions of the

HGWBMPA are shown in Table 5.1. The HGWBMPA is intended to operate at 5.0 GHz frequency. After considering the importance of DGS in improving the performance of MPAs as given in literature, DGS is employed in the proposed HGWBMPA to improve the performance of the antenna. A MPA without DGS produces the narrow bandwidth. The gain of the antenna is improved by incorporating the triangle strip into the partial GP to improve the performance of the antenna. The inset feeding method is used to feed the HGWBMPA. Inset feeding is easy to match with the input impedance of 50Ω by adjusting the inset at the input and it is easy of fabricate. A reflective plate is placed at the back of the antenna in order to further enhance the gain of the antenna. The position of the reflector surface is optimized and the optimum radiation properties are obtained for the gap of 2 mm between the reflector surface and the GP of the antenna. The reflector plate serves as a reflector to reflect the radiation in back lobes and improves the radiation properties of the antenna. Table 5.1 shows the optimized dimensions of the HGWBMPA.

Table 5.1: Dimensions of the proposed HGWBMPA

| S. No.	Parameter	Dimension (mm)
1	Wg	28.03
2	Lg	23.45
3	Wp	18.43
4	Lp	13.85
5	h	1.6
6	Fi	5.2
7	Wf	3.04
8	Gpf	0.1
9	ag	2
10	a	5
11	b	10
12	c	4.5
13	d	5.6

5.3   Results and Discussion

The HGWBMPA is designed on the FR-4 substrate and simulated using the CST Studio Suite. The three MPAs i.e. the MPA without DGS and reflector surface, the MPA with DGS and without reflector surface, the MPA with DGS and the reflector plane are analyzed. The proposed MPA with the DGSs and reflector surface achieves better
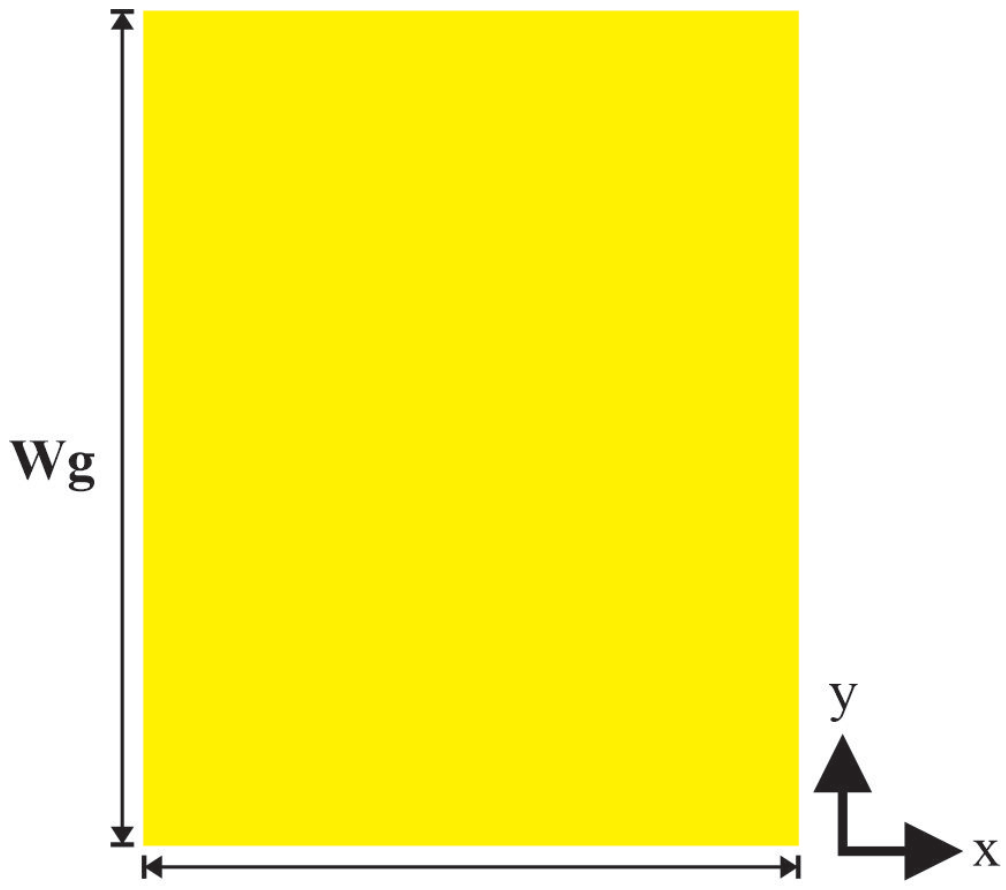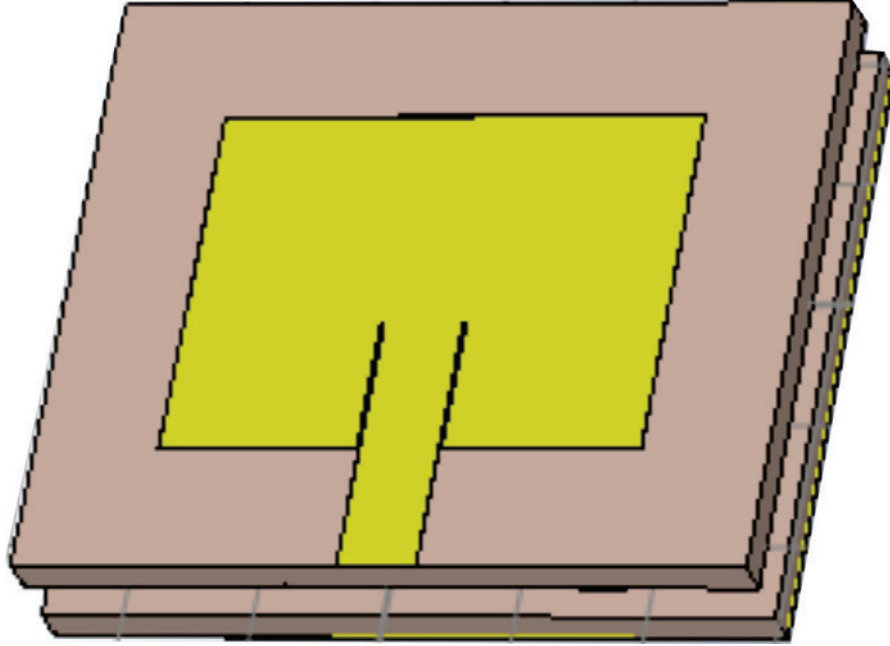
(a)

(b)

(c)
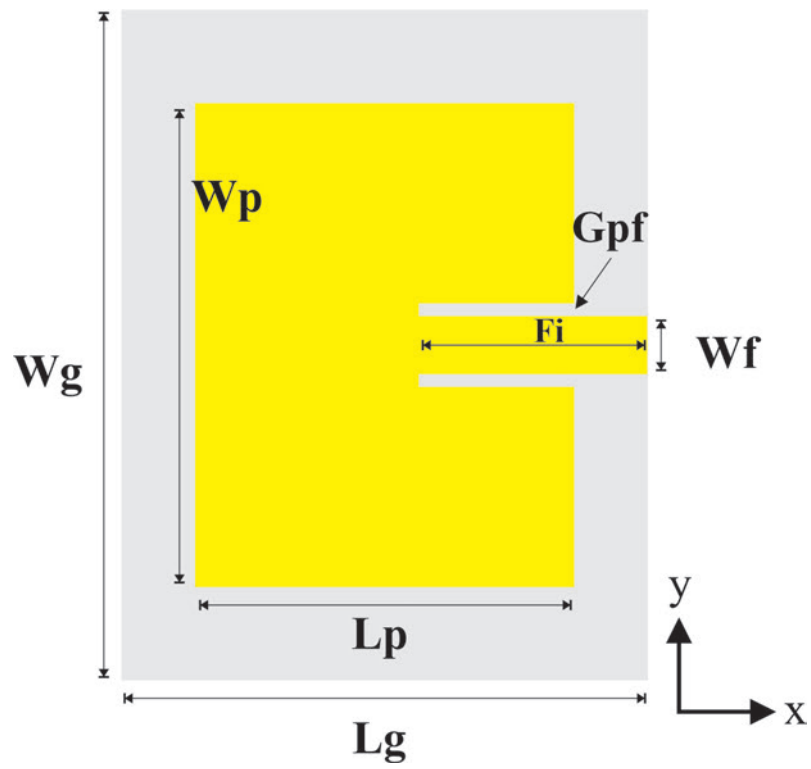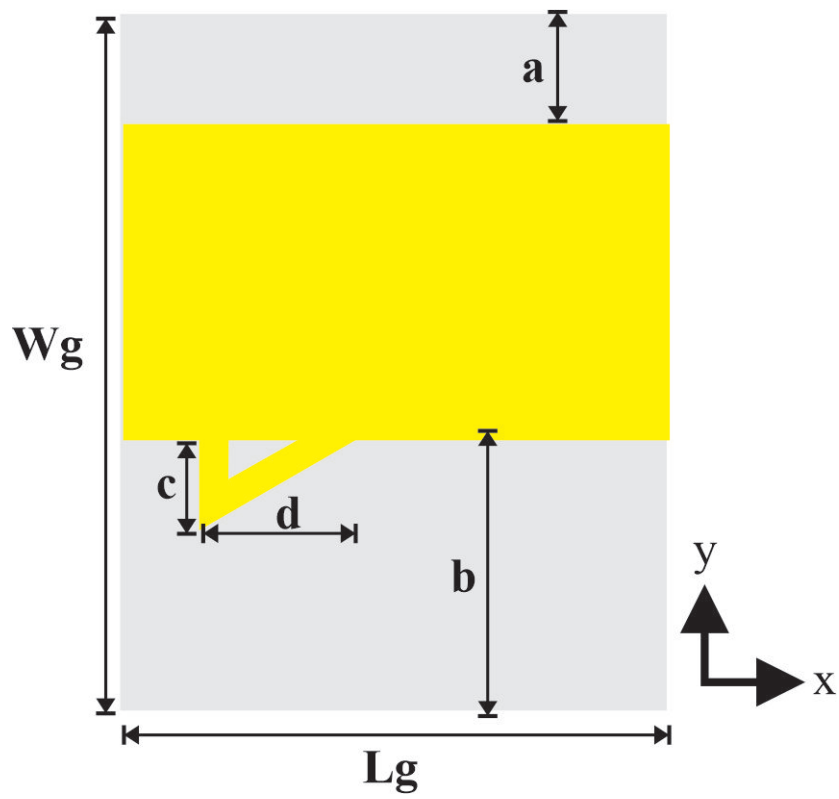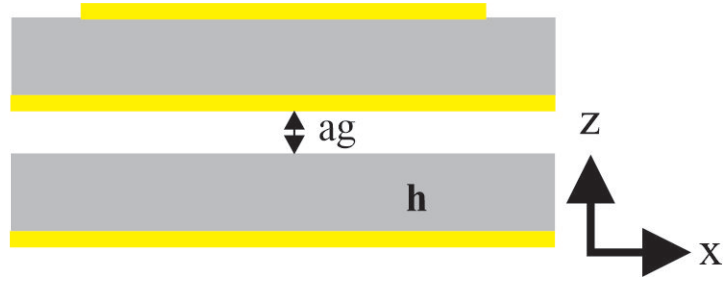
(d)

(e)

Figure 5.1: Antenna geometry of HGWBMPA, (a) top view, (b) ground plane (c) side view (d) back view (e) combined antenna

radiation properties when compared to the MPA without DGS and reflector surface, and the MPA with DGS only. Table 5.1 shows the optimized dimensions of the HGWBMPA. Fig. 5.2 (a) shows the reflection coefficient of the three different configurations. The MPA without DGS and reflector surface, the MPA with DGS and without reflector surface, the MPA with DGS and the reflector plane have the reflection coefficient of $-36\ dB$, $-26\ dB$ and $-18\ dB$, respectively. The MPA with DGS and the reflector plane also achieves the wide bandwidth from $4.921\ GHz$ to $5.784\ GHz$. Fig. 5.2 (b) shows the VSWR of the MPA without DGS and reflector surface, the MPA with DGS and without reflector surface, the MPA with DGS and the reflector plane.

Fig. 5.3 (a) and Fig. 5.3(b) show the 3D gain pattern and 3D directivity pattern of the HGWBMPA, respectively. The HGWBMPA has the maximum gain and maximum directivity of $6.21\ dB$ and $7.56\ dB$, respectively. This shows that the HGWBMPA has the high gain at the specified frequency of operation.

Fig. 5.4 (a) and Fig. 5.4 (b) show the normalised patterns of the the MPA without DGS and reflector surface, the MPA with DGS and without reflector surface, the MPA with DGS and the reflector plane at $4.8\ GHz$ in $phi = 90$ deg. plane and $phi = 0$ deg. plane, respectively. Fig. 5.5 (a) and Fig. 5.5 (b) present the normalised patterns of the MPA without DGS and reflector surface, the MPA with DGS and without reflector
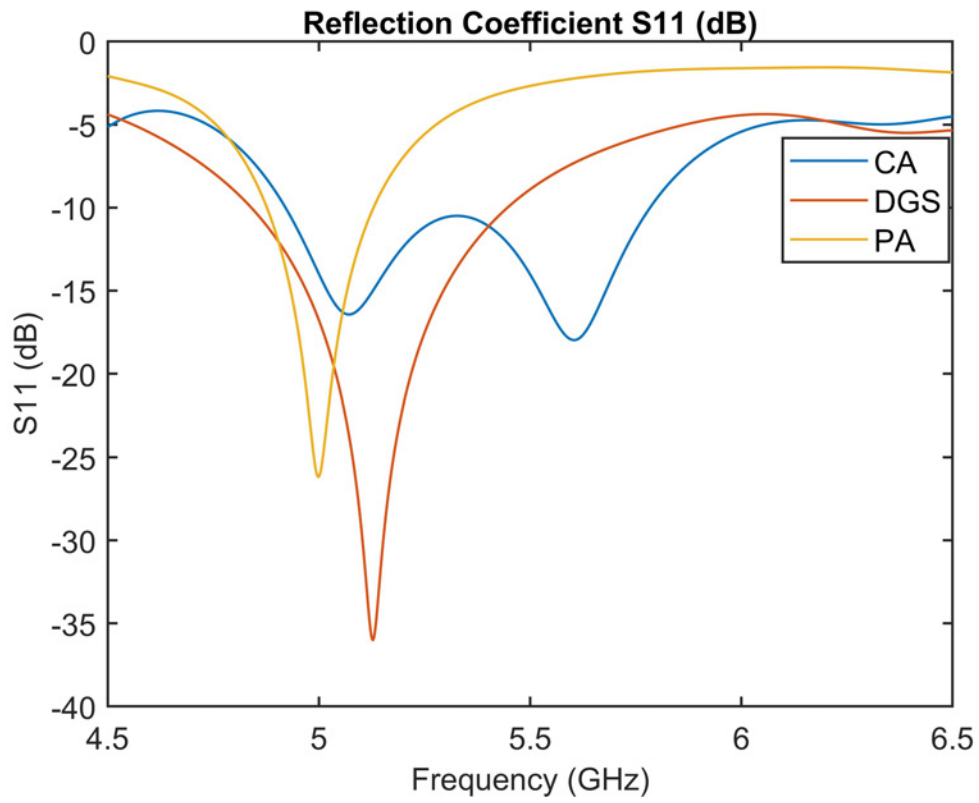
(a)
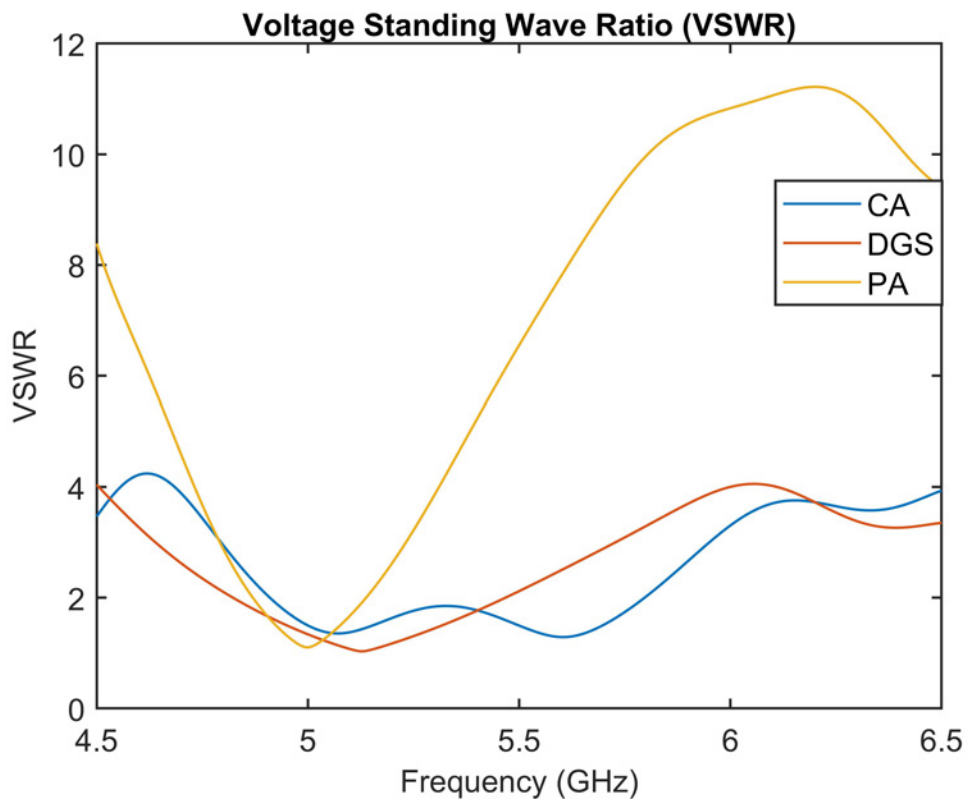
(b)

Figure 5.2: (a) reflection coefficient, (b) Voltage standing wave ratio

surface, the MPA with DGS and the reflector plane at 5.4 GHz in $phi = 90$ deg. plane and $phi = 0$ deg. plane, respectively. Fig. 5.6 (a) and Fig. 5.6 (b) show the normalised patterns at 5.8 GHz in $phi = 90$ deg. plane and $phi = 0$ deg. plane, respectively.
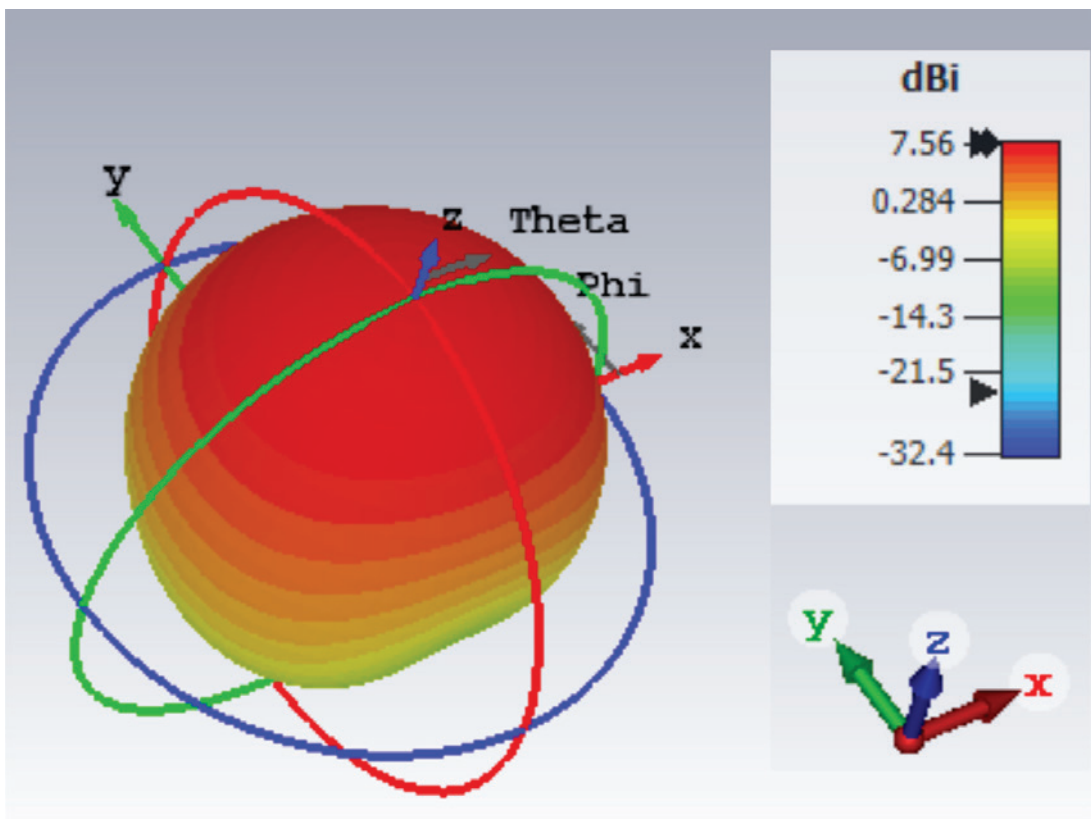
Fig. 5.7 (a) shows the gain of the MPA without DGS and reflector surface, the MPA with DGS and without reflector surface, the MPA with DGS and the reflector plane for the frequency range from 4.8 GHz to 5.8 GHz. The MPA with the DGS and reflector surface has the highest gain over the entire frequency range. Fig. 5.7 (b) shows the total efficiency of the MPA without DGS and reflector surface, the MPA with DGS and without reflector surface, the MPA with DGS and the reflector plane for the frequency range from 4.8 GHz to 5.8 GHz. The MPA with DGS and reflector plane has the highest total efficiency as compared to the MPA without DGS and reflector surface, and the MPA with DGS and without reflector surface. The efficiency of the MPA with DGS only seems good but for a narrow bandwidth when compared to the MPA with DGS and reflector plane.

Fig. 5.8 (a) shows the radiation efficiency of the three configurations. The MPA with the DGS and the reflector plane produces the good results due to minimum losses in side lobes and back lobes. Table 5.2 summarizes the main lobe direction and 3 dB beamwidth of the MPA without DGS and reflector surface, the MPA with DGS and without reflector surface, the MPA with DGS and the reflector plane at various frequencies in the frequency range from 4.8 GHz to 5.8 GHz. The 3 dB beamwidth for the antennas in $phi = 0$ plane shows that the three configurations show good 3 dB beamwidth close to 90 degrees. The 3 dB beamwidth in $phi = 90$ plane shows that the CA configuration has a good directional property close to 90 degree. Table 5.3 shows the maximum gain, maximum directivity, and the efficiency of the three configurations. From the results, it can be observed that the proposed HGWBMPA is suitable for the sub-6 GHz 5G communication band.

The fabricated HGWBMPA is presented in Fig. 5.9. The Fig. 5.10 (a) presents the simulated and measured reflection coefficient of the HGBWMPA. This figure shows that the minimum values of measured S11 and simulated S11 are -26 dB and -19 dB, respectively. The Fig. 5.10 (b) presents the voltage standing wave ratio of the HGWBMPA. The minimum values of simulated and measured VSWR are 1.11 and 1.29, respectively. The normalized patterns of the HGWBMPA at 4.8 GHz in $Phi = 90$ deg. plane and $Phi = 0$ deg. plane are presented in Fig. 5.11 (a) and Fig. 5.11 (b), respectively. The normalized
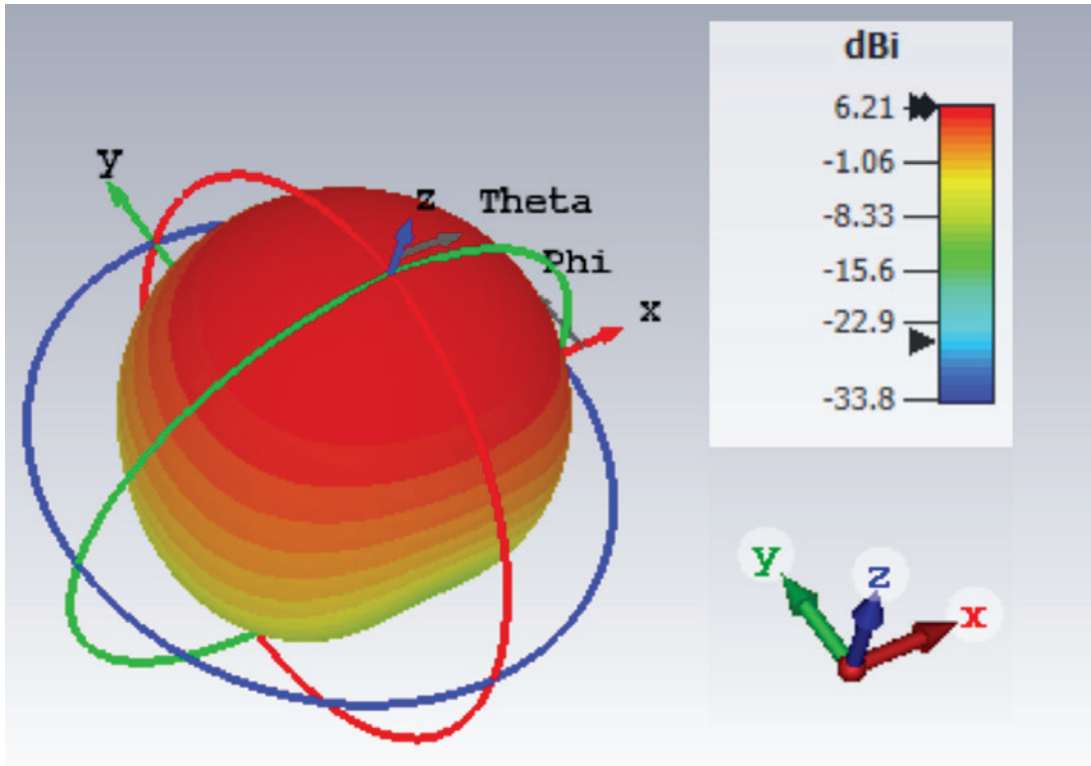
(a)

(b)

Figure 5.3: 3D Patterns of the HGWBMPA, (a) gain, (b) directivity
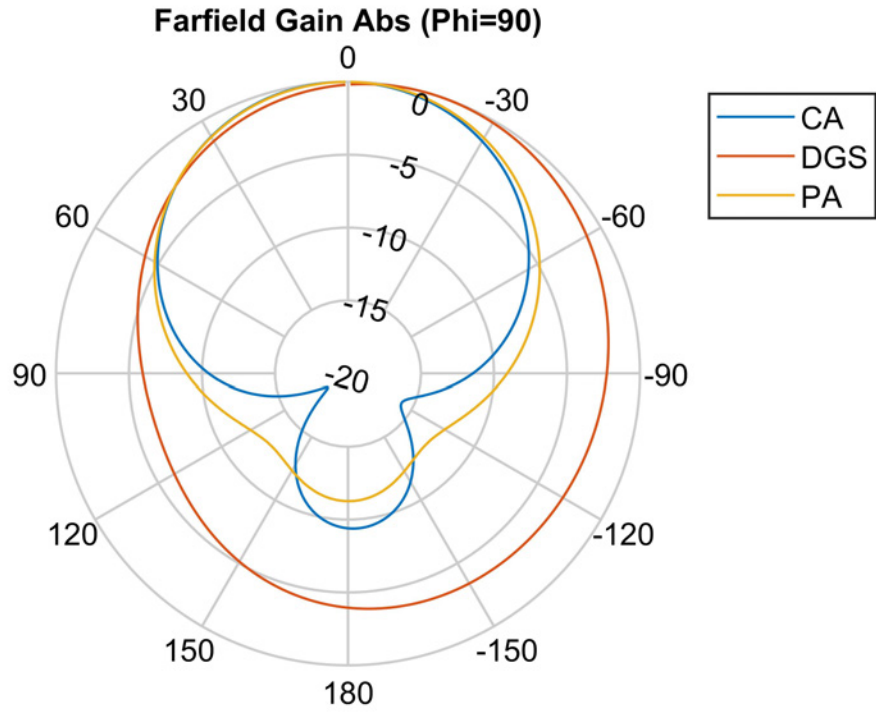
(a)
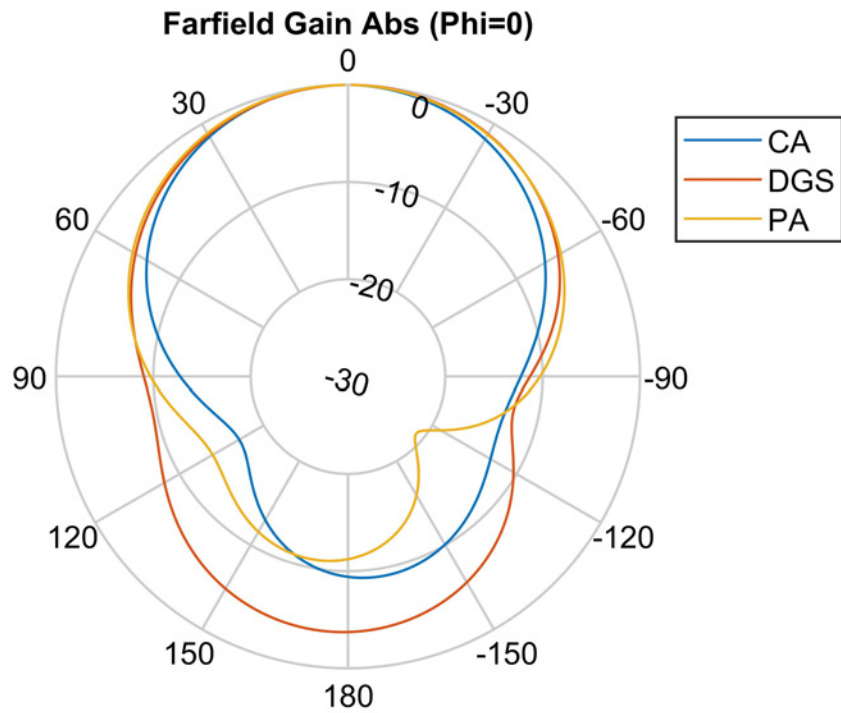
(b)

Figure 5.4: Normalized patterns of the MPA without DGS and reflector surface-PA, the MPA with DGS and without reflector surface-DGS, the MPA with DGS and the reflector plane-CA at 4.8 GHz, (a) $Phi = 90$ deg. plane, (b) $Phi = 0$ deg. plane

(a)

(b)

Figure 5.5: Normalized patterns of the MPA without DGS and reflector surface-PA, the MPA with DGS and without reflector surface-DGS, the MPA with DGS and the reflector plane-CA at 5.4 GHz (a) $Phi = 90$ deg. plane, (b) $Phi = 0$ deg. plane

(a)

(b)

Figure 5.6: Normalized patterns of the MPA without DGS and reflector surface-PA, the MPA with DGS and without reflector surface-DGS, the MPA with DGS and the reflector plane-CA at 5.8 GHz (a) $Phi = 90$ deg. plane, (b) $Phi = 0$ deg. plane

(a)

(b)

Figure 5.7: Gain and total efficiency of the MPA without DGS and reflector surface-PA, the MPA with DGS and without reflector surface-DGS, the MPA with DGS and the reflector plane-CA, (a) gain, (b) total efficiency

Figure 5.8: Radiation efficiency of the MPA without DGS and reflector surface-PA, the MPA with DGS and without reflector surface-DGS, the MPA with DGS and the reflector plane-CA

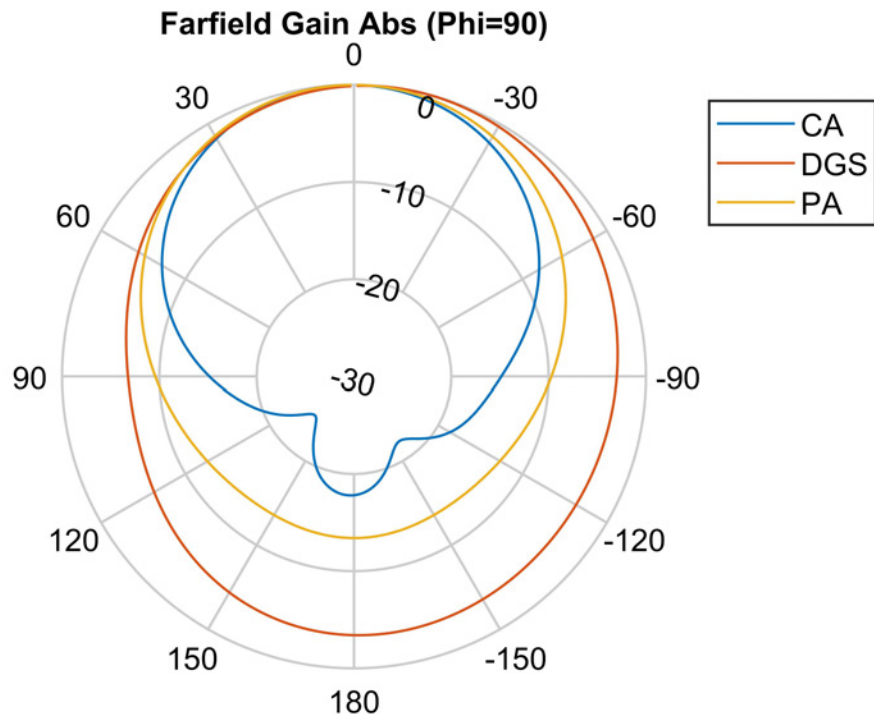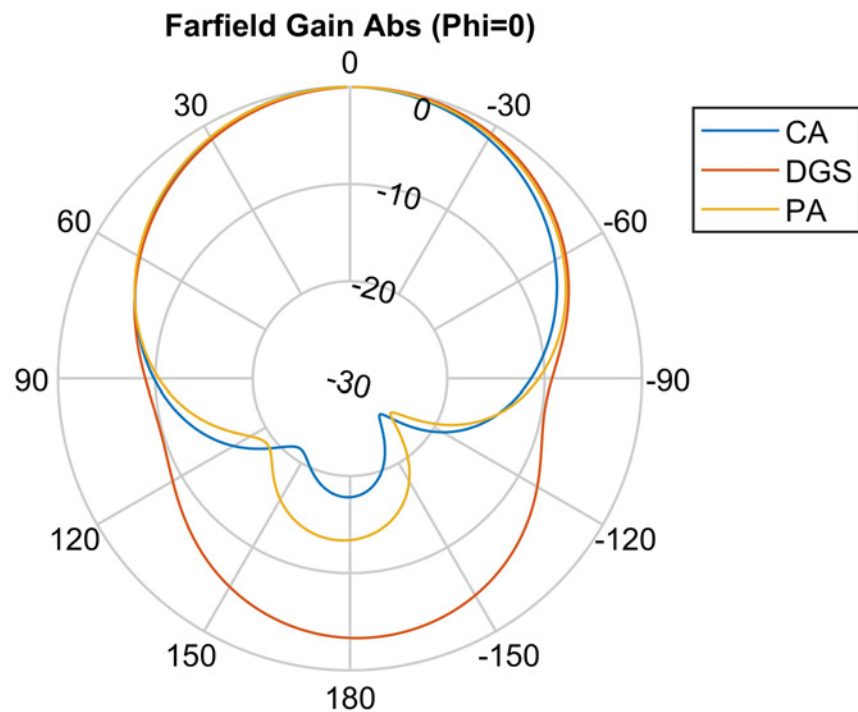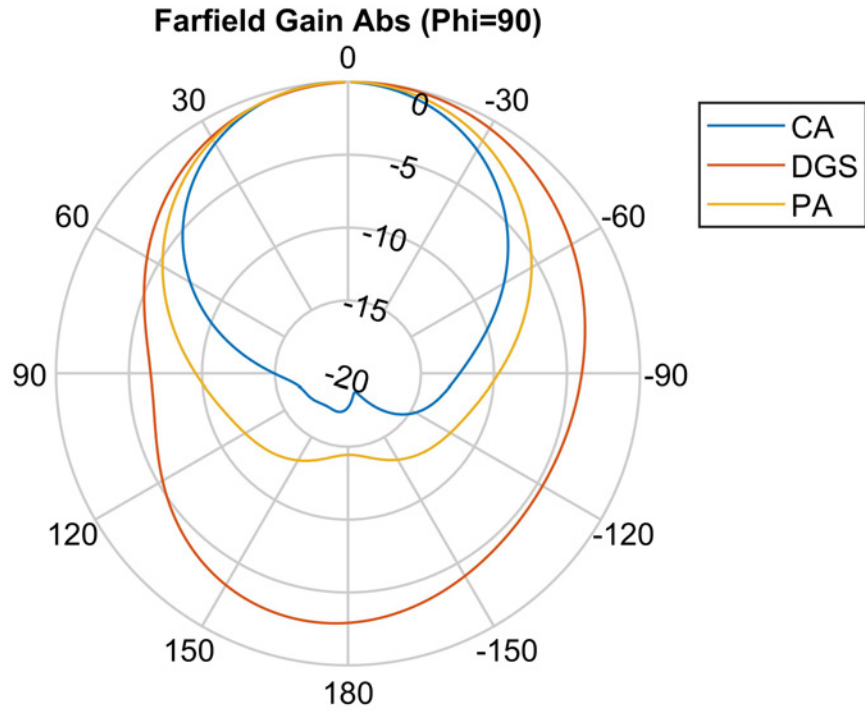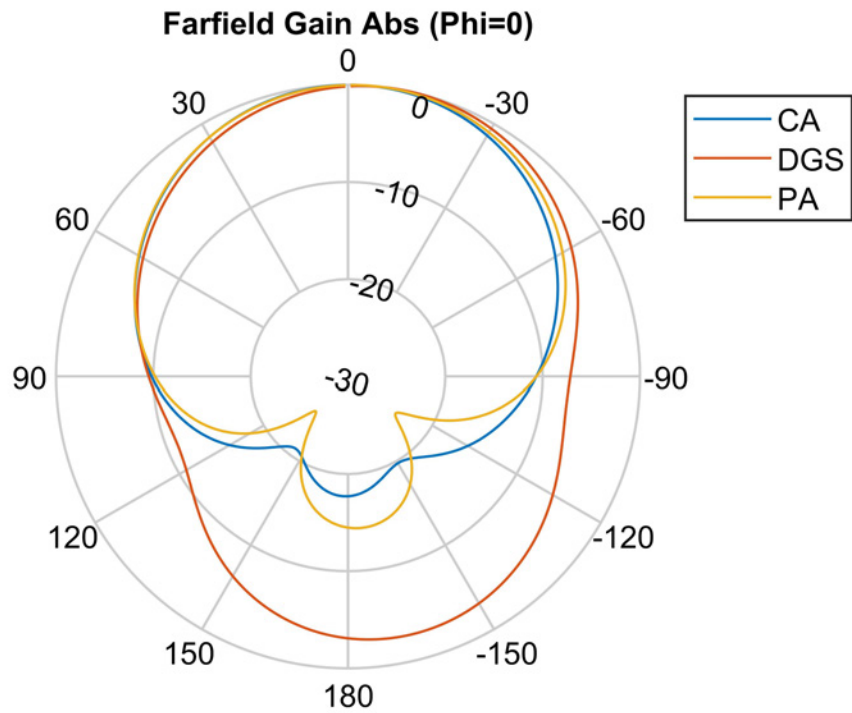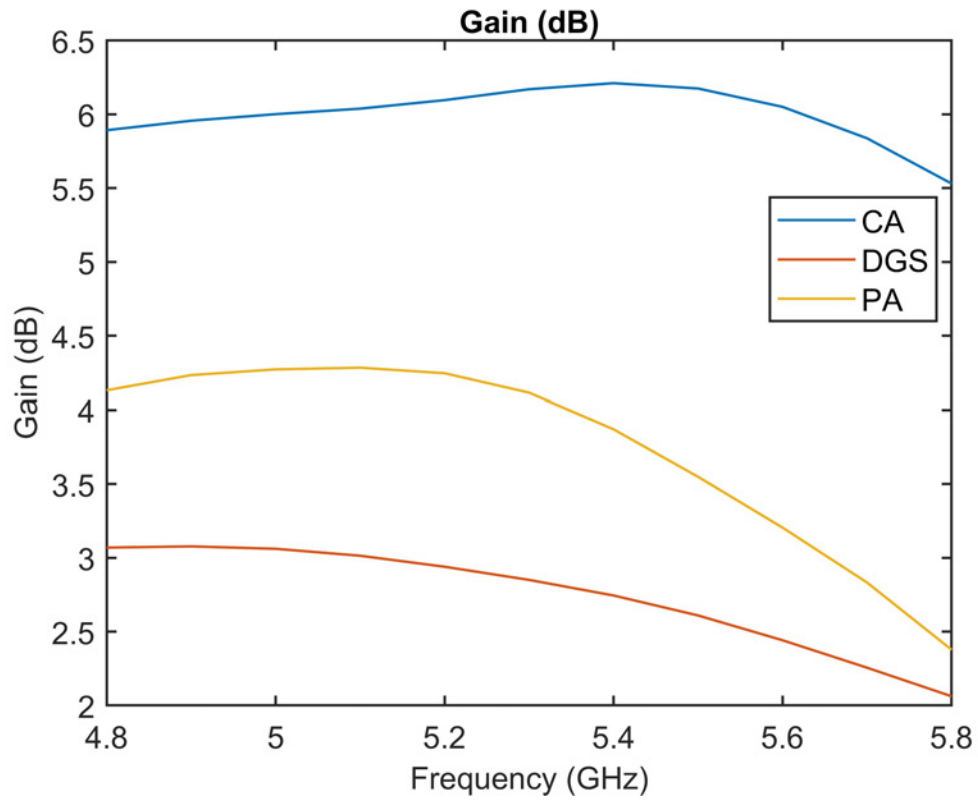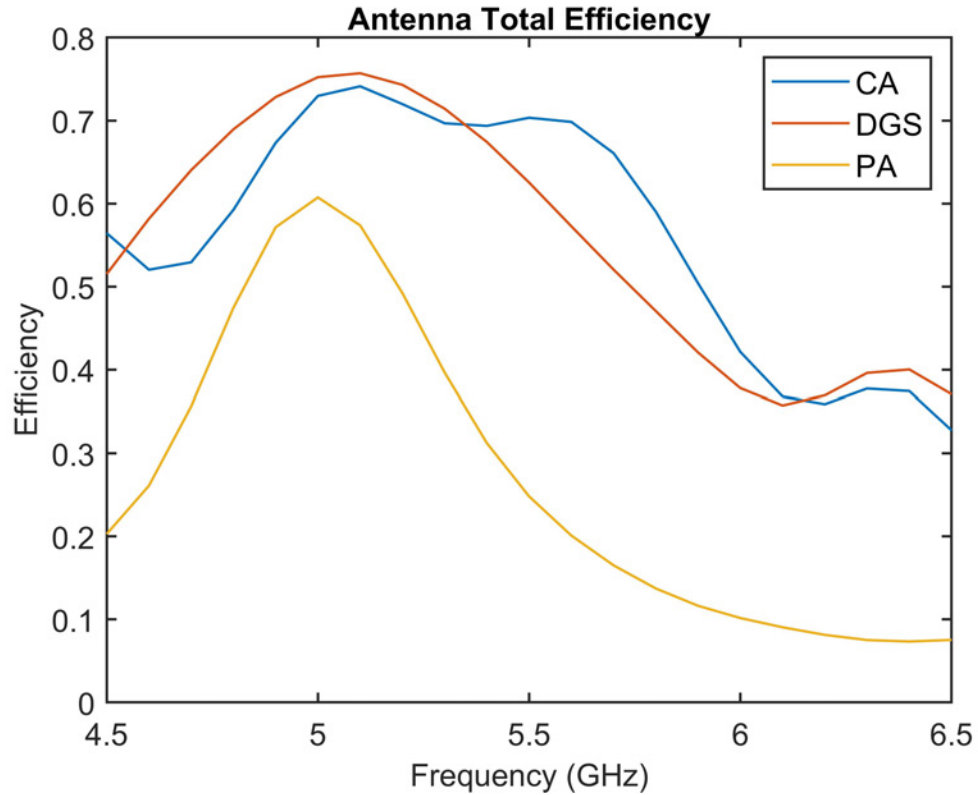Table 5.2: Main lobe direction and beamwidth of the MPA without DGS and reflector surface-PA, the MPA with DGS and without reflector surface-DGS, the MPA with DGS and the reflector plane-CA

Frequency (GHz)	Main lobe direction ($phi = 0$ deg plane) (in degrees)			Main lobe direction ($phi = 90$ deg plane) (in degrees)			3 dB beamwidth ($phi = 0$ deg) (in degrees)			3 dB beamwidth ($phi = 90$ deg) (in degrees)		
	CA	DGS	PA	CA	DGS	PA	CA	DGS	PA	CA	DGS	PA
4.8	1.0	2.0	0.0	1.0	16.0	0.0	80.8	93.0	96.0	88.3	167.8	92.5
4.9	1.0	2.0	0.0	1.0	15.0	0.0	82.7	93.0	95.6	87.3	161.7	91.6
5.0	0.0	2.0	0.0	1.0	15.0	0.0	84.5	93.1	95.1	85.3	155.9	90.7
5.1	0.0	3.0	0.0	1.0	14.0	0.0	86.0	93.1	94.7	82.6	150.0	89.8
5.2	0.0	3.0	1.0	1.0	13.0	0.0	87.2	93.2	94.4	79.4	144.6	89.0
5.3	0.0	4.0	1.0	2.0	12.0	0.0	87.8	93.4	94.0	76.3	139.9	88.2
5.4	0.0	5.0	2.0	1.0	11.0	0.0	87.9	93.5	93.8	74.0	135.8	87.5
5.5	0.0	6.0	2.0	1.0	10.0	0.0	87.6	93.5	93.5	72.8	131.7	86.9
5.6	1.0	8.0	3.0	1.0	9.0	0.0	87.3	93.7	93.3	72.4	127.7	86.3
5.7	1.0	9.0	3.0	1.0	7.0	0.0	87.1	93.8	93.1	72.5	124.0	86.0
5.8	2.0	11.0	4.0	2.0	5.0	0.0	87.2	94.0	93.0	73.0	120.4	86.0

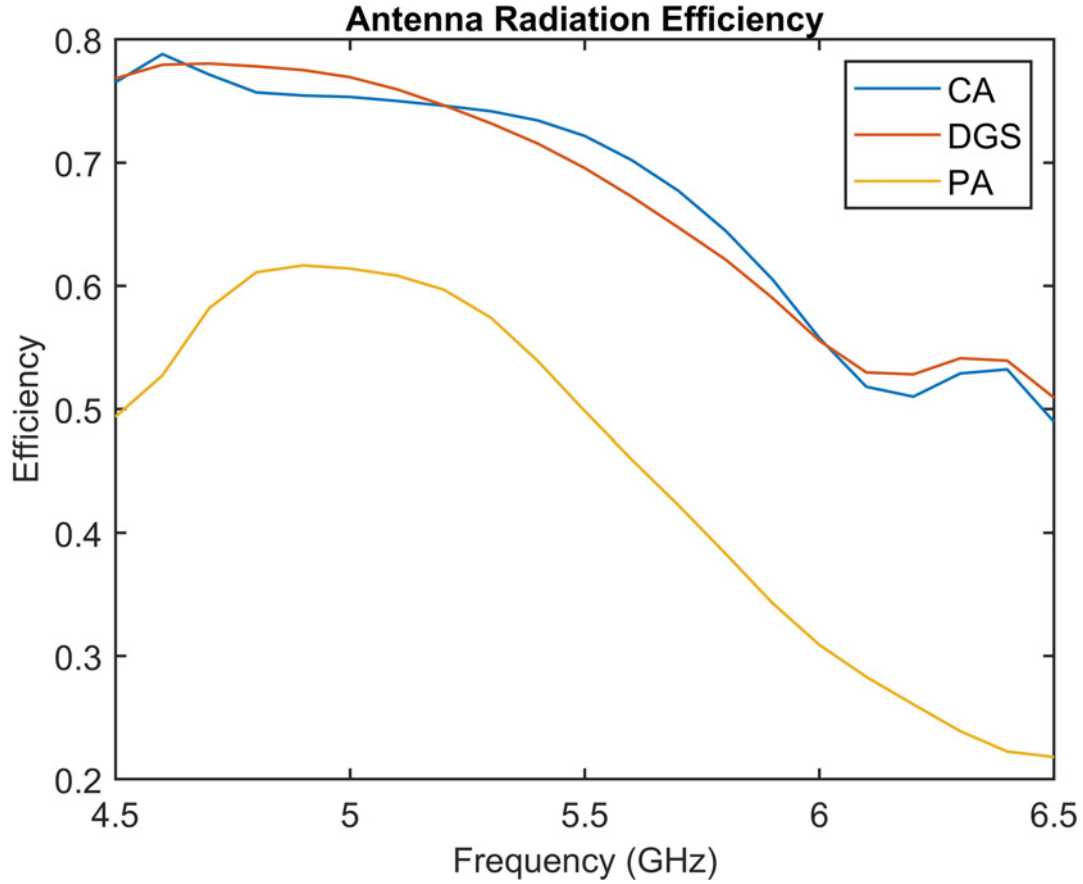Table 5.3: Maximum gain, maximum directivity and efficiencies of the MPA without DGS and reflector surface-PA, the MPA with DGS and without reflector surface-DGS, the MPA with DGS and the reflector plane-CA

Frequency (GHz)	Max. Gain (dB)			Max. Directivity (dB)			Total Efficiency (dB)			Radiation Efficiency (dB)		
	CA	DGS	PA	CA	DGS	PA	CA	DGS	PA	CA	DGS	PA
4.8	5.89	3.07	4.13	7.08	4.16	6.28	-2.25	-1.62	-3.24	-1.18	-1.09	-2.15
4.9	5.96	3.08	4.23	7.16	4.19	6.34	-1.70	-1.38	-2.43	-1.21	-1.11	-2.10
5.0	6.00	3.06	4.27	7.22	4.21	6.39	-1.36	-1.24	-2.17	-1.22	-1.14	-2.12
5.1	6.04	3.01	4.28	7.28	4.21	6.45	-1.30	-1.21	-2.42	-1.25	-1.20	-2.16
5.2	6.10	2.94	4.25	7.37	4.21	6.50	-1.43	-1.29	-3.08	-1.27	-1.27	-2.25
5.3	6.17	2.85	4.12	7.47	4.21	6.53	-1.57	-1.46	-4.02	-1.30	-1.36	-2.41
5.4	6.21	2.75	3.87	7.56	4.20	6.56	-1.60	-1.71	-5.06	-1.35	-1.46	-2.69
5.5	6.18	2.61	3.55	7.60	4.18	6.57	-1.53	-2.04	-6.05	-1.42	-1.58	-3.03
5.6	6.05	2.44	3.20	7.59	4.17	6.58	-1.56	-2.42	-6.97	-1.54	-1.72	-3.38
5.7	5.84	2.26	2.83	7.53	4.15	6.58	-1.80	-2.84	-7.82	-1.69	-1.89	-3.75
5.8	5.31	2.06	2.38	7.44	4.13	6.54	-2.29	-3.27	-8.63	-1.91	-2.07	-4.17

patterns of the HGWBMPA at 5.4 GHz in $Phi = 90$ deg. plane and $Phi = 0$ deg. plane are presented in Fig. 5.12 (a) and Fig. 5.12 (b), respectively. The normalized patterns of the HGWBMPA at 5.8 GHz in $Phi = 90$ deg. plane and $Phi = 0$ deg. plane are presented in Fig. 5.13 (a) and Fig. 5.13 (b), respectively. The simulated and measured patterns show good agreement. The Table 5.4 shows the comparison of the proposed HGWBMPA with the other antennas in literature. This table shows that the proposed HGWBMPA is compact in size and provides wide bandwidth and high gain. From the antenna characteristics, it can be observed that the proposed HGWBMPA is suitable for sub-6 GHz 5G wireless applications.

Table 5.4: Comparison of the HGWBMPA with the existing antennas in literature

Reference	Patch Size (mm^2)	Bandwidth (MHz)	Maximum Gain (dB)
[6]	38 × 22	200	4.61
[11]	40 × 40	400	4.91
[40]	35 × 40	100	7.43
[84]	29.50 × 33	170	4.46
[88]	38 × 22	360	2.24
[93]	38 × 16	700	2.5
Proposed	18.43 × 13.85	863	6.21
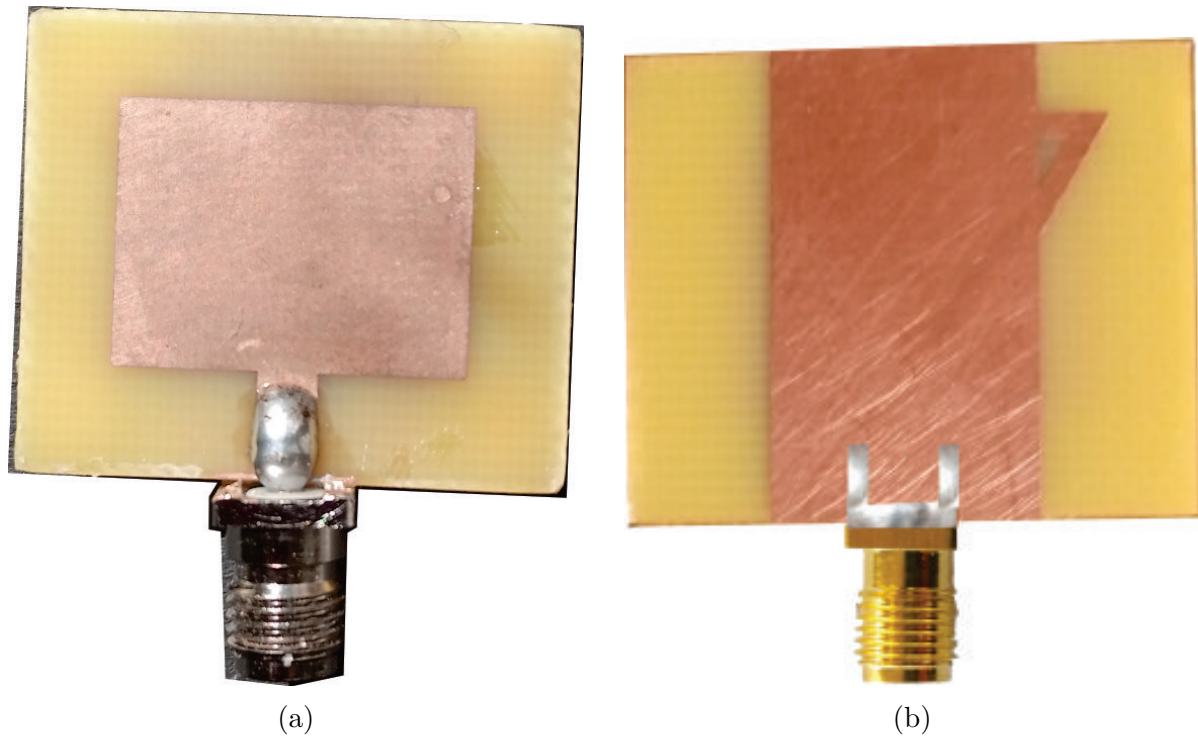
Figure 5.9: Fabricated HGWBMPA, (a) top view, (b) back view.

5.4 Summary

In this chapter, the design and development of the HGWBMPA for sub-6 GHz 5G applications have been presented. The presented HGWBMPA utilizes the triangular slot in the partial ground plane along with a reflector surface. The antenna is simulated and optimized using the commercial EM tool i.e. CST Studio Suite. The antenna provides the maximum gain and maximum directivity of 6.21 dB and 7.29 dB, respectively. The presented compact high gain HGWBMPA is suitable sub-6GHz 5G wideband applications.
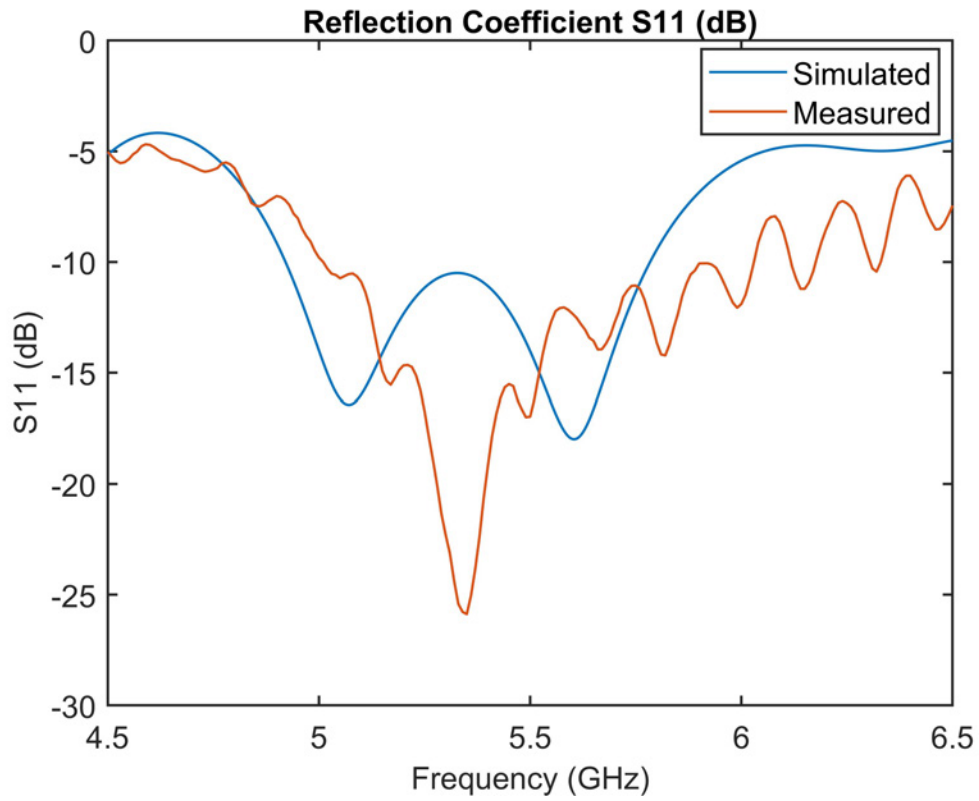
(a)
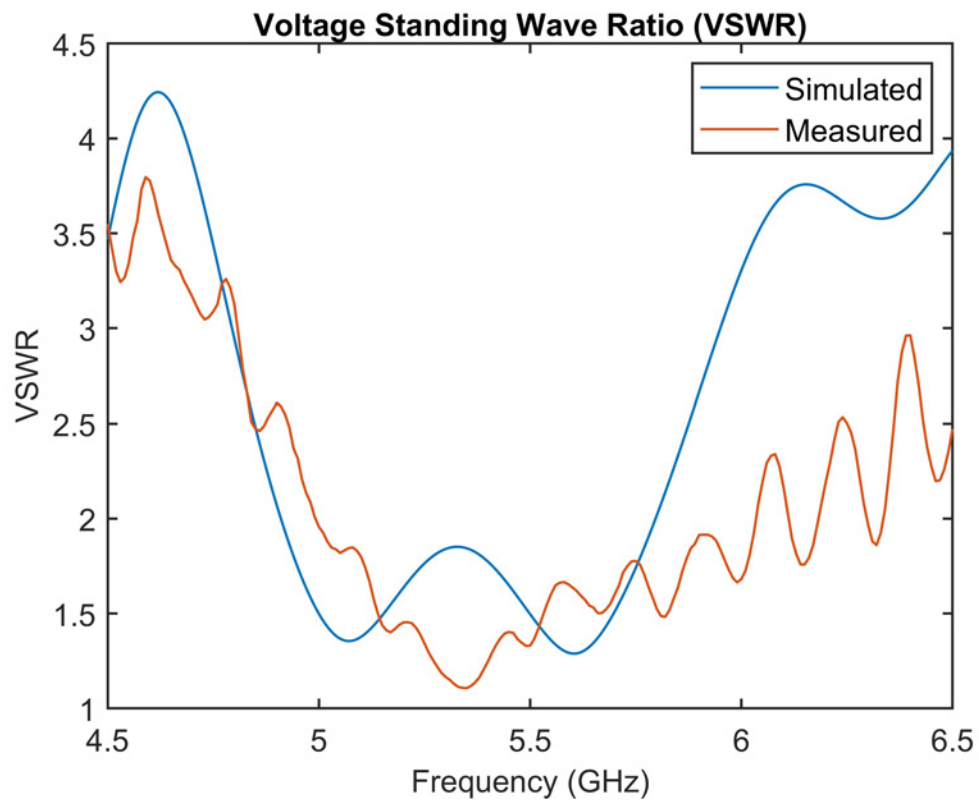
(b)

Figure 5.10: Reflection coefficient and VSWR of the HGWBMPA, (a) reflection coefficient (S11), (b) VSWR
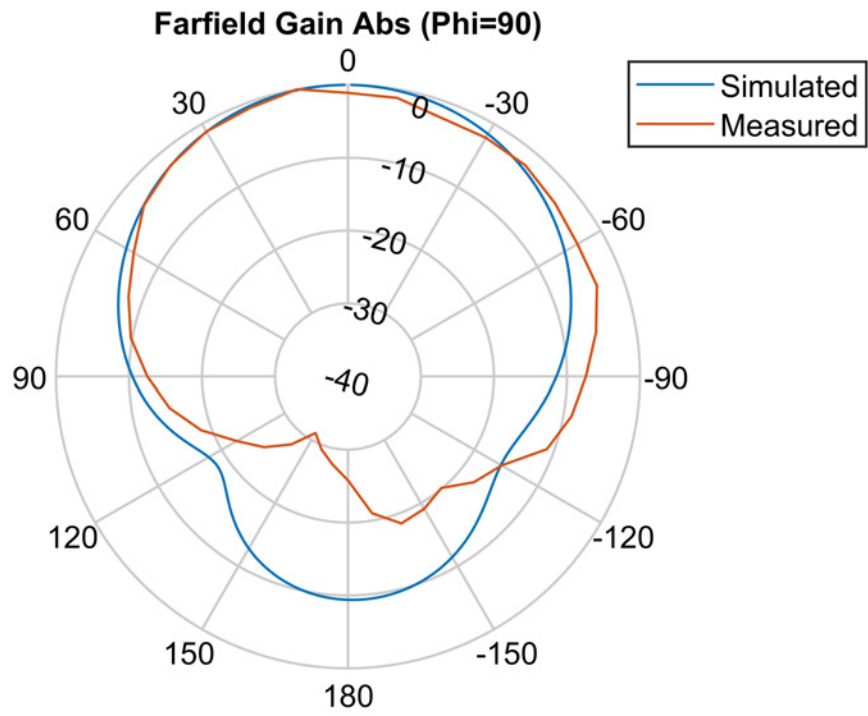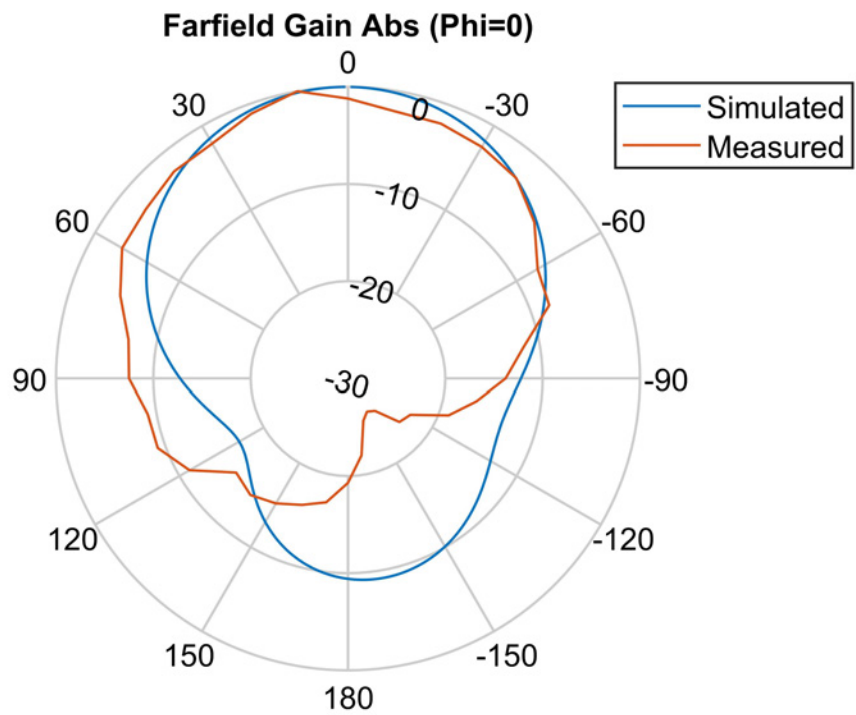
Figure 5.11: Radiation patterns of the HGWBMPA at 4.8 GHz, (a) $Phi = 90$ deg. plane, (b) $Phi = 0$ deg. plane

Figure 5.12: Radiation patterns of the HGWBMPA at 5.4 GHz, (a) $Phi = 90$ deg. plane, (b) $Phi = 0$ deg. plane

Farfield Gain Abs (Phi=90)

(a)

Farfield Gain Abs (Phi=0)
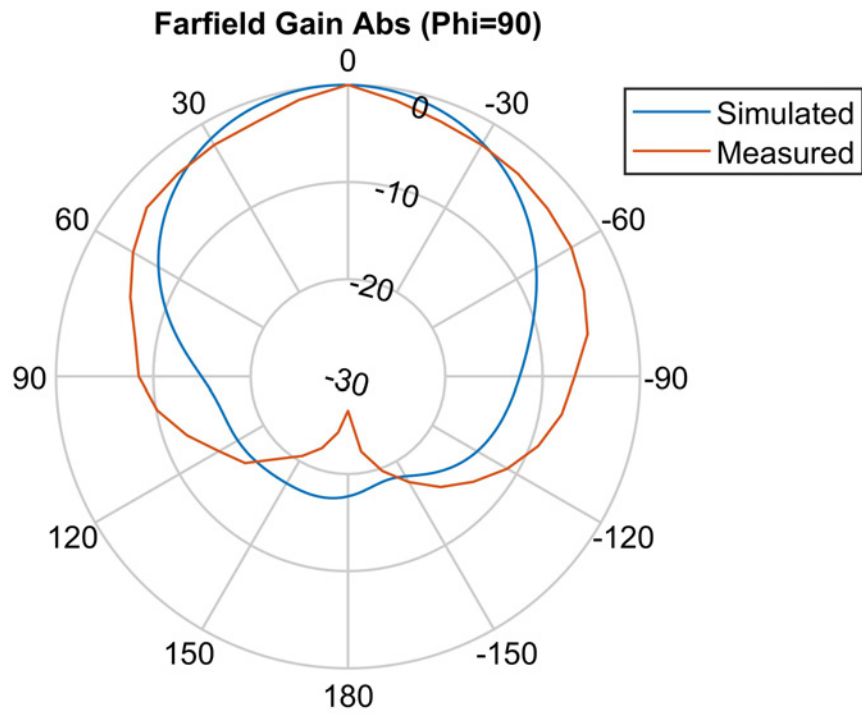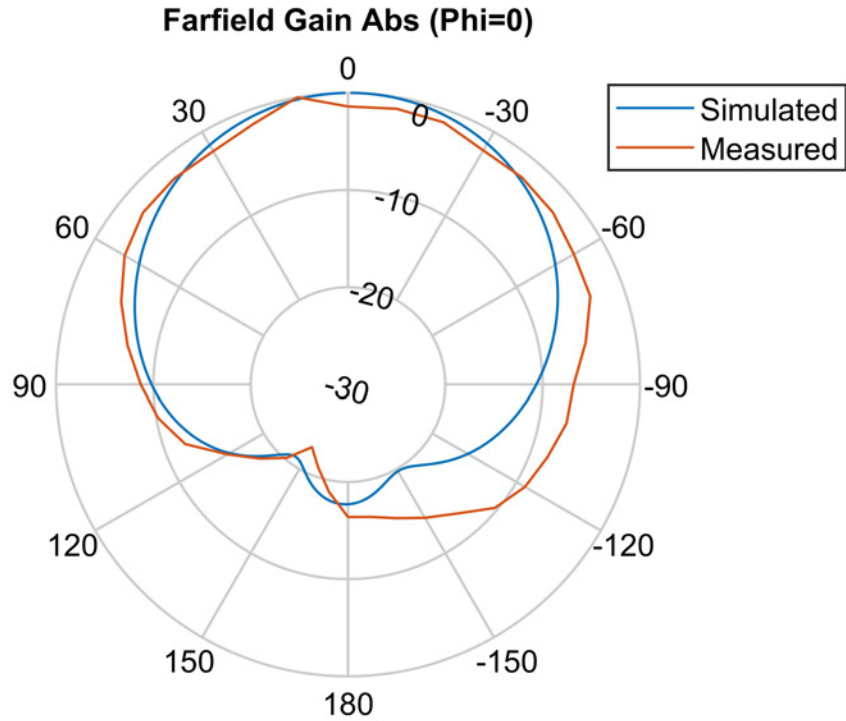
(b)

Figure 5.13: Radiation patterns of the HGWBMPA at 5.8 GHz, (a) $Phi = 90$ deg. plane, (b) $Phi = 0$ deg. plane

Chapter 6

Conclusions and Recommendations for Future Work

6.1   Conclusions

In this dissertation, the design and development of HGRMPA and HGWBMPA for sub-6 GHz 5G communications have been presented. The presented antennas utilize DGS to improve the gain and bandwidth. DGS provides various advantages when used in the MPAs. DGS technology based MPAs are easy to fabricate and give better performance. DGS can improve several antenna parameters such as gain, bandwidth etc. After choosing the substrate material and height of the substrate, the antennas are designed using transmission line model. In the proposed HGRMPA, the slot in the patch, the DGS and the reflector surface are utilized to improve the performance of the antenna. The reflector surface helped to suppress the side and back lobes of the antenna. The HGRMPA is designed and optimized using the CST microwave studio. The HGRMPA with optimized dimensions is fabricated. The measured results are compared with the simulated results. The comparison between the simulated and the measured results of HGRMPA shows good agreement. The maximum gain and maximum directivity of the antenna are 5.49 dB and 7.12 dB, respectively.

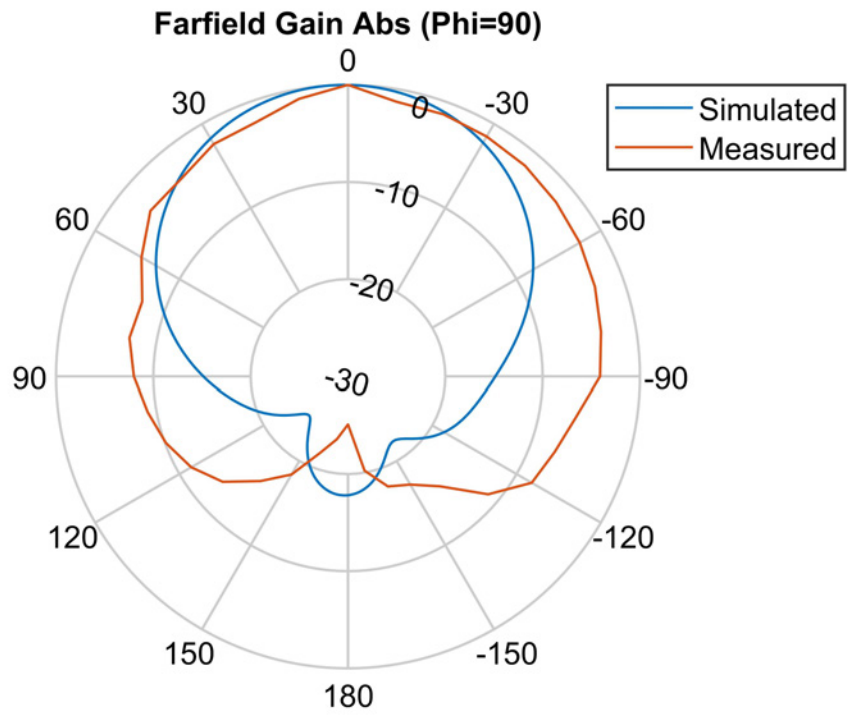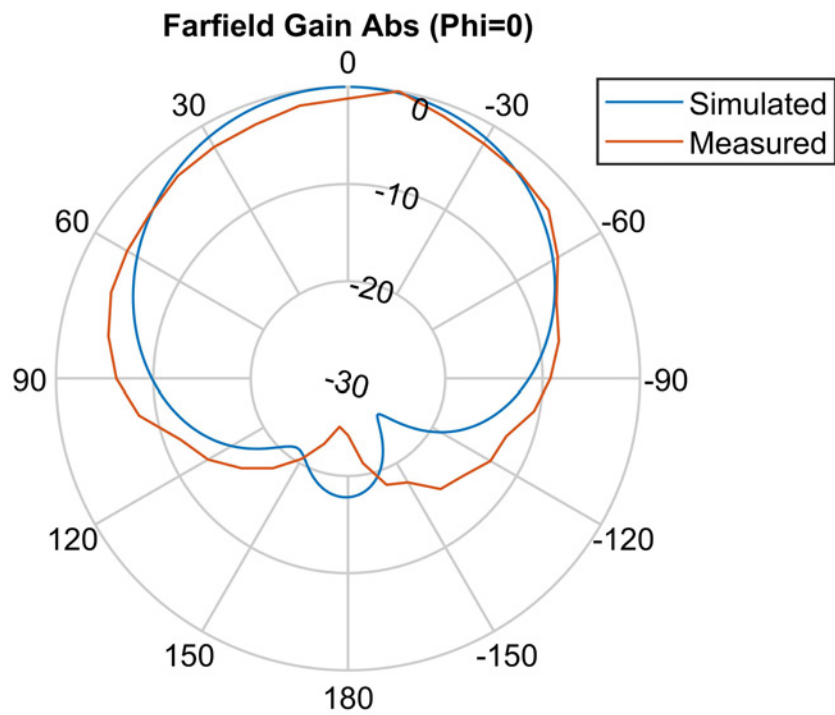To make the HGRMPA suitable for sub-6GHz 5G wideband applications, the design and development of HGWBMPA has been presented. Wideband behavior is achieved by replacing the C lacerated ground plane of the antenna by the partial ground plane with the triangular strip. The HGWBMPA gives the wide bandwidth ranging from 4.9 GHz to

5.8 GHz. The gain of the HGWBMPA has been improved by using the reflector surface below the ground plane. The maximum gain and maximum directivity of the HGWBMPA are 6.21 dB and 7.29 dB, respectively. The prototype of the designed and optimized HGWBMPA is fabricated. The comparison between the simulated and measured results of HGWBMPA shows good agreement. The size of the HGWBMPA is 28.03 $mm \times$ 23.45 $mm \times$ 5.35 mm with the patch size of 18.43×13.85 mm^2. The bandwidth of the HGRMPA and HGWBMPA lies in the sub-6 GHz frequency range. The antennas provide high gain and can be used for various wireless applications such as WiFi, WLAN etc. The proposed HGRMPA and HGWBMPA are suitable for sub-6 GHz 5G compact devices.

6.2   Recommendations for Future Work

For the future work, the gain of the proposed antennas can be further enhanced by designing the array antenna using the proposed antennas as the elements of the array. To enhance the capacity of the wireless communication systems, the design of the proposed antennas may be extended for multiple-input multiple-output systems. FSS, metamaterial etc. can also be utilized to further improve the performance of the proposed antennas.

Bibliography

[1] N. Singh and M. Sharma, "Antenna and its application," *International Journal of Computer Science and Technology*, vol. Vol 6.1 SP, no. 1, pp. 95–97, 2015.

[2] S. K. Gupta, H. K. Jangam, and N. Sharma, "Theory of antennas, its advantage & applications in communication systems," *International Journal of Engineering Development and Research*, vol. 6, no. 1, pp. 925–930, 2018.

[3] M. K. Pandian and T. Chinnadurai, "Design and optimization of rectangular patch antenna based on FR4, teflon and ceramic substrates," *Recent Advances in Electrical & Electronic Engineering*, vol. 12, no. 4, pp. 368–373, 2019.

[4] J. Volakis, R. C. Johnson, and H. Jasik, *Antenna Engineering Handbook, Fourth Edition*. McGraw-Hill's Access Engineering, McGraw-Hill Education, 2007.

[5] C. A. Balanis, *Antenna Theory Analysis and Design*. Hoboken, New Jersey: John Wiley & Sons, Inc., fourth ed., 2016.

[6] D. Nataraj and G. Karunakar, "Design and research of miniaturized micro strip slot with and without defected ground structure," *International Journal of Recent Technology and Engineering*, vol. 8, no. 2 Special Issue 11, pp. 391–398, 2019.

[7] Y. Liu, L.-M. Si, M. Wei, P. Yan, P. Yang, H. Lu, C. Zheng, Y. Yuan, J. Mou, X. Lv, and H. Sun, "Some recent developments of microstrip antenna," *International Journal of Antennas and Propagation*, vol. 2012, 2012.

[8] A. Taggu, B. Patir, and U. Bhattacharjee, "A dual band omni-directional antenna for WAVE and Wi-Fi," in *2017 2nd International Conference on Communication Systems, Computing and IT Applications (CSCITA)*, pp. 1–4, IEEE, 2017.

[9] R. Garg, P. Bhartia, I. J. Bahl, and A. Ittipiboon, *Microstrip Antenna Design Handbook*. Artech house, 2001.

[10] D. Guha, S. Biswas, and C. Kumar, "Printed antenna designs using defected ground structures: A review of fundamentals and state-of-the-art developments," *Forum for Electromagnetic Research Methods and Application Technologies (FERMAT)*, vol. 2, no. 1, pp. 1–13, 2014.

[11] R. H. Thaher and Z. S. Jamel, "New design of dual-band microstrip antenna for wi-max and WLAN applications," in *2018 1st International Scientific Conference of Engineering Sciences-3rd Scientific Conference of Engineering Science (ISCES)*, pp. 131–134, IEEE, 2018.

[12] B. R. Guan and Z. H. Zhang, "An ultra broadband antenna (UWB) loaded with defected ground structure (DGS)," in *2011 International Conference on Electronics, Communications and Control (ICECC)*, pp. 1872–1874, IEEE, 2011.

[13] R. H. Prasad, D. Vakula, and M. Chakravarthy, "A novel fractal slot DGS microstrip antenna for wi-fi application," in *2018 IEEE Indian Conference on Antennas and Propogation (InCAP)*, pp. 1–4, IEEE, 2018.

[14] G. P. Mishra, A. B. Sahoo, S. Hota, and B. B. Mangaraj, "Direct and electromagnetically coupled compact microstrip antenna design with modified fractal DGS," *International Journal of RF and Microwave Computer-Aided Engineering*, vol. 29, no. 10, p. e21887, 2019.

[15] R. A. Pandhare, P. L. Zade, and M. P. Abegaonkar, "Miniaturized microstrip antenna array using defected ground structure with enhanced performance," *Engineering Science and Technology, an International Journal*, vol. 19, no. 3, pp. 1360–1367, 2016.

[16] V. Sarin, M. Nishamol, D. Tony, C. Aanandan, P. Mohanan, and K. Vasudevan, "A wideband stacked offset microstrip antenna with improved gain and low cross polarization," *IEEE Transactions on Antennas and Propagation*, vol. 59, no. 4, pp. 1376–1379, 2011.

[17] M. K. Khandelwal, B. K. Kanaujia, and S. Kumar, "Defected ground structure: fundamentals, analysis, and applications in modern wireless trends," *International Journal of Antennas and Propagation*, vol. 2017, 2017.

[18] N. M. Salleh, I. M. M. Yusoff, A. A. Azlan, and M. T. Ali, "The design of quarter-wave EBG antenna," *RFM 2018 - 2018 IEEE International RF and Microwave Conference, Proceedings*, pp. 266–269, 2018.

[19] M. Asaadi, I. Afifi, and A.-R. Sebak, "High gain and wideband high dense dielectric patch antenna using FSS superstrate for millimeter-wave applications," *IEEE Access*, vol. 6, pp. 38243–38250, 2018.

[20] S. Hota, G. P. Mishra, and B. Mangaraj, "Sensitivity analysis of fractal DGS integrated microstrip patch antenna for X-band radar applications," *2018 International Conference on Computing, Power and Communication Technologies (GUCON)*, pp. 504–507, 2018.

[21] H. H. M. Ghouz, M. F. A. Sree, and M. A. Ibrahim, "Novel wideband microstrip monopole antenna designs for WiFi/LTE/WiMax devices," *IEEE Access*, vol. 8, pp. 9532–9539, 2020.

[22] V. S. Melkeri, S. Mallikarjun, and P. Hunagund, "Microstrip antenna with defected ground structure: A review," *International Journal of Electrical Electronics and Telecommunication Engineering*, pp. 2051–3240, 2015.

[23] G. A. Deschamps, "Microstrip microwave antennas," in *Proceedings of the Third Symposium on the United States Air Force (USAF) Antenna Research and Development Program*, pp. 18–22, Oct 1953.

[24] K. F. Lee, "A personal overview of the development of microstrip patch antennas," in *2016 IEEE International Symposium on Antennas and Propagation (APSURSI)*, pp. 689–690, IEEE, 2016.

[25] R. Mishra, "An overview of microstrip antenna," *HCTL Open International Journal of Technology Innovations and Research (IJTIR)*, vol. 21, no. 2, pp. 1–17, 2016.

[26] S. Khadka, *Evaluation of Radio Anechoic Chamber*. Metropolia Ammattikorkeakoulu, 2017.

[27] M. F. Salbani, A. Halim, M.A, A. H. Jahidin, and M. M. Ali, "Helical antenna design for wireless power transmission: A preliminary study," in *2011 IEEE International Conference on System Engineering and Technology*, pp. 192–195, IEEE, 2011.

[28] A. Pandey, *Practical Microstrip and Printed Antenna Design*. Artech House, 2019.

[29] S. N. Makarov, *Antenna and EM Modeling with MATLAB*. Princeton University Press, 2002.

[30] A. Q. Khan, M. Riaz, and A. Bilal, "Various types of antenna with respect to their applications: a review," *International Journal of Multidisciplinary sciences and Engineering*, vol. 7, no. 3, pp. 1–8, 2016.

[31] N. Kaur, N. Sharma, and N. Singh, "A study of different feeding mechanisms in microstrip patch antenna," *International Journal of Microwaves Applications*, vol. 6, no. 1, pp. 4–8, February 2017.

[32] N. Kumar and N. Sharma, "The various feeding techniques of microstrip patch antenna using HFSS," *International Journal of Electronics and Communication Engineering*, vol. 6, no. 6, pp. 23–29, 2019.

[33] A. Bansal and R. Gupta, "A review on microstrip patch antenna and feeding techniques," *International Journal of Information Technology*, vol. 12, no. 1, pp. 149–154, 2020.

[34] P. Gour and R. Mishra, "Bandwidth enhancement of a backfire microstrip patch antenna for pervasive communication," *International Journal of Antennas and Propagation*, vol. 2014, 2014.

[35] R. Waterhouse, *Microstrip patch antennas: a designer's guide*. Springer Science & Business Media, 2013.

[36] K. Ding, C. Gao, T. Yu, and D. Qu, "Wideband CP slot antenna with backed FSS reflector," *IET Microwaves, Antennas & Propagation*, vol. 11, no. 7, pp. 1045–1050, 2017.

[37] R. Mondal, P. S. Reddy, D. C. Sarkar, and P. P. Sarkar, "Compact ultra-wideband antenna: improvement of gain and FBR across the entire bandwidth using FSS," *IET Microwaves, Antennas & Propagation*, vol. 14, no. 1, pp. 66–74, 2020.

[38] H. Attia, M. L. Abdelghani, and T. A. Denidni, "Wideband and high-gain millimeter-wave antenna based on fss fabry–perot cavity," *IEEE Transactions on Antennas and Propagation*, vol. 65, no. 10, pp. 5589–5594, 2017.

[39] A. El Yassini, L. Aguni, S. Ibnyaich, S. Chabaa, and A. Zeroual, "Design of circular patch antenna with a high gain by using a novel artificial planar dual-layer metamaterial superstrate," *International Journal of RF and Microwave Computer-Aided Engineering*, vol. 29, no. 11, p. e21939, 2019.

[40] R. Li, Q. Zhang, Y. Kuang, X. Chen, Z. Xiao, and J. Zhang, "Design of a miniaturized antenna based on split ring resonators for 5g wireless communications," in *2019 Cross Strait Quad-Regional Radio Science and Wireless Technology Conference (CSQRWC)*, pp. 1–4, IEEE, 2019.

[41] J. Park, M. Jeong, N. Hussain, S. Rhee, S. Park, and N. Kim, "A low-profile high-gain filtering antenna for fifth generation systems based on nonuniform metasurface," *Microwave and Optical Technology Letters*, vol. 61, no. 11, pp. 2513–2519, 2019.

[42] S. Narayan, G. Gulati, B. Sangeetha, and R. U. Nair, "Novel metamaterial-element-based fss for airborne radome applications," *IEEE Transactions on Antennas and Propagation*, vol. 66, no. 9, pp. 4695–4707, 2018.

[43] S. Ghanem, A. Allam, and R. Uyguroglu, "Designs for leaky-wave antennas using metamaterial structures," in *2018 18th Mediterranean Microwave Symposium (MMS)*, pp. 83–86, IEEE.

[44] R. Parikh and B. Singh, "Effects of slots on resonant frequencies of a microstrip patch antenna," in *2018 Fourth International Conference on Computing Communication Control and Automation (ICCUBEA)*, pp. 1–5, IEEE, 2018.

[45] S. P. Gangwar, K. Gangwar, and A. Kumar, "A compact microstrip patch antenna with five circular slots for wideband applications," in *2018 3rd International Conference on Microwave and Photonics (ICMAP)*, pp. 1–2, IEEE, 2018.

[46] Y. Yin and K. Wu, "Dual band dual mode low cross-polarization slot-patch antenna fed by microstrip line," *IET Conference Publications*, vol. 2018, no. CP741, pp. 3–6, 2018.

[47] B. Ngobese and P. Kumar, "A high gain microstrip patch array for 5 GHz WLAN applications," *Advanced Electromagnetics*, vol. 7, no. 3, pp. 93–98, 2018.

[48] V. Platero, P. Ferguson, R. Jayaraman, and D. Isleifson, "2-in-1 smart panels: Embedding phased array patch antennas within satellite structures," *Acta Astronautica*, vol. 175, pp. 51–56, 2020.

[49] K. S. Kola, A. Chatterjee, and D. Patanvariya, "Design of a compact high gain printed octagonal array of spiral-based fractal antennas for dbs application," *International Journal of Microwave and Wireless Technologies*, vol. 12, no. 8, pp. 769–781, 2020.

[50] M. Y. Mohamed, A. M. Dini, M. M. Soliman, and A. Z. M. Imran, "Design of 2×2 microstrip patch antenna array at 28 GHz for millimeter wave communication," in *2020 IEEE International Conference on Informatics, IoT, and Enabling Technologies (ICIoT)*, pp. 445–450, IEEE, 2020.

[51] A. Zaidi, A. Baghdad, A. Ballouk, and A. Badri, "High gain microstrip patch antenna, with PBG substrate and PBG cover, for millimeter wave applications," in *2018 4th International Conference on Optimization and Applications (ICOA)*, pp. 1–6, IEEE, 2018.

[52] G. Á. Jiménez-Guzmán, J. A. Tirado-Mendez, A. Rangel-Merino, L. A. Vasquez-Toledo, and R. Marcelin-Jimenez, "Improving the performance of a patch antenna array by using photonic bandgap structures at X-band," *Journal of Electromagnetic Waves and Applications*, vol. 34, no. 16, pp. 2130–2146, 2020.

[53] P. R. T. Naidu, C. Saha, K. V. Krishna, L. A. Shaik, J. Y. Siddiqui, and Y. Antar, "Compact multiple EBG cells loaded UWB-narrowband antenna pair with high isolation for cognitive radio (CR) based MIMO applications," *AEU-International Journal of Electronics and Communications*, p. 153420, 2020.

[54] C. Kumar, M. I. Pasha, and D. Guha, "Defected ground structure integrated microstrip array antenna for improved radiation properties," *IEEE Antennas and Wireless Propagation Letters*, vol. 16, pp. 310–312, 2016.

[55] N. Nhlengethwa and P. Kumar, "Microstrip patch antenna with enhanced gain for 2.4 GHz wireless local area network applications," in *Micro-Electronics and Telecommunication Engineering*, pp. 583–591, Springer, 2020.

[56] R. Garg, I. Bahl, and M. Bozzi, *Microstrip lines and slotlines*. Artech house, 2013.

[57] D. Ahn, J.-S. Park, C.-S. Kim, J. Kim, Y. Qian, and T. Itoh, "A design of the low-pass filter using the novel microstrip defected ground structure," *IEEE transactions on microwave theory and techniques*, vol. 49, no. 1, pp. 86–93, 2001.

[58] H. J. Naibaho, M. Yunus, A. Munir, *et al.*, "Coupling reduction between two elements of array antenna using u-shaped defected ground structure," in *2017 International Conference on Control, Electronics, Renewable Energy and Communications (ICCREC)*, pp. 29–32, IEEE, 2017.

[59] A. Kakkar, S. Sah, *et al.*, "A tri-band circular patch microstrip antenna with different shapes in DGS for Ku and K applications," in *2017 2nd International Conference on Telecommunication and Networks (TEL-NET)*, pp. 1–5, IEEE, 2017.

[60] Z.-L. Wen, Y.-N. Han, X.-Y. Sun, R. Tao, J.-N. Xia, X.-M. Chen, Y.-J. Chen, and Z.-D. Chen, "Design of miniaturized low-pass filter with improved koch fractal DGS," in *2017 IEEE 5th International Symposium on Electromagnetic Compatibility (EMC-Beijing)*, pp. 1–4, IEEE, 2017.

[61] R. A. Panda, D. Mishra, D. Ghosh, and S. Dey, "Modified dumbbell shaped patch with defective ground structure for 24 GHz ISM band application," in *2019 IEEE International Conference on Electrical, Computer and Communication Technologies (ICECCT)*, pp. 1–4, IEEE, 2019.

[62] B. S. Reddy and D. Vakula, "Compact zigzag-shaped-slit microstrip antenna with circular defected ground structure for wireless applications," *IEEE Antennas and Wireless Propagation Letters*, vol. 14, pp. 678–681, 2014.

[63] M. Yunus, Z. L. Patriana, E. Wismiana, T. Firmasyah, and A. Munir, "Planar array-antenna with improved radiation characteristic using spiral shaped DGS," in *2018 International Conference on Applied Electromagnetics, Signal Processing and Communication (AESPC)*, vol. 1, pp. 1–4, IEEE, 2018.

[64] A. K. Belbachir, M. Boussouis, and N. Amar Touhami, "High-performance LPF using coupled C-shape DGS and radial stub resonators for microwave mixer," *Progress In Electromagnetics Research*, vol. 58, pp. 97–103, 2016.

[65] A. I. Hammoodi, H. Raad, and M. Milanova, "Mutual coupling reduction between two circular patches using h-shape DGS," in *2018 IEEE International Symposium on Antennas and Propagation & USNC/URSI National Radio Science Meeting*, pp. 1371–1372, IEEE, 2018.

[66] M. F. Nakmouche, D. E. Fawzy, A. Allam, H. Taher, and M. F. A. Sree, "Dual band siw patch antenna based on h-slotted DGS for Ku band application," in *2020 7th International Conference on Electrical and Electronics Engineering (ICEEE)*, pp. 194–197, IEEE, 2020.

[67] K. Wei, J.-Y. Li, L. Wang, Z.-J. Xing, and R. Xu, "Mutual coupling reduction of microstrip antenna array by periodic defected ground structures," in *2016 IEEE 5th Asia-Pacific Conference on Antennas and Propagation (APCAP)*, pp. 389–390, IEEE, 2016.

[68] D.-J. Woo, T.-K. Lee, and J. W. Lee, "Equivalent circuit model for a simple slot-shaped DGS microstrip line," *and Wireless Components Letters*, vol. 23, no. 9, pp. 447–449, 2013.

[69] B. D. Wulandari and A. Munir, "Equivalent circuit for microstrip bandpass filter," in *2016 2nd International Conference on Wireless and Telematics (ICWT)*, pp. 14–19, IEEE, 2016.

[70] E. Van Nechel, F. Ferranti, Y. Rolain, and J. Lataire, "Model-driven design of microwave filters based on scalable circuit models," *IEEE Transactions on Microwave Theory and Techniques*, vol. 66, no. 10, pp. 4390–4396, 2018.

[71] C. Garg and M. Kaur, "A review of defected ground structure (DGS) in microwave design," *International Journal of Innovative Research in Electrical, Electronics, Instrumentation and Control Engineering*, vol. 2, no. 3, pp. 1285–1290, 2014.

[72] Shivnarayan and B. R. Vishvakarma, "Analysis of slot-loaded rectangular microstrip patch antenna," *Indian Journal of Radio and Space Physics*, vol. 34, pp. 424–430, December 2005.

[73] L. H. Weng, Y.-C. Guo, X.-W. Shi, and X.-Q. Chen, "An overview on defected ground structure," *Progress In Electromagnetics Research*, vol. 7, pp. 173–189, 2008.

[74] J.-I. Park, C.-S. Kim, J. Kim, J.-S. Park, Y. Qian, D. Ahn, and T. Itoh, "Modeling of a photonic bandgap and its application for the low-pass filter design," in *1999 Asia Pacific Microwave Conference. APMC'99. Microwaves Enter the 21st Century. Conference Proceedings (Cat. No. 99TH8473)*, vol. 2, pp. 331–334, IEEE, 1999.

[75] N. C. Karmakar, S. M. Roy, and I. Balbin, "Quasi-static modeling of defected ground structure," *IEEE Transactions on Microwave Theory and Techniques*, vol. 54, no. 5, pp. 2160–2168, 2006.

[76] C. Caloz, H. Okabe, T. Iwai, and T. Itoh, "A simple and accurate model for microstrip structures with slotted ground plane," *IEEE Microwave and Wireless Components Letters*, vol. 14, no. 3, pp. 127–129, 2004.

[77] A. Kumar and M. Kartikeyan, "Design and realization of microstrip filters with new defected ground structure (DGS)," *Engineering Science and Technology, an International Journal*, vol. 20, no. 2, pp. 679–686, 2017.

[78] R. Krishna, K. Sharma, R. Gupta, and M. S. Naruka, "Design of compact coplanar band stop filter composed on open loop ring resonator and defected ground structure (DGS)," in *2020 International Conference on Contemporary Computing and Applications (IC3A)*, pp. 102–105, IEEE, 2020.

[79] D. S. Jose, A. S. Kumar, T. Shanmugantham, *et al.*, "A band pass coupled line filter with DGS for ultra-wide band application," *Procedia Computer Science*, vol. 171, pp. 561–567, 2020.

[80] T. K. Rekha, P. Abdulla, P. M. Jasmine, and A. R. Anu, "Compact microstrip lowpass filter with high harmonics suppression using defected structures," *AEU-International Journal of Electronics and Communications*, vol. 115, p. 153032, 2020.

[81] E. A. Casu, A. A. Müller, M. Fernández-Bolaños, A. Fumarola, A. Krammer, A. Schüler, and A. M. Ionescu, "Vanadium oxide bandstop tunable filter for Ka frequency bands based on a novel reconfigurable spiral shape defected ground plane CPW," *IEEE Access*, vol. 6, pp. 12206–12212, 2018.

[82] V. Komarov, O. Barybin, and Y. V. Rassokhina, "Low-pass load matching network design using dumbbell-shaped DGS for high-efficiency microwave power amplifiers," in *2019 International Conference on Information and Telecommunication Technologies and Radio Electronics (UkrMiCo)*, pp. 1–4, IEEE, 2019.

[83] G. Immadi, K. Swetha, M. V. Narayana, M. Sowmya, and R. Ranjana, "Design of microstrip patch antenna for WLAN applications using back to back connection of two E-shapes," *International Journal of Engineering Research and Applications (IJERA)*, vol. 2, no. 3, pp. 319–323, 2012.

[84] K. O. Mabusha and P. Kumar, "A rectangular microstrip patch antenna for dual band wireless applications," *Recent Advances in Electrical & Electronic Engineering*, vol. 13, no. 2, pp. 212–218, 2020.

[85] M. Mabaso and P. Kumar, "A dual band patch antenna for bluetooth and wireless local area networks applications," *International Journal of Microwave and Optical Technology*, vol. 13, no. 5, pp. 393–400, 2018.

[86] M. Mabaso and P. Kumar, "A microstrip patch antenna with defected ground structure for triple band wireless communications," *Journal of Communications*, vol. 14, no. 8, pp. 684–688, 2019.

[87] N. Rasool, K. Huang, A. B. Muhammad, and Y. Liu, "A wideband circularly polarized slot antenna with antipodal strips for WLAN and C-band applications," *International Journal of RF and Microwave Computer-Aided Engineering*, vol. 29, no. 11, p. e21945, 2019.

[88] J. Ashish and A. P. Rao, "Design and implementation of compact dual band u-slot microstrip antenna for 2.4 GHz WLAN and 3.5 GHz WiMAX applications," in *2019 International Conference on Smart Systems and Inventive Technology (ICSSIT)*, pp. 1084–1086, IEEE, 2019.

[89] H. Davoudabadifarahani and B. Ghalamkari, "High efficiency miniaturized microstrip patch antenna for wideband terahertz communications applications," *Optik*, vol. 194, p. 163118, 2019.

[90] J. Baker-Jarvis, M. D. Janezic, B. Riddle, C. L. Holloway, N. Paulter, and J. Blendell, *Dielectric and Conductor-Loss Characterization and Measurements on Electronic Packaging Materials.* NIST Technical Note 1520, 2001.

[91] W. L. Stutzman and G. A. Thiele, *Antenna Theory and Design.* John Wiley & Sons, 2012.

[92] S. N. Njokweni and P. Kumar, "Salt and sugar detection system using a compact microstrip patch antenna," *International Journal on Smart Sensing and Intelligent Systems*, vol. 13, pp. 1–9, 2020.

[93] A. Kapoor, R. Mishra, and P. Kumar, "Compact wideband-printed antenna for sub-6 ghz fifth-generation applications," *International Journal on Smart Sensing and Intelligent Systems*, vol. 13, pp. 1–10, 2020.